

3.2 First-Principles Calculation of Material Properties

First-principles statistical thermodynamics simulations on the structure and reactivity of heterogeneous catalysts

Teruo HIRAKAWA, Fahdzi MUTTAQIEN, Sasfan Arman WELLA, Yuji HAMAMOTO,
Kouji INAGAKI, Hidetoshi Kizaki, and Yoshitada MORIKAWA

*Department of Precision Science and Technology,
Osaka University, Yamada-oka, Suita, Osaka 565-0871*

In our research project, we investigated chemical reactions at surfaces and interfaces including CO₂ adsorption and hydrogenation on Cu surfaces, naphthalene on graphite surfaces, ligand-free Suzuki-Miyaura cross coupling reactions in aqueous solutions, and stability of Pd atoms dissolved into LaFeO₃ perovskite oxides. In the present report, we explain some of our recent progresses.

The Suzuki-Miyaura reaction (SMR) is one of the most efficient palladium-catalyzed cross-coupling reactions for the formation of carbon-carbon bonds, in particular for the formation sp²-sp² carbon-carbon of biaryls in organic synthesis [1-3]. The SMR has been developed mainly with ligands, especially phosphine ligands to make the palladium catalyst stable and optimize its reactivity in an organic solvent.

The SMR without any ligands, that is "ligand free" in a water solvent, was suggested, and it has been attracting enormous interest recently [4-6]. Most theoretical studies for the SMR reported so far, used a simple solvent model to

simulate the cross coupling mechanisms in an organic solvent. In these studies, the solvent effect is approximately treated using a polarizable continuum model (PCM). However, solvent molecules may play important roles in ligand-free Pd cross coupling reactions, explicitly including solvent. Thus, in the present study we focus on the oxidative addition step of the SMR in a water solvent explicitly including solvent molecules in our calculation models and perform full quantum mechanical molecular dynamics (MD) simulations[7].

All of the calculations are based on the density functional theory (DFT) within the generalized gradient approximation (GGA-PBE) as implemented in the STATE-Senri code [8]. We used ultrasoft pseudo potentials and a plane-wave basis set with cutoff energies of 25 Ry and 225 Ry for wave functions and charge densities, respectively.

The results show that the energy barrier on the oxidative addition step is quite low especially for PhBr, which is significantly different from the conventional SMR with ligands in organic solvents. This may be the reason why the SMR in water without any ligands can achieve a high TON and low-leaching of the Pd catalyst. Conversely, the barrier of the oxidative addition for PhCl is sizable, indicating that the reaction can proceed at room temperature or above, but the rate is rather slow compared with PhBr. Therefore, the lifetime of the η^2 complex of PhCl-Pd is elongated, causing the sintering of Pd to degrade the catalyst. We observed that the activation barriers of the oxidative addition of PhX to the PdX⁻ anion complex are similar to those of the oxidative addition of PhX to a single Pd⁽⁰⁾ atom in a water solvent. The final state of the oxidative addition step, however, becomes significantly destabilized by the additional coordination of a halogen anion to the central Pd atom, and this should have an important effect for the following transmetalation step. The coordination of anions to the Pd atom should also prevent the aggregation of the Pd atom to form the Pd black. Therefore, the halogen anion can act as a "ligand" in a ligand-free system.

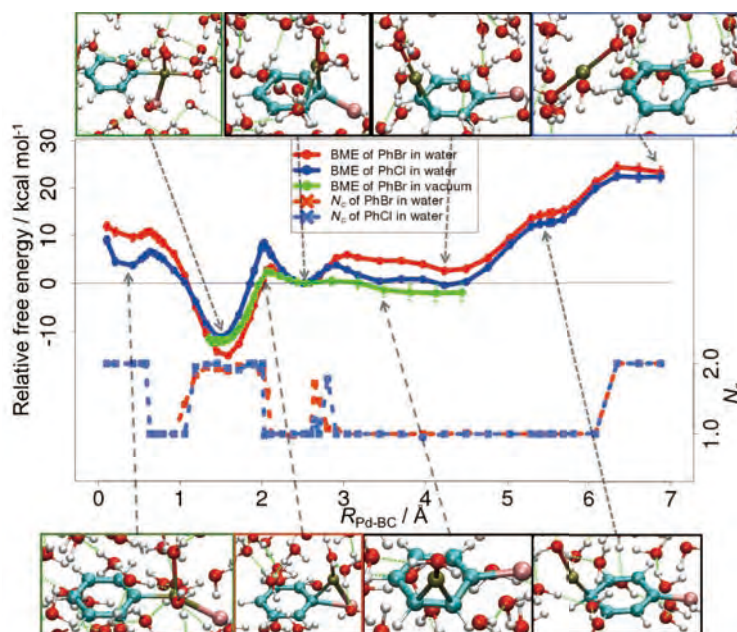


Fig. 1. Relative free energy profile and the number of coordinated H₂O to Pd for the oxidative addition step. The top and bottom panels show snapshots of the oxidative addition

References

- [1]. N. Miyaura and A. Suzuki, *J. Chem. Soc., Chem. Commun.*, **19**, 866–867 (1979).
- [2]. N. Miyaura, K. Yamada, and A. Suzuki, *Tetrahedron Lett.*, **20**, 3437–3440 (1979).
- [3]. N. Miyaura, A. Suzuki, *Chem. Rev.*, **95**, 2457–2483 (1995).
- [4]. M.D. Smith, A.F. Stepan, C. Ramarao, P.E. Brennan, S.V. Ley, *Chem. Commun.*, 2652–2653 (2003).
- [5]. S.P. Andrews, A.F. Stepan, H. Tanaka, S.V. Ley, M.D. Smith, *Adv. Synth. Catal.*, **347**, 647–654 (2005).
- [6]. N.J. Hill, M.D. Bowman, B.J. Esselman, S.D. Byron, J. Kreitinger, N.E. Leadbeater, *J. Chem. Educ.*, **91**, 1054–1057 (2014).
- [7]. T. Hirakawa, Y. Uramoto, D. Mimura, A. Takeda, S. Yanagisawa, T. Ikeda, K. Inagaki, and Y. Morikawa, *J. Phys. Chem. B*, **121**, 164–173 (2017).
- [8]. Y. Morikawa, *Phys. Rev. B*, **51**, 14802 (1995).

Analyses on atomic structure magnetism and electronic structure in spintronics materials and molecular magnets

Tatsuki ODA^{1,2}, Tomosato KANAGAWA², Nurul IKHSAN²,
Yosuke FUNATO², Hasan Al RASYID², Masao OBATA²

¹*Institute of Science and Engineering, Kanazawa University, Kanazawa, Ishikawa 920-1192*

²*Graduate School of Natural Science and Technology, Kanazawa University, Kanazawa, Ishikawa, 920-1192*

We studied the several topics involved with this project; Rashba's effect of surface, magnetic anisotropy and its electric field (EF) effect in the thin film related with spintronic devices, and magnetic effects in molecular system. We also developed a method of van der Waals density functional (vdW-DF) approach for magnetic systems. These investigations have been done by employing the home-made density functional code, which has run efficiently in the architectures in Systems B in ISSP.

Rashba's effect of surface

The heavy-element-covered semiconductor surfaces show a giant Rashba-type spin splitting and many experiments have been reported for spintronics applications. We found the peculiar magnetic configuration in momentum space (spin texture) around the Fermi level for the surface band of Tl/Si(110). This is novel, compared with the normal Rashba spin texture, in which the spin lies along concentric circles in plane. The spin texture obtained forms an alignment to the direction perpendicular to the mirror plane of system. This may be very useful for spintronics application because of the suppressed spin scattering. The silicon based materials are still recommended as a new material in the next generation electronics (spintronics). Such

research has been published in the collaboration with the experimental group of photoemission measurement [1].

The Rashba's effect obtained in Tl/Si(110) is explained in a combination of two usual Rashba spin textures. The one arises from the origin in the momentum space, and the other from the cross point which has both the mirror and glide-plane symmetries. At the middle point between the two, the spin direction tends to align within the surface plane along the direction perpendicular to the mirror plane. In such region, fortunately, the surface single band can form the small hole pocket with a peanut form. This enable us to have a single uniform spin valley when adjusting the Fermi level. These theoretical results not only agree well with the experimental result, but also work efficiently as a useful guide for the accomplishment of experimental measurement.

Magnetic anisotropy and electric field effect

Magnetic anisotropy energy (MAE) and its EF effect were investigated in the slab system of Cr/Fe/MgO by using first-principles calculation. Such system keeps the Fe/MgO interface and has a possibility to improve the perpendicular magnetic anisotropy by introducing intrinsic deflections from the under layer (Cr). We estimated MAEs and voltage-control magnetic anisotropy (VCMA)

coefficient and analyzed the electronic structures. The calculation results revealed a more concrete relation between electronic structures and MAE, compared with the previous achievements. The publishing paper is now in preparation.

The slab system which consists of a part of spintronics device, PtCo/ZnO, has been studied. This may be categorized to one of multi-ferroic interfaces. This is because one can expect an electric polarization from ZnO and a magnetism from PtCo metal. By introducing the external electric field or magnetic field, one can control a multi-function of such interface. The first paper, published in the collaboration with the experimental group of magnetic tunnel spectral [2], theoretically reported interface models of different electric polarizations in ZnO layer, as shown in Fig.1. This can be made by the effective screened medium (ESM) method, which easily allows the electric polarization in slab system. At the barrier layer (ZnO), a monotonic variation superpositioned on a rapid oscillation indicates an internal depolarization electric field opposite to the

respective polarization. Note that this field cancels out the polarization to maintain a zero electric flux. The publishing paper which describes effects on spin-orbit interaction in the magnetic layer is now in preparation.

Van der Waals density functional approach

The vdW-DF approach is one of promising methods to overcome the problem that the density functional approach, such as local density approximation or generalized gradient approximation, cannot describe van der Waals (vdW) force properly. We have proposed the extension of vdW-DF to spin-polarized (magnetic) systems, vdW-DF-SGC (SGC stands for spin-polarization-dependent gradient correction), and demonstrated the usefulness. We also focused on the effect of SGC which described the spin dependent semi-local electron correlation effect, and found that it plays an important role in antiferromagnetic interactions.

Another spin van der Waals method (svdW-DF) was developed in 2015. The relation between vdW-DF-SGC and svdW-DF should be clarified in several applications. Therefore we also implemented this method in the house-DFT code, and investigated the oxygen systems and the absorption system which contains magnetic materials, namely, graphene on Ni(111) surface. Comparing these results with those of our method, we found that the svdW-DF also corrected the antiferromagnetic coupling and gave almost the same binding property as the vdW-DF-SGC.

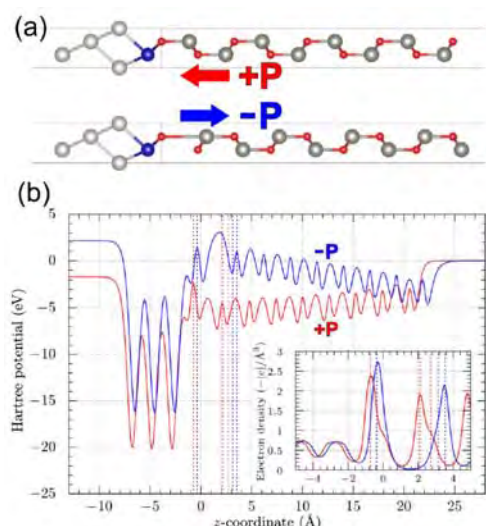


Figure 1. (a) Slab models for the electric polarizations and (b) electrostatic potential profiles along the layer thickness.

- [1] E. Annese, et al., Chem. Phys. Rev. Lett. **117** (2016) 16803.
- [2] M. Belmoubarik et al., Appl. Phys. Lett., **109** (2016) 173507.

Exciton wave function analysis for [n]CPPs (n = 3-16)

Yoshifumi NOGUCHI

Institute for Solid State Physics,

The University of Tokyo, Kashiwa-no-ha, Kashiwa, Chiba 277-8581

As cycloparaphenylenes molecules (CPP), known as the shortest armchair-type carbon nanotube with hydration terminated edges, were successfully synthesized experimentally in 2008 [1], their structural and optical properties have attracted attention. As one of the interesting features, it has been reported that the optical gap is sensitive to the molecular size in the photo emission spectra but is insensitive to the same in the photoabsorption spectra. However, the theoretical studies within the framework of time-dependent density functional theory (TDDFT) have never successfully explained this experimental fact.

In this study, we applied the first-principles *GW*+Bethe-Salpeter method to [n]CPPs ($n = 3-16$) and discussed the optical properties [2]. The simulated spectra are in a good agreement with the experimental UV-vis absorption spectra particularly from the viewpoints of the peak positions and peak heights. More importantly, the results are consistent with the experimentally observed insensitivity of the optical gap to the molecular size. As the first exciton (S_1) is dark (or experimentally invisible) for all the sizes, the experimentally

observed molecular size insensitivity is for the higher excitons ($i \geq 2$). To investigate the first dark and bright excitons in detail, we estimated the expectation value for an arbitrary operator (O) by using the exciton wave functions ($\Psi^i(r_1, r_2) = \sum_{e,h} A_{e,h}^i \psi_e(r_1) \psi_h^*(r_2)$), where $A_{e,h}^i$ is the eigenvector obtained when the Bethe-Salpeter equation is solved and $\psi_e(\psi_h)$ is the LDA wave function at the excited electron (created hole) level [3]. The overlap strength between the electron and hole wave functions (Λ), the exciton size (d_{exc}), the electron-hole separation distance ($d_{e \rightarrow h}$), the electron (hole) delocalization (σ_e, σ_h), and the exciton binding energy (E^b) exhibit common features for larger sized CPPs ($n \geq 9$). These observations nicely explain why the optical gap is insensitive to the molecular size.

References

- [1] R. Jasti, J. Bhattacharjee, J. B. Neaton, and C. R. Bertozzi: *J. Am. Chem. Soc.*, **130** (2008) 17646.
- [2] Y. Noguchi and O. Sugino: *J. Chem. Phys.* **146** (2017) 144304.
- [3] D. Hirose, Y. Noguchi, and O. Sugino: *J. Chem. Phys.* **146** (2017) 044303.

Development of first-principles electronic-structure and transport calculation method based on real-space finite-difference approach

Tomoya ONO

*Center for Computational Sciences, University of Tsukuba
Tenno-dai, Tsukuba, Ibaraki 305-8577*

1 Introduction

SiC is attracted much attention due to its excellent physical properties, such as a high thermal conductivity, high breakdown strength, and large band gap. However, unlike Si metal-oxide-semiconductor field-effect transistors (MOSFETs), SiC-MOSFETs, primarily of the n-channel type, suffer from unacceptably low carrier mobility. Large amount of defects at SiC/SiO₂ interface, which are generated in oxidation process, is expected to be one of the origins for the low carrier mobility.

Among various polytypes, 4H-SiC, in which Si and C atoms can occupy one of three positions along the $[1\bar{1}00]$ direction, normally labelled ABCBAB... is the most widely used polytype for SiC-MOSFETs. Within these four bilayers, there are two inequivalent lattice sites, usually known as h (hexagonal) and k (quasi-cubic) based on the site occupied by the Si atoms in the neighboring bilayers. It is found that interface type determines whether conduction band edge (CBE) internal-space states at the interface are affected by the presence of O defects, as with h type, or not, as with k type.[1]

In this study, we performed first-principles calculation to investigate how the electron scattering property of the SiC/SiO₂ interface changes depending on the stacking of SiC bilayers at the interface, i.e. h and k types, and when O atoms are subsequently introduced.[2]

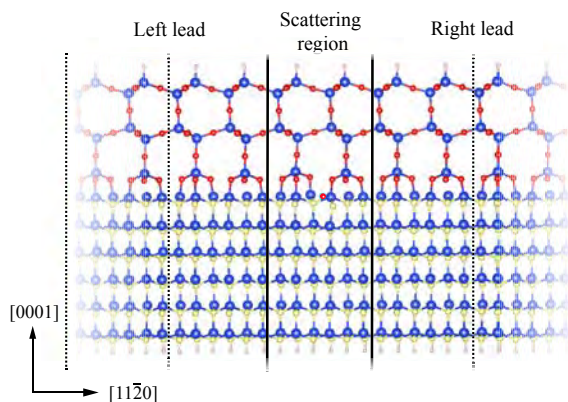


Figure 1: Schematic image of the transport-calculation model. The boundary between the scattering region and the semi-infinite leads is distinguished by solid lines. Supercells of leads are bounded by dotted lines. Blue, yellow, red, and white spheres are Si, C, O, and H atoms, respectively. Reprinted with permission from Ref. 3.

2 Method

Calculations are carried out using RSPACE.[3] To perform the transport calculation, we adopt the Green's function method and the Landauer-Büttiker formalism within the framework of density functional theory. Figure 1 illustrates schematics of the computational models used for the transport calculations, in which the whole system is divided into three parts: a left lead, a central scattering region, and a right lead. The central

scattering region is composed of the SiC/SiO₂ interface including the oxygen related structures or carbon-related defects. We investigate three models, one O atom O_{if}, two O atoms O_{sub}+O_{if}, and VCO₂, which appears after introducing three excess O atoms and removing a CO molecule to relieve the interface stress caused by lattice constant mismatch. The left (right) lead is a semi-infinite slab along the [11 $\bar{2}$ 0] ($\bar{1}\bar{1}$ 20) direction and its atomic structures correspond to those of the initial interface. The other details of the computational method are introduced elsewhere.[2]

3 Results

Figures 2 and 3 show the channel current with respect to the applied bias. A significant reduction of the current due to the existence of the O atoms is observed for the h type while the amount of the current is unaffected for the k type. This is because the local density of states (LDOS) at CBE is very sensitive to insertion of the O atoms in the case of h type. Two physical phenomena combine to prevent electron transmission in the h type. First, the internal-space states appear from the top of the interface in the h type. Second, the energy level of the internal-space states is shifted upward by the Coulomb interaction with inserted O atoms or defects.

For comparison, the transmissions through the h and k types with carbon-related defects are also examined. Similarly to the case of the oxygen-related structures, it is found that the transmission at the h type is markedly decreased. It is surprising that the oxygen-related structures, which are naturally generated at the SiC/SiO₂ interface during dry oxidation, cause the electron scattering because the oxygen-related structures considered here have been reported to be electrically inactive. According to the discussion about the LDOS at the interface, the internal-space states will play important role for the carrier scattering

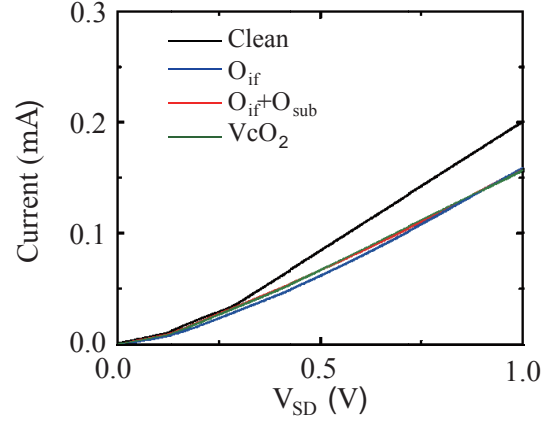


Figure 2: Calculated channel current for h type.

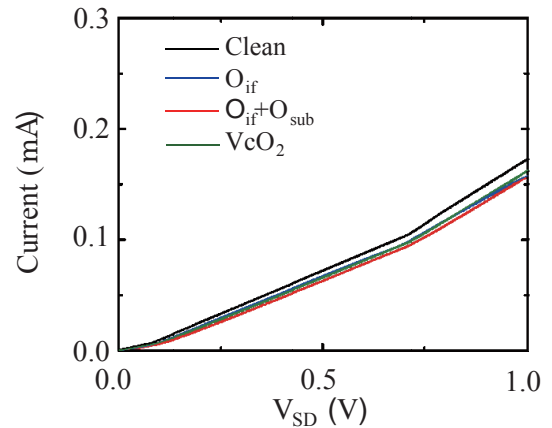


Figure 3: Calculated channel current for k type.

at the n-channel MOSFET.

References

- [1] C. J. Kirkham and T. Ono: J. Phys. Soc. Jpn. **85** (2016) 024701.
- [2] S. Iwase, C. J. Kirkham and T. Ono: Phys. Rev. B **95** (2017) 041302.
- [3] K. Hirose, T. Ono, Y. Fujimoto, and S. Tsukamoto: *First Principles Calculations in Real-Space Formalism, Electronic Configurations and Transport Properties of Nanostructures* (Imperial College, London, 2005).

Analyses on protein-folding process by automatic detection of structural transitions with molecular dynamics simulations

Yasuteru SHIGETA

Center for Computational Sciences,

University of Tsukuba, 1-1-1 Tennodai, Tsukuba, Ibaraki 305-8577, Japan

Structural transitions of proteins are strongly related to biological functions. In order to theoretically reproduce the structural transitions of proteins at the atomic level, molecular dynamics (MD) simulations have been widely used to generate atomic trajectories as time-series data for the structural transitions. If one can ideally perform sufficiently long-time MD simulations, the atomic trajectories would be utilized for analyzing the biological functions and calculating several physical properties on an equal footing, since the Ergodic hypothesis indirectly guarantees that the sufficiently long-time trajectories include structural transitions relevant to the biological functions and might be regarded as a statistically reliable ensemble.

However, conventional timescales of the biological functions are in a range within the order of milliseconds to seconds, which are far from the accessible timescales of conventional MD simulations, i.e. the order of nanoseconds to microseconds. As a strategy for enhancing the conformational sampling of the conventional MD simulations and reproducing these kinds of biologically important rare events, special purpose machines like Anton

series enable one to perform extremely long-time MD simulations but the usages of these special purpose machines are limited. Also, the conformational transitions relevant to the biological functions are stochastic processes. It does not ensure that the long-time MD simulations inevitably capture the essential conformational transitions during every MD simulation. Therefore, one might perform several long-time MD simulations starting from distinct initial structures to remove dependence on initial conditions. That is why it is desirable to develop enhanced conformational sampling methods for reproduction of biologically important rare events instead of conventional MD simulations.

As an alternative conformational sampling method to CMD, the Parallel Cascade Selection MD (PaCS-MD) [1] and variants have been proposed by our group as a distributed computing for generating structural transition pathways between a given reactant and product under a condition that the both end-point structures are known *a priori*. In PaCS-MD, the initial structures are selected from obtained snapshots by referring to a structural similarity

of them with respect to the product at the end of each cycle. By repeating the cycles of conformational resampling from the reasonably selected structures, PaCS-MD generates candidates of structural transition pathways from the reactant to the product. To efficiently perform PaCS-MD, the number of the initial structures, n_{initial} , is one of essential parameters. However, it has not been clarified how the choice of n_{initial} affects conformational sampling efficiency of PaCS-MD.

In this work, the conformational sampling efficiency was assessed by changing n_{initial} in performing PaCS-MD. As the assessments, we addressed how a number of initial structures, n_{initial} , affected the conformational sampling efficiency. It is confirmed that the large n_{initial} accelerated the structural transitions. In contrast, the small n_{initial} showed a high conformational sampling efficiency as an accumulated simulation time over cycles, indicating that the both n_{initial} s are suitable for promoting the structural transitions [2].

Besides the PaCS-MD, we have also proposed TaBoo SeArch (TBSA) algorithm [3]. In TBSA, an inverse histogram of the original distribution projected onto a set of reaction coordinates is constructed from trajectories, and rarely occurring states of the protein are statistically selected as new initials based on the inverse histogram, and resampling via

restarting MD simulations. In this process, a definition of the inverse histogram, which characterizes the rarely occurring states, is crucial for an efficiency of TBSA.

In this work, we also propose a simple modification of the inverse histogram to further accelerate the convergence of TBSA. As demonstrations of the modified TBSA, hydrogen bonding rearrangements of Met-enkephalin, large-amplitude domain motion of Glutamine binding protein, and folding processes of a B domain of *Staphylococcus aureus* Protein A are shown. In all demonstrations, it is numerically proven that the modified TBSA successfully reproduced these biologically important rare-events with nanosecond-order computational costs, although a set of microsecond-order canonical MD simulations failed to reproduce them, indicating the high efficiency of the modified TBSA[4].

References

- [1] R. Harada, Kitao, *J. Chem. Phys.*, **139**, 035103 (2013).
- [2] R. Harada, Y. Shigeta, *Chem. Lett. in press* (2017).
- [3] R. Harada *et al.* *J. Comput. Chem.*, **36**, 763 (2015) and *Chem. Phys. Lett.*, **630**, 68 (2015).
- [4] R. Harada, Y. Takano, Y. Shigeta, *J. Chem. Theor. Comput.* **12**, 2436(2016).

DFT sampling studies on interfacial reactions in catalysts and batteries

Yoshitaka TATEYAMA

Center for Green Research on Energy and Environmental Materials (GREEN), National Institute for Materials Science (NIMS), 1-1 Namiki, Tsukuba, Ibaraki 305-0044; Elements Strategy Initiative for Catalysts & Batteries (ESICB), Kyoto University, Goryo-Ohara, Nishikyo-ku 615-8245.

Transformation of energy management systems via success of efficient utilization of renewable energy and CO₂ zero emission is an urgent challenge in our society. To step toward its realization, improvement of energy storage and conversion is indispensable. However, establishments of high-efficiency techniques as well as high reliability are not satisfactory yet for practical implementation. Due to the difficulty in the experimental observations, these atomistic mechanisms are still open questions.

We addressed such issues with well-optimised first-principles calculations. Regarding the CeO₂/Pt particle/H₂O catalytic interface, we found the electron transfer between the oxide and the metal cluster, basicity of the CeO₂ surface, and the fast proton/hydroxide transfer upon the oxide interface [1]. The observed atomistic mechanism gives an insight into the catalytic reactions upon the oxide materials.

For the battery field, we have examined microscopic origins of the interfacial resistance

(e.g. space-charge layer model, reaction layer model) as well as the buffer layer effect in solid-state batteries (SSBs) by using first-principles DFT+U calculations [2]. As a representative model system, LiCoO₂ (LCO), β -Li₃PS₄ (LPS), and LiNbO₃ (LNO) were selected for cathode, sulfide electrolyte, and buffer layer, respectively. We carried out first-principles calculations of the several possible interface configurations and obtained the stable structures and the electronic states. Besides, we calculated the site-dependent Li chemical potentials with respect to Li metal. The results indicate that the Li depletion can proceed at the beginning of the charge process, which may correspond to the space-charge layer scenario, and the interposition of buffer layer can suppress the depletion. Furthermore, we evaluated the interfacial ion diffusion by examining possible exchange of cations between the cathode and the electrolyte. The results show that the Co and P exchange is preferred at the LCO/LPS interface, and the LNO interposition can suppress these mixings

(Fig.1). Interestingly, the Li-depletion tendency still exists under these circumstances [2]. Therefore, the Li-depletion is likely to be a major factor of the interfacial resistance. These aspects would be useful for future improvement of the interfacial resistance of SSBs

We are keeping intensive collaborations with the experimentalists as well as the industries, and solving crucial issues for fundamental science and industrial application on the atomic scale. In the near future, our computational researches may play a decisive role in the transformation of energy management in our society.

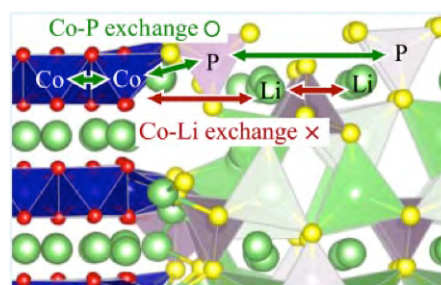


Fig. 1: Schematic picture of cation exchange at the LCO cathode / LPS electrolyte interface. The Co-P exchange turns out to be energetically preferable.

References

- [1] M. F. Camellone, F. N. Ribeiro, L. Szabova, Y. Tateyama, S. Fabris, *J. Am Chem. Soc.* **138**, 11560-11567 (2016).
- [2] J. Haruyama, K. Sodeyama, Y. Tateyama, *ACS Appl. Mater. Interfaces*, **9** 286-292 (2017).

First-principles calculations of iron solid solution effects on the lattice thermal conductivity of lower mantle minerals

Haruhiko DEKURA

Geodynamics Research Center

Ehime University, 2-5 Bunkyo-cho, Matsuyama 790-8577, Japan

Iron-bearing Bridgmanite (Mg,Fe)SiO₃ would be the most constituent mineral in the earth's lower mantle. Determination of the phonon transport property, *i.e.*, lattice thermal conductivity (κ), of the material should be therefore a key to understanding the dynamics and evolution of the earth's deep interior. Lattice anharmonicity owing to the phonon-phonon interaction strongly relates the phonon transport. The primary purpose of this project in this period is to determine the anharmonic properties of the iron-bearing system at deep mantle pressure conditions.

We have performed density-functional theoretic calculations combined with the LDA+*U* method [1] and have extracted the large number of harmonic and anharmonic force constants (AFC) by numerical derivatives of the adiabatic potential surface [2]. The simulation cell of (Mg_{0.9375},Fe²⁺_{0.0625})SiO₃ that includes totally 160 atoms was adopted in this study. The ferrous iron was treated in the high spin state ($S = 2$). Since the crystal point group symmetry is broken associated with the

incorporation of the iron atoms as impurities into the system, the number of SCF calculations is enormous (more than 10,000). The use of the supercomputers in ISSP allowed us to deal with it.

During this period, by the use of supercomputer (system B), we have finished the determination of the 3rd order AFC at 100 GPa relevant to an earth's lowermost mantle condition. Using the calculated force tensors, we have solved the phonon Boltzmann transport equation and have succeeded in describing κ at temperatures ranging from 300 K to 4000 K [3]. To the best of our knowledge, this is the first time to predict solid solution effects on κ of Fe-bearing lower mantle minerals by fully *ab initio* calculations.

References

- [1] T. Tsuchiya and X. Wang: *J. Geophys. Res.* **118** 83 (2013).
- [2] H. Dekura and T. Tsuchiya, *Phys. Rev. B* **95**, 184303 (2017).
- [3] H. Dekura and T. Tsuchiya, *in prep* (2017).

First-principles study of quantum transport in nanostructures

NOBUHIKO KOBAYASHI

Institute of Applied Physics, University of Tsukuba

1-1-1 Tennodai Tsukuba Ibaraki 305-8573

1 Introduction

The aim of this project is to reveal charge, heat and spin transport in materials from first-principles. Quantum nature is essential in nanoscale systems, and atomistic analysis based on detailed electronic states calculations are indispensable to discuss the transport property. In order to analyze transport properties, we have developed the nonequilibrium Green's function (NEGF) method, and the time dependent wave-packet diffusion (TD-WPD) method. Using these methods, we have investigated charge, heat and spin transport properties of materials.

2 Charge Transport

The recent progress in the fabrication technology of organic single-crystal semiconductors and thin-film field-effect transistors with very high carrier mobility up to $40 \text{ cm}^2/\text{Vs}$ requires us to elucidate the mechanisms of carrier transport in organic semiconductors, which are assemblies of p-conjugate molecules weakly bonded by van der Waals interactions. Observations of the crossover from the hopping transport of localized carriers to bandlike transport with a diffusive nature are expected to provide us with clues allowing us to reveal the carrier transport mechanisms.

We studied the carrier coherence factor α and the thermally induced fluctuations of transfer energies with neighboring molecules. The thermal fluctuation effects of molecular motion have been discussed for transport properties of organic semiconductors. We analyzed numerical data of transfer energy fluctuations of pentacene at various temperatures and pres-

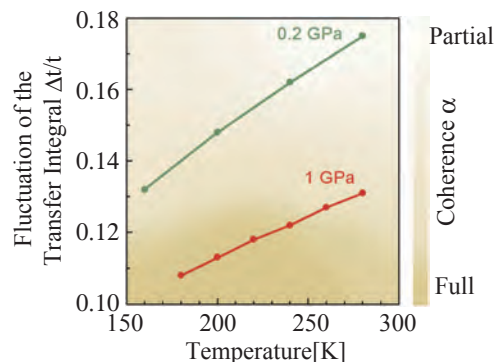


Figure 1: Reduction of the relative thermal fluctuation $\Delta t/t$ of the transfer integral at high pressure and low temperature for pentacene. [1]

ures. We showed that the value of $\Delta t/t$ is approximately 20% at room temperature, and that the effect of thermal fluctuations is significant and therefore reduces the electronic coherence. Moreover, plotting the temperature dependence of $\Delta t/t$, we showed that the value rapidly decreases towards 10%, which is favorable for the emergence of coherent electronic states. These calculations show that reducing the dynamic disorder resulting from thermal fluctuations is important to observe coherent charge transport. Thus, synthesizing molecules with steric hindrance is crucial to achieving full coherence under ambient conditions. [1]

3 Thermoelectricity

Highly efficient thermoelectric materials have been attracting much attention because of their potential applications, especially for energy harvesting by waste heat. A challenge is to improve the relatively low conversion ef-

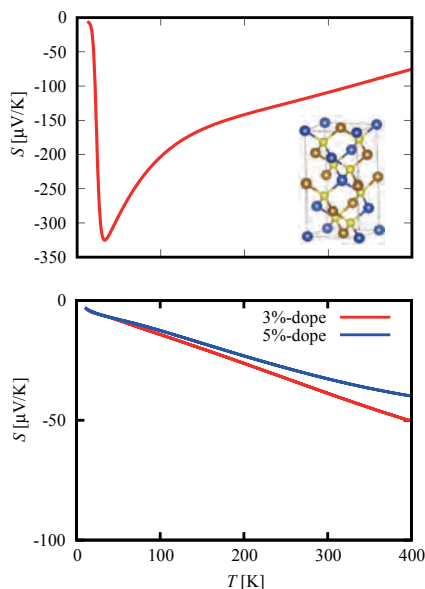


Figure 2: The Seebeck coefficients of CuFeS2 and the doped systems. [2]

efficiency, which is a function of the figure of merit $ZT = \sigma S^2 T / \kappa$. It is difficult to simply enhance ZT because of the typical trade-off between the Seebeck coefficient and electrical conductivity, and a material that should conduct electricity well, without conducting heat, is also somewhat paradoxical.

We analyze the thermoelectric properties of a magnetic semiconductor CuFeS2 based on density functional theory. We reproduce the Seebeck coefficient of CuFeS2, such as a peak structure at a low temperature and weak temperature dependence around room temperature, and elucidated the mechanism of the high performance thermoelectric material. Furthermore, we discuss the temperature dependence of the doped systems.[2]

4 O(N) Method

We developed the O(N) TD-WPD method for the quantum transport calculation of huge systems of up to 100 million atoms a decade or so ago. We calculated the conductance and the mobility of the system with micron-order lengths at room temperature based on the Kubo-Greenwood formula. Using this method we can study the transport properties from diffusive to ballistic regimes including the effect of realistic electron-phonon scattering, and determine the mean free path and relaxation time

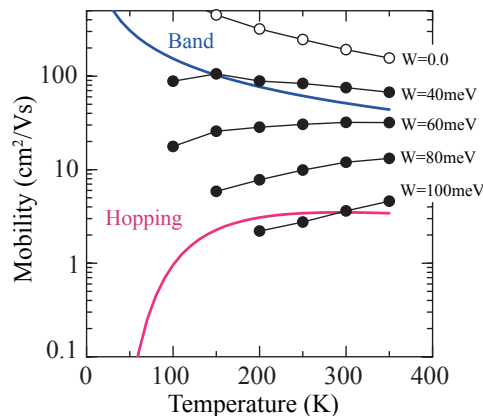


Figure 3: Calculated mobility of a rubrene single crystal along the a axis as a function of temperature for several magnitudes of static disorder W . [3]

from an atomistic viewpoint. We performed DFT calculations of electronic structures and interactions between molecules of pentacene and rubrene single-crystal organic semiconductors including the effect of the van der Waals interaction, and applied the TD-WPD method to the analysis of transport properties of the organic semiconductors.

We have studied charge transport using the TD-WPD method with maximally localized Wannier functions based on density functional theory including van der Waals interactions. The strong electron-phonon interactions due to thermal fluctuation are appropriately included as intrinsic effects. We analyzed the transport properties of pentacene and rubrene single crystals. We also find the temperature-dependent behavior from bandlike to thermally activated behavior due to extrinsic disorder effects, which correspond to experimental observations.

References

- [1] K. Sakai, Y. Okada, T. Uemura, J. Tsurumi, R. Hausermann, H. Matsui, T. Fukami, H. Ishii, N. Kobayashi, K. Hirose and J. Takeya, *NPG Asia Materials*, 8, e252 (2016).
- [2] H. Takaki, K. Kobayashi, M. Shimono, N. Kobayashi, K. Hirose, N. Tsujii, T. Mori, *Appl. Phys. Lett.* 110, 072107 (2017)
- [3] H. Ishii, N. Kobayashi, K. Hirose, *Phys. Rev. B* 95, 035433 (2017)

Theoretical Analyses on Ionic Transport Properties, Electrical Properties and Interfacial Electronic States of Nanostructures

Satoshi WATANABE

*Department of Materials Engineering, the University of Tokyo
7-3-1 Hongo, Bunkyo-ku, Tokyo, 113-8656*

1 Introduction

For designing and controlling novel nanoscale information and energy devices, our understanding is still insufficient especially on complicated situations and phenomena at nanoscale, such as the effects of interface between novel two-dimensional materials and substrates and ionic transport in metal-oxide heterostructures.

So we have been performing theoretical analyses on these topics based on atomic/electronic level simulations (mainly based on density functional theory (DFT)), taking various nanostructures as target systems. In the followings, some of our results in the fiscal year 2016 are described.

2 Electric field effects in organic molecular layers

Organic semiconductors have attracted increasing attention as promising materials for electronic devices. In α - ω -dihexyl sexithiophene (DH6T) crystal, one of the most famous molecules for organic semiconductor, fluorescence-yield X-ray adsorption spectra (FY-XAS) have taken under the external electric fields [1].

To understand the electric field effects seen in the observed spectra, we have performed theoretical analysis based on DFT calculations (using Quantum-Espresso package) [2].

Comparing the results with/without electronic fields, we have found that the change of total density of states (DOS) is similar to the projected DOS at the hexyl group in DH6T layer. This means that the charge polarization induced by the electric field is mainly localized at the hexyl group in the DH6T molecule, which is in good agreement with the experiment [1]. We conclude that the external electric field is strongly screened by the hexyl group which makes the changes in the electronic state in the thiophene backbone negligible.

3 Search for relevant 2D substrates for Germanene and stanene

Germanene and stanene have attracted much attention recently and have been synthesized on several substrates like Al(111), Au(111) and Pt(111). However, they still lack suitable semi-conducting substrates that can preserve their fascinating electronic properties and topology.

We have explored such substrates by using the combination of DFT calculations (using Quantum-Espresso package) and data mining of Inorganic Crystal Structure Database [3]. We have found several candidates including some of the CdI₂-type materials, CuI, and GaGeTe. All of them can preserve the quasi-free-standing geometry, stability and band structure of germanene or stanene. Among them, CdI₂ and ZnI₂ can open a band gap of 0.16-0.18 eV in germanene, larger than

all 2D substrates previously found manually, while preserving Dirac-cone-like band structures. The mobility of supported germanene is as high as $1-8 \times 10^5 \text{ cm}^2/\text{Vs}$. Moreover, the Z_2 invariants of germanene on CuI and stanene on CaI_2 are found to be non-trivial. In addition, from the analysis of germanene on substrates based on a low-energy tight-binding Hamiltonian, strong linear correlations are found among the effective electric field, external Rashba coefficient and charge transfer.

4 Li Diffusion in amorphous Li_3PO_4

Deeper understand on atom diffusion is necessary for further development of some of novel information and energy devices. Simulations based on DFT are powerful for this, but are computationally very heavy for certain systems such as amorphous materials. So we have explored the applicability of neural network potentials (NNP), a recently developed machine learning technique, to studying atom diffusion in amorphous materials, using Li_3PO_4 as a benchmark system [4].

We adopted the NNP proposed by Behler and Parrinello [5], and used about 17,000 Li_3PO_4 structures and corresponding DFT energies (calculated using VAPS package) to train our NNP, and 28,000 structures as independent testing data. The residual mean square error (RMSE) of NNP is 7.6 meV/atom for the training dataset and 6.5 meV/atom for the testing dataset.

Our NNP can reproduce the DFT results of Li atom diffusion paths, barrier energies, diffusion coefficients and effective activation energies in amorphous- Li_3PO_4 . For example, the average barrier energies are 0.58 eV and 0.56 eV in the DFT and NNP calculations, respectively, and the mean absolute error of barrier energy prediction is 0.05 eV. We would like to note that the calculation speed of NNP is about 3 to 4 orders of magnitude faster than DFT.

References

- [1] H.S. Kato, H. Yamane, N. Kosugi and M. Kawai: Phys. Rev. Lett. **107** (2011) 147401.
- [2] T. Moriya, E. Minamitani and S. Watanabe: in preparation.
- [3] Z. Ni, E. Minamitani, Y. Ando and S. Watanabe: submitted to Phys. Rev. B.
- [4] W. Li, Y. Ando, E. Minamitani and S. Watanabe: in preparation.
- [5] J. Behler and M. Parrinello: Phys. Rev. Lett. **98** (2007) 146401.

First Principles Calculations of Muon and Positron in Solids

Mineo SAITO

Institute of Science and Technology, Kanazawa University

Kakuma, Kanazawa, 920-1192 Japan

Recently, the spin polarized positron annihilation experiment attracted scientific interests because it provides useful information on electron spin polarization. We study the momentum densities of the ferromagnet Fe. The two dimensional momentum densities of majority and minority spins are found to have strong anisotropy, i.e., the momentum densities on the Σ line are larger than those on the Δ line. We analyze the origin of this anisotropy based on the group theory. For this purpose, we develop a code that can identify irreducible representations of spin-polarized bands. We find that the number of the totally symmetric bands on the Σ line are larger than those on the Δ line. We conclude that this difference in the number of the totally symmetric bands is the origin of the fact that the momentum densities on the Σ line are larger than those on the Δ line since only the totally symmetric bands contribute to the momentum densities. The difference in the number is due to the fact that the symmetry on the Σ line (C_{2v}) is lower than that on the Δ line (C_{4v}).

We next study the one dimensional momentum density distribution. The distribution of the majority spin is found to be broader than

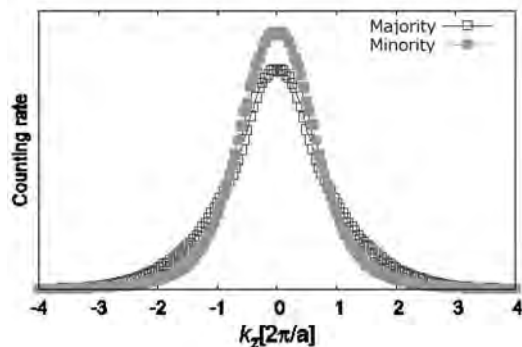


Fig. 1 One dimensional momentum density in Fe

that of the minority spin (Fig. 1). This difference between the two spins is expected to be due to the fact that the distribution in space in the majority spin is narrower than that of the minority spin.

We also study muon in GaN. A paramagnetic neutral muonium was observed and the hyperfine structure was found to show strong anisotropy [1]. We find that the Fermi contact term is small compared with the cases of Si and GaAs and the dipole term induces the anisotropy.

[1] K. Shimomura et al., Phys. Rev. Lett., 92,135505 (2004).

Exploration of structure motifs characterizing metal oxides

Kazuto AKAGI

WPI-Advanced Institute for Materials Research,

Tohoku University, Katahira, Aoba-ku, Sendai, Miyagi 980-8577

We continued the exploration of key structural motifs in metal oxides leading to their properties as preparation for data driven approach.

Polaron and hydrogen in a-HfO₂

Hafnium oxide is a high dielectric constant material used as a gate insulator in modern transistors. However, charge trapping centers in its complicated amorphous structure degrades the electrical performance. Therefore, in-depth understanding of the electronic structure of this material is needed. The molecular dynamics calculations were performed in both the classical and first-principles ways to model the amorphous structures hosting different defects. Screened hybrid functional (HSE06) was used to investigate the geometrical and electronic structures.

First, it turned out that extra electron/holes in the amorphous hafnium oxides (a-HfO₂) can be trapped spontaneously on intrinsic structural precursors like longer Hf-O bonds or under-coordinated atoms. Electrons can get trapped in deep states in the gap. These results show deep polaron in amorphous oxides are inherent and do not require any bond rupture to form

precursor sites [1].

The interaction of hydrogen atom (H) in a-HfO₂ was also investigated. Hydrogen in many wide gap crystalline oxides exhibits negative-U behavior with the +1 or -1 charge states lower in energy for all Fermi-level positions. The obtained results demonstrate that hydrogen in a-HfO₂ also gives negative-U feature, with charged states being the most thermodynamically stable at all Fermi level positions. However, a metastable atomic hydrogen can share an electron with intrinsic electron trapping precursor sites forming a [$e^-_{tr} + O-H$] center, which is lower in energy on average by about 0.2 eV. These electron-trapping sites can affect both the kinetics and thermodynamics of the interaction of hydrogen with a-HfO₂ and the electrical behaviour of amorphous hafnia films in CMOS devices.

Shallow Acceptor Level in Rh:SrTiO₃

Photocatalytic water splitting uses sunlight to produce hydrogen from water. Rh-doped SrTiO₃ (Rh:SrTiO₃) has the potential for visible-light water splitting due to the formation of in-gap states. It is known that the valence state of Rh can be changed between +4 and +3,

and only Rh^{3+} provides photocatalytic activity [2]. The photo-carrier lifetime measurement found $\text{Rh}^{3+}:\text{SrTiO}_3$ has a longer carrier lifetime of about 10ps, which indicates there must be an impurity level close to the conduction band bottom, forming a shallow acceptor level. Since the valence state of Rh can be controlled by the introduction of oxygen vacancies (V_o) into $\text{Rh}:\text{SrTiO}_3$, the interaction between V_o and Rh must play an important role in the electronic structure change.

We systematically performed first-principles calculations to search for the origin of this shallow acceptor level considering the various configurations between V_o and Rh dopant. The hybrid-functional (HSE06) was necessary to reproduce experimental band gap and a $4 \times 4 \times 4$ SrTiO_3 unit cell was used. The obtained results show that Rh exists in +3 state and there is no impurity level near conduction minimum as far as Rh and V_o are in the separate configuration. While Rh located next to V_o can be further reduced to +2/+1 states and this $\text{Rh}^{3+}-\text{V}_\text{o}$ complex results in a gap state within 1eV below

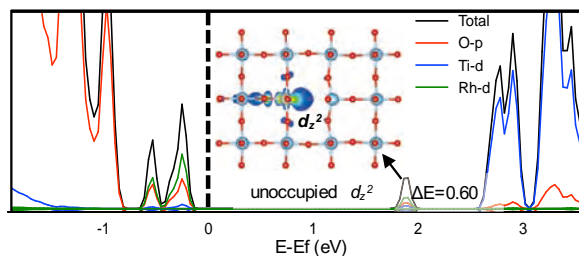


Fig. 1: DOS of the $\text{Rh}^{3+}-\text{V}_\text{o}$ complex and wave-function character of the corresponding shallow acceptor level.

conduction band minimum. The origin of this shallow acceptor level was unoccupied d_{z^2} orbital of Rh (Fig. 1). These results can be well interpreted by the octahedral crystal field theory.

Li_2O_2 formation in a Li-O₂ battery

Li-Air battery is one of the candidates for next generation batteries. Control of the Li_2O_2 formation during discharge is necessary to improve the energy density. It is believed that LiO_2 is formed first and converted to $\text{Li}_2\text{O}_2 + \text{O}_2$ by self-redox reaction, but even the size dependence has not been clarified.

In order to elucidate it, ab initio random structure search (AIRSS) method developed by C. J. Pickard and implemented to CASTEP was applied to form many Li_nO_{2n} ($n=3$ to 10) clusters in vacuum (*e.g.* 1,000 samples for $n=8$) and self-redox events were statistically analyzed. There was no critical threshold for n , but the ratio of O_2^{2-} becomes dominant at $n \geq 9$. Spatial distribution of Li_2O_2 domain seems to be inhomogeneous, but further analysis is ongoing.

References

- [1] M. Kaviani, J. Strand, V. V. Afanas'ev, A. Sluger, Phys. Rev. B, **94**, 020103(R) (2016).
- [2] R. Kosta, T. Ishii, H. Kato, and A. Kudo, J. Phys. Chem. B **108**, 8992 (2004).

First-Principles Study of Excited Electron Dynamics of Nanostructures and Positron States at Surfaces

Kazuyuki WATANABE, Yasumitsu SUZUKI, Elena SILAEVA, Satoshi HAGIWARA, Yoshihiro UEDA, Kazuki UCHIDA, Hironari MIYAUCHI, Shota MIYAUCHI, Daisuke IWASAKI

Department of Physics, Tokyo University of Science

1-3 Kagurazaka, Shinjuku-ku, Tokyo 162-8601

In the project we investigated the following six topics this year. 1) Secondary electron emission from nanographene, 2) electron transmission through bilayer graphene (BLG), 3) electron excitation and emission from a nanoribbon under pulsed laser irradiation, 4) dielectric functions of carbon nanotubes with adsorbed water, 5) Bohmian mechanics in the exact factorization of electron-nuclear wave functions, and 6) positron states at Li- and O-adsorbed Fe(001) ferromagnetic surfaces by two-component density functional theory (TCDFT).

1) *Secondary electron emission from nanographene* [1]: We have observed secondary electron emission (SEE) from nanosurface by home-made time-dependent density functional theory (TDDFT) code, KENS. We obtained the incident-electron energy dependence and bilayer effect on the amount of secondary electron (SE) about finite-size graphene flakes. The dynamics of SEE and collective density oscillations, which are electronic excitations induced by electron impact and have a frequency specific to the target graphene flake, were demonstrated numerically. The dynamics of SEE from graphene flakes were also elucidated by the time-dependent occupation numbers of the Kohn-Sham electronic levels, which show consistency with typical properties observed in experiments. We also obtained k-resolved energy spectrum of SEs from various atomic sheets, which are

infinite and periodic systems, and revealed relationship between band structure, electron excitation, and SEE. The calculations have been performed using System B.

2) *Electron transmission through bilayer graphene* [2]: We investigated electron scattering by AA-stacked and AB-stacked BLG using KENS code, and obtained energy-dependent transmittances that exhibit an unexpected crossing. The crossing behavior is successfully interpreted using the diffraction intensity distribution of single-layer graphene (SLG). Importantly, the crossing behavior holds for simulated BLG with reduced or increased layer distances compared with the real graphite gap. The present study not only revealed the close relationship between BLG transmittance and SLG diffraction for low-energy electron scattering but also provides relevant knowledge that will be useful for various surface analysis techniques based on electron scattering spectroscopy. The calculations have been performed using System B.

3) *Electron excitation and emission from a nanoribbon under pulsed laser irradiation* [3]: TDDFT simulations of laser-assisted electron excitation and emission from a SiNR were conducted, and the energy spectrum of emitted electrons was obtained. The energy spectrum in the low and intermediate energy regions was successfully interpreted by the excitation dynamics of one-photon and two-photon absorption and by that of multiphoton absorption,

respectively. The calculations have been performed using System B.

4) *Dielectric functions of carbon nanotubes with adsorbed water* [4]: We studied the optical properties of carbon nanotubes (CNTs) with adsorbed water by calculating the dielectric functions of CNTs following water adsorption using density functional theory and random phase approximation. Our calculations reproduced the redshifts of the peak position in the absorption spectrum that were reported in recent experimental studies. We demonstrated that they can be attributed to decreases in the band gaps, which result from electronic coupling between the CNTs and the water molecules. We also performed the calculations based on the many-body perturbation theory, i.e., the GW method and Bethe-Salpeter equation, to take into account the screening and excitonic effects. All calculations were performed with ABINIT code in System B.

5) *Bohmian mechanics in the exact factorization of electron-nuclear wave functions* [5]: The exact factorization theory allows us to define the time-dependent potential energy surfaces (TDPEs) that are responsible for the correlated electron-nuclear dynamics. We are developing a novel first-principle non-adiabatic molecular dynamics simulation method based on the TDPEs. We studied whether the propagation of multiple classical trajectories can reproduce the quantum nuclear motion in strong-field processes when their motions are governed by the quantum Hamilton-Jacobi equation derived by applying Bohmian mechanics to the exact factorization theory. We demonstrated that multiple classical trajectories propagated by the force from the gradient of the exact TDPEs plus the Bohmian quantum potential can reproduce the strong-field dissociation dynamics of a one-dimensional model of the hydrogen molecular ion. The preliminary calculations that required a lot of memory were performed using System B.

6) *Positron states at Li- and O-adsorbed*

Fe(001) ferromagnetic surfaces studied by TCDFDFT [6]: We investigated the positron states for a ferromagnetic Fe(001) surface with and without Li and O adsorption by using TCDFDFT, and we determined annihilation life time τ , binding energies, and the change in the electron work function. τ is found to be sensitive to changes in the electron and positron density distributions, which are induced by adatoms. The spin-polarization fraction at Li- and O-adsorbed Fe(001) surfaces, which are estimated by τ is in good agreement with that at the topmost surfaces obtained by using DFT. Thus, positron density distributions, which are localized around the topmost surface, capture the information of spin states at the topmost surface. Since τ is sensitive to the surface electronic states and spins, spin-polarized positron annihilation spectroscopy can be an important tool for detecting surface magnetization. The calculations have been performed using System B.

References

- [1] Y. Ueda, Y. Suzuki, and K. Watanabe, Phys. Rev. B **94**, 035403 (2016).
- [2] H. Miyauchi, Y. Ueda, Y. Suzuki, and K. Watanabe, Phys. Rev. B **95**, 125425 (2017).
- [3] S. Miyauchi and K. Watanabe, J. Phys. Soc. Jpn **86**, 035003 (2017).
- [4] D. Iwasaki, Y. Suzuki, and K. Watanabe, Appl. Phys. Express **10**, 045101 (2017).
- [5] Y. Suzuki and K. Watanabe, Phys. Rev. A **94**, 032517 (2016).
- [6] S. Hagiwara and K. Watanabe, J. Phys. Soc. Jpn **85**, 114703 (2016).

First-principles study of anomalous thermoelectric effect

Fumiyuki ISHII, Yo Pierre MIZUTA, Hikaru SAWAHATA

*Faculty of Mathematics and Physics, Institute of Science and Engineering,
Kanazawa University, Kanazawa, 920-1192, Japan*

The Berry curvature, a geometric quantity associated with electronic Bloch states of crystalline materials, is one of the key ingredients of various transport phenomena. For example, the behavior of the anomalous Hall effect (AHE) and anomalous Nernst effect (ANE) is sensitively determined by the landscape of Berry curvature in reciprocal space.

The ANE, which is closely related to AHE, is a thermoelectric (TE) effect that generates electric current transversely to the applied temperature gradient.

Our aim is to find or design materials with large ANE, which could be useful in the future realization of highly efficient conversion of waste heat into electric power. As candidate systems that promisingly realize such TE conversion, we have investigated two classes of materials, namely (i) and (ii) described below, in each of which an effective magnetic field that induces AHE and ANE essentially stems from spin-orbit coupling or non-coplanar magnetic configuration.

(i) **(Coplanar) magnetic Heusler alloys** (real systems) :

There have been several studies on Heusler compounds in which time-reversal symmetry is broken due to magnetic order, often resulting in a very large AHE [1]. Since large ANE can be expected as well in such systems if the conductivity of AHE has a strong dependence on Fermi energy, we aim to study the ANE of these compounds as promising candidates for Berry-curvature-driven good TE materials.

In preparation for future investigations in such direction, we have clarified the fundamental electronic structure from first-principles using an open-source package OpenMX [2], choosing some of the Co-based Heusler systems.

(ii) **Non-coplanar magnetic structures** (model systems):

Motivated by a previous report of large AHE in a model of *Skymion crystal* phase [3], one of non-coplanar magnetic configurations, we studied a similar model from **first-principles**. The procedure was as follows:

1. The electronic structure calculations with OpenMX [2], which supports the assumption of arbitrary magnetic configurations.
2. Identification of *Chern number*=(Band-resolved integration of Berry curvature) characterizing the geometric nature of each band, with our own implementation of a lattice gauge theoretical formalism [4].
3. Construction of a set of Wannier basis via Wannier90 [5] from the Bloch states obtained in the first step.
4. Evaluation of all the transport quantities of interest in the Wannier representation via postprocessing modules of Wannier90 package [6, 7] and some additional integration to evaluate ANE.

In the above procedure, a set of Wannier orbitals was successfully constructed from a large

number of electronic Bloch bands via Wannier90 [5], by exploiting the big memory size of the ISSP Supercomputer for storing large matrices. Subsequent evaluation of the conductivity of AHE from the Wannier orbitals, which required lots of sampling points for integration, was efficiently performed by making use of massive parallelization of the Supercomputer.

These computations revealed a surprisingly large ANE due to the peculiar geometric character of the electronic bands[8]. The variation of such behavior with respect to the magnetic configuration was also examined, which illuminated the uniqueness of the particular configuration of Skyrmion [9].

We hope that our above-described first-principles methods will be widely applied in quest for real materials that realize such noticeable TE effect.

nano-spin conversion science & quantum spin dynamics, Tokyo, Oct. 14, 2016.

References

- [1] J-C. Tung and G-Y. Guo, *New J. Phys.* **15** (2013) 033014.
- [2] T. Ozaki *et al.*, <http://www.openmx-square.org/>
- [3] K. Hamamoto, M. Ezawa, and N. Nagaosa, *Phys. Rev. B* **92** (2015) 115417.
- [4] T. Fukui, Y. Hatsugai, and H. Suzuki, *J. Phys. Soc. Jpn.* **74** (2005) 1674.
- [5] A.A. Mostofi *et al.*, *Comput. Phys. Commun.* **185** (2014) 2309.
- [6] X. Wang *et al.*, *Phys. Rev. B* **74** (2006) 195118.
- [7] G. Pizzi *et al.* , *Comput. Phys. Commun.* **185** (2014) 422.
- [8] Y.P. Mizuta and F. Ishii, *Sci. Rep.* **6** (2016) 28076.
- [9] H. Sawahata, Y.P. Mizuta, and F. Ishii, Poster Q-22, International workshop on

First-principles calculations of oxide thin-films and heterostructures

Fumiyuki ISHII, Yo Pierre MIZUTA, Hikaru SAWAHATA, Naoya YAMAGUCHI
*Faculty of Mathematics and Physics, Institute of Science and Engineering,
 Kanazawa University, Kanazawa, 920-1192, Japan*

Oxides-based thin films and heterostructures are an attractive playground for both basic and applied sciences because of the rich physics that can be manipulated by nano-engineering their structures.

One example is the thermoelectric (TE) effect: The heat-to-electricity conversion efficiency could be better in two-dimensional(2D) systems such as oxide films compared to 3D bulk [1]. The other example is inverse Rashba-Edelstein effect[2]: The spin-to-charge current conversion at interface of oxide and non-magnetic metals[3].

In the context of magnetism, a whirling magnetic configuration called *Skymion crystal* is considered to be more stabilized in 2D than in 3D, which can drive a TE effect named the anomalous Nernst effect (ANE). The ANE is a thermoelectric (TE) effect that generates electric current transversely to the applied temperature gradient due to non-zero *Berry curvature* reflecting the magnetic configuration.

Our idea is, by combining these two, to explore the TE behavior of 2D oxide films when the electrons therein form Skymions. As specific ingredients that connect the TE effects and magnetic Skymions, we focused on the anomalous Hall effect (AHE) and the related anomalous Nernst effect (ANE), which are among the transverse transport phenomena arising due to non-zero *Berry curvature*, which in turn, can originate from non-coplanar magnetic structures such as Skymion crystal.

We chose EuO as a target material, since

the appearance of Skymion-like state has been experimentally implied there [4]. More specifically, what we considered is a monolayer of EuO on which Skymion crystal is formed by unit Skymion composed of 4×4 Eu atoms with $S = 7/2$ electronic spin on each.

Firstly, we computed its self-consistent electronic states via OpenMX [5]. Secondly, the geometric (topological) character of each of the obtained bands was analyzed by band-resolved integration of Berry curvature (= *Chern number*) via our implementation of the formalism of Ref. [6, 7]. Thirdly, a set of hundreds of Wannier orbitals was constructed via Wannier90 [8] from the states obtained in the first step, and all the transport quantities of interest were evaluated in the Wannier representation via postprocessing modules of Wannier90 package [9, 10].

In the above procedure, the big memory size of the ISSP Supercomputer was exploited for storing large matrices associated with large number of relevant bands, and the massive parallelization of the computer was essential for the evaluation of ANE, which required a lot of sampling points for integration.

Our study showed the presence of a substantial strength of Berry curvature in the lowest conduction bands, which is reflected in a large ANE when the carriers are doped into those bands. Furthermore, the ANE and the conventional longitudinal Seebeck effect added up constructively to make the transverse TE voltage even larger. This situation, if realized,

would be very beneficial for efficient TE conversion. As a future task, we need to identify energetically stable Skyrmion crystals, unlikely to the present one, which is higher in energy as compared to ferromagnetic state as found in our calculations.

In addition to ANE in magnetic skyrmion, we have studied spin-orbit coupling parameters and spin structures in momentum space (effective magnetic field in momentum space) at the Bismuth surface alloys[11] and interfaces for several oxide systems, such as interfaces of $\text{Bi}_2\text{O}_3/(\text{Cu}, \text{Ag}, \text{Au})$. We have focused on Rashba effect and investigated its parameters and the spin structure. We have estimated Rashba coefficients α_R for $\text{Bi}_2\text{O}_3/(\text{Cu}, \text{Ag}, \text{Au})$ at 0.37-0.94, 0.48-0.75 and 0.39-0.67 in units of $\text{eV}\cdot\text{\AA}$ respectively, and investigated the sign of the Rashba spin splitting, analyzing spin textures in momentum space. We also discussed a trend of the Rashba parameters for interfaces of $\text{Bi}_2\text{O}_3/(\text{Cu}, \text{Ag}, \text{Au})$ compared to that for surface alloys of $\text{Bi}/(\text{Cu}, \text{Ag}, \text{Au})$ [11].

References

- [1] L. Hicks and M. Dresselhaus, Phys. Rev. B **47** (1993) 12727.
- [2] V.M. Edelstein, Solid State Commun. **73** (1990) 233.
- [3] Karube et al, Appl. Phys. Express **9** (2016) 033001.
- [4] Y. Ohuchi, Y. Kozuka, M. Uchida, K. Ueno, A. Tsukazaki, and M. Kawasaki, Phys. Rev. B **91** (2015), 245115.
- [5] T. Ozaki *et al.*, <http://www.openmx-square.org/>
- [6] T. Fukui, Y. Hatsugai, and H. Suzuki, J. Phys. Soc. Jpn.**74** (2005) 1674.
- [7] Y.P. Mizuta and F. Ishii, Sci. Rep. **6** (2016) 28076.

- [8] A.A. Mostofi *et al.*, Comput. Phys. Commun. **185** (2014) 2309.
- [9] X. Wang *et al.*, Phys. Rev. B **74** (2006) 195118.
- [10] G. Pizzi *et al.* , Comput. Phys. Commun. **185** (2014) 422.
- [11] N.Yamaguchi, H. Kotaka and F. Ishii, J. Cryst. Growth. *in press*, arXiv:160909782.

Atomic structure and electronic properties of metal/oxide interfaces

Hongping Li¹, Mitsuhiro Saito^{1,2}, Kazutoshi Inoue¹, Yuichi Ikuhara^{1,2}

¹*Advanced Institute for Materials Research, Tohoku University, Sendai, Miyagi, 980-8577*

²*Institute of Engineering Innovation, The University of Tokyo, Yayoi, Tokyo, 113-8656*

Metal/oxide hetero-interfaces are common and important in engineering devices. Their microstructure often plays a critical role in the macroscopic properties. To obtain atomic-scale understanding of the impact of buried interface behavior on electronic properties, it is of great importance to perform precise examinations of the local atomic structure and the detailed bonding characteristics at the metal/oxide interface. However, it is difficult to simply describe the nature of the interfacial bonding by a particular chemical bonding state due to their dissimilar electronic and crystal structures. In this work, we combined the high-resolution and scanning transmission electron microscopy with the first-principles DFT calculations to systematically investigate the atomic-scale structure and their bonding mechanism of the largely mismatched Pd/ZnO interface.

The molecular beam epitaxy method was applied to grow a thin film of Pd on both ZnO (0001) and ZnO (000 $\bar{1}$) surfaces and found a successful epitaxial growth between largely mismatched lattices (18%) [1]. The atomic model of the hetero-interface contained 968 atoms. The first-principles DFT calculations have been performed using the Vienna ab-initio simulation package (VASP). We applied the projector augmented-wave method with a plane wave cut-off energy of 400 eV. Geometry optimization was performed using the PBE functional with a $1 \times 1 \times 1$ Gamma point centered k-point grid. All atoms in the

supercells were fully optimized with respect to interatomic force tolerance of 1.0×10^{-4} eV/Å. By estimating the adhesion energies, it has been revealed that two different Zn-terminated interfaces are formed between Pd and polarized ZnO, and their large lattice misfit was accommodated periodically by the incoherent interface. Charge density analysis showed that effective chemical bonding was formed along the interface from covalent bonding to ionic bonding according to their site-dependent character. This study opened up a novel avenue to straightforward understanding of the largely mismatched metal/oxide heterointerfaces, which is particularly important in designing interface structure and properties, and uncovering the origin of interface-related phenomena [2].

References

- [1] M. Saito, T. Wagner, G. Richter, and M. Rühle, “High-resolution TEM investigation of structure and composition of polar Pd/ZnO interfaces”, *Phys. Rev. B*, 80, 134110 (2009).
- [2] H. Li, D. Yin, M. Saito, K. Inoue, C. Chen and Y. Ikuhara, “Atomic structure and electronic properties of metal/oxide interfaces”, (2017), preprint.

Theoretical Design for Topological Materials Based on First-Principles Simulation

Kunihiko YAMAUCHI

ISIR-SANKEN, Osaka University, Ibaraki, Osaka 567-0047

Topological matters are known as a new class of materials which exhibits quantum-Hall-like behavior. As aiming at finding novel topological insulators, we have explored the possibility to engineer the coupling of spin and valley physics in ferroelectric transition-metal oxide heterostructures. After we surveyed about hundred combinations between 5d element perovskite and ferroelectric host perovskite, we finally found $\text{BiAuO}_3/\text{BiAlO}_3$ combination as the best candidate material for the topological spin-valley ferroelectric system as shown in Figure 1.

In the wide energy gap of host BiAlO_3 , $\text{Au-}e_g$ orbital states forms the 2D graphene-like molecular-orbital bands with Dirac cone at the K point of the hexagonal Brillouin zone. Due to the ferroelectric ionic distortion, breaking of space-inversion leads to the spin splitting of the Dirac cone bands and results in the ideal spin-valley coupling both at the conduction and valence bands. We showed that the polar structural distortion is also responsible for a topological transition from a topological-insulating phase to a trivial band insulator. The spin-valley physics is influenced by the topological band inversion in a nontrivial way. When the valley-dependent spin polarization of both conduction and valence bands is preserved, a change of the Berry curvature and of spin-valley selection rules is predicted, leading to so-called spin-valley Hall effects.[1]

We have also studied theoretically Weyl semimetals in order to support ARPES experiments performed in Tohoku University. Trig-

onal tellurium crystalizes in the chiral crystal structure with infinite helical chains along the [001] axis. The chirality, *i.e.* lack of the mirror and inversion symmetries, allows the presence of the Weyl points at the symmetric points, such as the H point. By DFT computation, we successfully reproduced the electronic bandstructure which had been observed through ARPES measurement.[2]

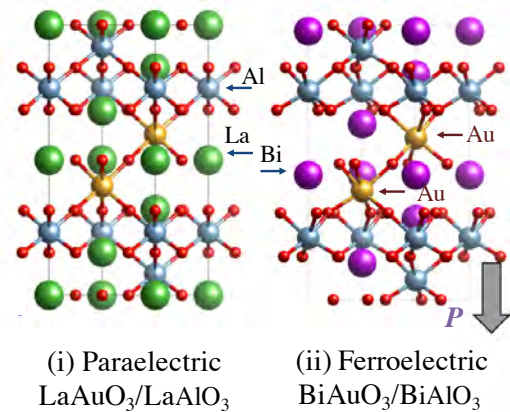


Figure 1: Theoretically designed ferroelectric topological oxide heterostructure.

References

- [1] K. Yamauchi, P. Barone, S. Picozzi, Phys. Rev. B **95**, 035146 (2017).
- [2] K. Nakayama, M. Kuno, K. Yamauchi, S. Souma, K. Sugawara, T. Oguchi, T. Sato, and T. Takahashi, Phys. Rev. B **95**, 125204 (2017).

The role of Ti interstitial in adsorption of O₂ on reduced rutile TiO₂ (110) surface

Kenji Yasuoka

Department of Mechanical Engineering,

Keio University, Kohoku, Yokohama, Kanagawa 223-8522

TiO₂(110), a wide-gap semiconductor, have attracted considerable attention due to its potential applications as solar cell, photocatalysis and biocompatible materials. Among many surface reactions, adsorption of O₂ was studied as a surface model reaction. It have been reported that reducing TiO₂(110) surface enhances O₂ absorption rate[1]. This change in absorption rate was explained by excess electrons. Until recent, surface bridging-oxygen vacancy was attributed main source of these excess electrons. However, recent experimental result suggested that subsurface Ti interstitial (Ti_{int}) is the main source of these

excess electrons [2]. The influence of excess electrons introduced by Ti_{int} for O₂ absorption is still an open question. In order to study the chemistry of this surface, we have performed ab initio molecular dynamics simulation (AIMD).

As a result of AIMD, we were able to obtain the spatial distribution of excess electrons. The change in the distribution by time is shown in Figure 1. Taking account the fact that excess electrons induce by magnetic moment of $\pm 1.0 \mu_B$, the location of excess electrons were analyzed using the magnetic moment. The vertical lines represent hopping of excess

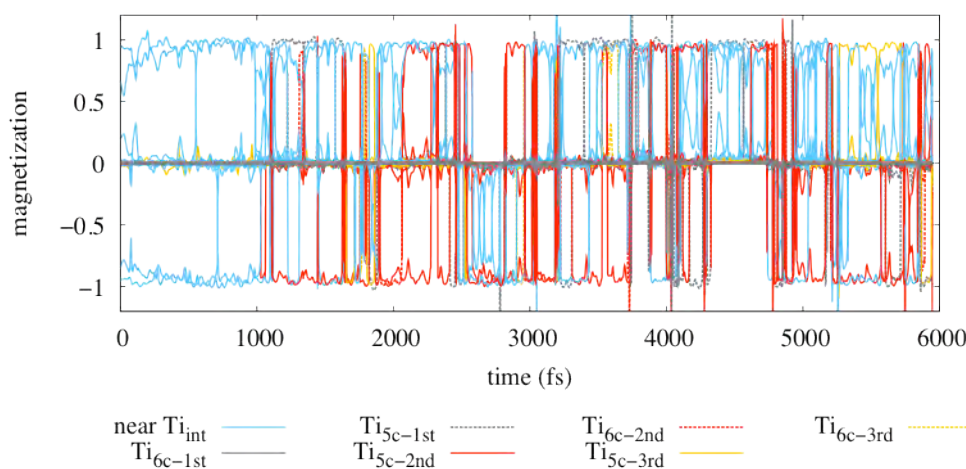


Figure 1: Change in the magnetic moment of a particular Ti site. Coloring is done by the group of Ti sites.

electrons, indicating that spontaneous excess electron hopping is occurring. Furthermore, excess electrons have shown stability in the near-surface region, suggesting that excess electrons introduced by Ti_{int} can contribute to the absorption of O_2 .

References

- [1] Y. Yoon, Y. Du, J. C. Garcia, Z. Zhu, Z. Wang, N. G. Petrik, G. A. Kimmel, Z. Dohnalek, M. A. Henderson, R. Rousseau, N. A. Deskins, and I. Lyubinetsky: *ChemPhysChem*. **16** (2015) 313-321.
- [2] S. Wendt, P. T. Sprunger, E. Lira, G. K. H. Madsen, Z. Li, J. Ø. Hansen, J. Matthiesen, A. Blekinge-Rasmussen, E. Lægsgaard, B. Hammer, and F. Besenbacher: *Science* **320** (2008) 1755.

Surface reactions of hydrogen and oxygen on oxide materials

WILSON AGERICO DIÑO

*Department of Applied Physics, Osaka University, Suita, Osaka 565-0871, Japan
Center for Atomic and Molecular Technologies Osaka University, Suita, Osaka 565-0871,
Japan*

*Joining and Welding Research Institute, Osaka University, Ibaraki, Osaka
567-0047, Japan*

We investigated oxygen ion migration in oxide materials using supercomputer system at ISSP.

Our original code “NANIWA” has allowed us to investigate various quantum states appeared in the reactions. In addition to electronic states, which can be calculated by conventional methods, NANIWA can simulate motions and stationary states of nuclei based on quantum theory. Therefore, this method is applicable to analyze quantum effects like tunneling, and has been successful to reveal reaction mechanisms in the atomic level.

Ceria based materials have been attracting considerable attention as a potential candidate for solid oxide fuel cells (SOFCs). Rare earth doping and lattice strain have been discussed as important factors to reduce the operating temperature of SOFC.

Oxygen ion migration in ceria based materials is essentially affected by covalent interactions resulting from the delocalization of

electrons to oxygen sites. We investigated migration barrier for oxygen ion in ceria-based materials using density functional theory based calculation with Hubbard U correction [1]. From our calculations, we emphasized that the treatment of 4f electrons with variable occupancy is crucial for describing the covalent interactions. Furthermore, we conducted quantum dynamics calculation for oxygen ion migration in Sm doped ceria using NANIWA. We identified 4% lattice compression of Sm doped ceria as the optimum for oxygen ion migration. Making use of the quantum effects in oxygen ion migration, we successfully achieved reduction of SOFC operation temperature from 600°C to 300°C.

References

- [1] M. Alaydrus, M. Sakaue, H. Kasai: Phys. Chem. Chem. Phys. 18 (2016) 12938.

Development and Application of Extended Ensemble Method Coupled with First-Principles Electronic Structure Calculations

Masaaki Araidai

*Institute of Materials and Systems for Sustainability, Nagoya University
Furo-cho, Chikusa-ku, Nagoya, 464-8603*

First-principles calculation method is a powerful tool to obtain electronic states and optimized atomic configurations in nanoscale. They have achieved many great successes for revealing experimentally inaccessible microscopic processes. In general, electronic states and optimized atomic configurations are calculated at zero temperature from a few initial guesses which can capture the nature of system of interest. Therefore, thermodynamical or statistical aspects of system are often missing in the first-principles electronic-states calculations. There are many physical and chemical phenomena induced by complex motion of a great number of atoms or molecules with charge transfer. Accordingly, free energy calculation method coupled with the first-principles electronic-states calculation method is essential for understanding those kinds of phenomena.

In this project, we developed multicanonical Monte Carlo (MUCA-MC) simulation code[1] coupled with VASP (Vienna ab-initio simulation package) code[2]. We refer to the code as MUCA-MC-VASP hereafter. In the code, the multicanonical weight is generated by the Wang-Landau algorithm[3].

Figure 1 shows the potential of mean force of

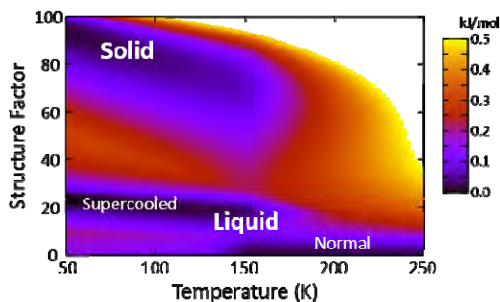


Fig.1 Potential of mean force of Lennard-Jones fluids.

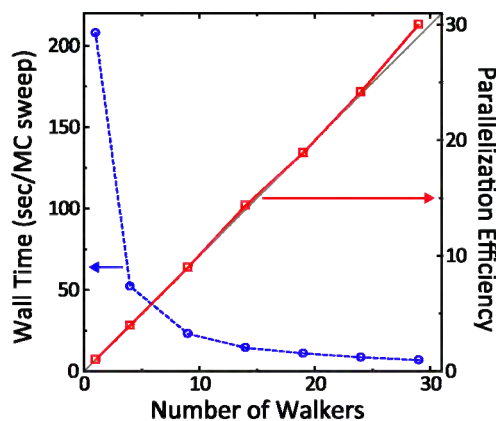


Fig.2 Wall time and parallelization efficiency of the developed code.

Lennard-Jones fluids. There are 108 argon atoms in the system. We are aiming at the reproduction of the results, using the MUCA-MC-VASP code. Figure 2 shows the wall time per one MC sweep (dotted line) and parallelization efficiency (solid line) as a function of the number of random walkers. The wall time is the average value over 500 MC sweeps. It is immediately obvious that our code possesses an excellent parallelization efficiency.

After the reproduction, we plan to apply the developed code to redox reaction at solid-gas interface, electrochemical reaction at solid-liquid interface, atomic diffusion process on surface, thermodynamical stability of matter, and so on.

This work was supported by Grants-in-Aid for Scientific Research (Grant No. 16K17551) from MEXT of Japan.

References

- [1] B. A. Berg and T. Neuhaus, Phys. Rev. Lett. **68**, 9 (1992).
- [2] G. Kresse and J. Hafner, Phys. Rev. B **47**, 558 (1993).
- [3] F. Wang and D. P. Landau, Phys. Rev. Lett. **86**, 2050 (2001).

Large-scale computational simulations of non-equilibrium transport phenomena

Yoshihiro Asai, Marius Bürkle, Jun-ichi Ozaki

*Research Center for Computational Design of Advanced Functional Materials,
National Institute of Advanced Industrial Science and Technology (AIST),
Central 2, Umezono 1-1-1, Tsukuba, Ibaraki 305-8568*

We have studied the following subjects in non-equilibrium transport in terms of large-scale computational simulations:

- 1-1) Transport calculations based on an order-N DFT method for large channel materials.
- 1-2) Phonon transport calculation based on the first-principles DFT theory.
- 1-3) Comparisons of first-principles transport calculations with conductance measurements using scanning tunneling microscope molecular break junction experiments.
- 2-1) Time-dependent density matrix renormalization group study of the electric conductance of strongly correlated Hubbard chain.

In the following we outline these subjects and give the main results:

- 1-1) Non-equilibrium Green's function (NEGF) techniques were combined with the order-N code CONQUEST for large scale transport calculations. The method has been applied to highly conducting polymers of length between

50 nm to 100 nm (Fig. 1). **[1. (Unpublished)]**

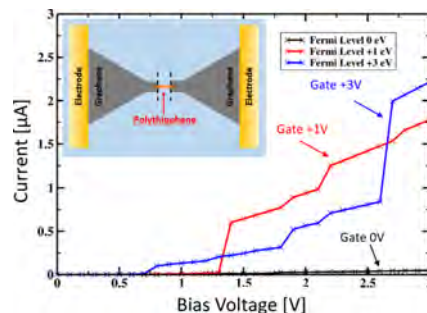


Fig. 1 Calculated I/V for different gate voltages

- 1-2) Ballistic phonon transport calculations based on (i) first-principles methods and (ii) classical molecular dynamic simulations were made for two terminal devices with a single molecule as a channel material. **[2.]**

- 1-3) Using accurate first-principle (DFT+ Σ) based calculations of the conductance we investigated the orbital selection rule for molecular conductance, showing excellent agreement with experiment. **[3.]**

- 2-1) The electric conductance of Hubbard chain bridging two electrodes at finite bias

voltage was studied, using massive parallel computer simulations. The time-dependent density matrix renormalization group [4] is adopted to simulate the real-time dynamics of electric transport changing bias voltage. Here we have used the real-space parallelization [5] to overcome the expensive calculation cost.

Fig. 2 shows a differential conductance as a function of bias voltage at various wire length (site number) for a non-particle-hole-symmetric wire [6]. The differential of I-V curve oscillates with a length-dependent period. The period is an increasing function of the wire length.

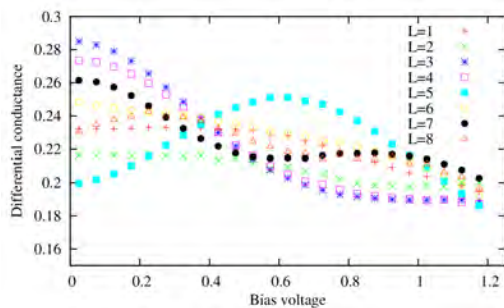


Fig.2: Differential conductance of Hubbard chain

References

- [1] Unpublished
- [2] M. Buerkle, Y. Asai, **Sci. Rep.**, 7, 41898 (2017)
- [3] M. Buerkle, L. Xiang, G. Li, A. Rostamian, T. Hines, S. Guo, G. Zhou, N. Tao, Y. Asai, **J. Am. Chem. Soc.**, 139 (8), 2989 (2017)
- [4] S. R. White and A. E. Feiguin, *Phys. Rev. Lett.* 93, 076401 (2004).
- [5] E. M. Stoudenmire and S. R. White, *Phys. Rev. B* 87, 155137 (2013)
- [6] J. Ozaki and Y. Asai, in preparation

Development & Application of Rational Drug Design Method using First-Principles Calculations & Bioinformatics

Vladimir Sladek and Hiroaki TOKIWA

*Research Center for Smart Molecules, Department of Chemistry,
Rikkyo University, 3-34-1 Nishi-Ikebukuro, Toshima, Tokyo 7-8501*

We have applied energy interaction analysis based on the first-principles calculations using the energy decomposition techniques: SAPT (Symmetry Adapted Perturbation Theory) [1] and the FMO – PIEDA (Fragment Molecular Orbital – Pair Interaction Energy Decomposition Analysis) [2] to Golgi α -mannosidase II (GM) system. The GM is a pharmaceutical target for the design of inhibitors with anti-cancer activity. The known potent GM inhibitors enter complex interactions with Zn^{2+} ion and the active-site amino acids, many of which contain ionisable functional groups. In our project, the physical insight into the ligand-receptor interactions was provided for a large GM active-site cluster. Protonation dependent molecular recognition in Golgi α -mannosidase is demonstrated for five inhibitors and mannose, as a model for native GM substrate. The Zn^{2+} ion and Asp472 induce the key interactions with the deprotonated inhibitors (bearing an amino group in neutral state) followed by Asp92 and Asp341. This interaction pattern is consistent for all of the studied inhibitors and is similar to the interaction pattern of the enzyme native

substrate – mannose. The interactions with the Zn^{2+} ion become repulsive for the protonated states of the inhibitors (bearing an amino group with +1 charge) and the importance of Asp92 and Asp204 raises considerably while the interactions with Asp472 and Asp341 are modified slightly. The interaction pattern for the protonated ligands seems to have an oxocarbenium transition state-like character rather than a Michaelis complex of GM. The electrostatic interactions with amino acids coordinating the zinc ion are of key importance for both the neutral and protonated states of the inhibitors. The ligands diol group which coordinates zinc is an essential structural feature of the potent inhibitors which is consistent with experimental findings. Based on the calculations either the protonated or deprotonated state of the ligand may be the active form of the GM inhibitor exhibiting different interacting patterns.

References

- [1] R. Bukowski, et al., Chem. Phys. Lett., **414** (2005) 111.
- [2] D. G. Fedorov, et al., Phys. Chem. Chem. Phys., **14** (2012) 7562

Reduction of Rare Metals in Fuel Cell Catalysts and Oxygen Sorption Materials

Yuji KUNISADA

*Center for Advanced Research of Energy and Materials, Faculty of Engineering,
Hokkaido University, Sapporo, Hokkaido 060-8628*

We investigated the Pt adsorption and diffusion properties on non-metal element doped graphene and local electronic structure of oxygen sorption materials, with the aid of the first principles calculation based on the density functional theory (DFT).

At first, we investigated adsorption and diffusion properties of a single Pt atom on non-metal element doped graphene. We performed the total energy and electronic structure calculations using VASP code. We installed parallelized VASP with Intel® MPI Library and Intel® Math Kernel Library. We found that the adsorption energies increase by non-metal element doping into graphene lattice. We also calculated the dopant dependence of diffusion constants of a single Pt atom at 100 °C which is operating temperature of typical polymer electrolyte fuel cell. From these calculations, we found that the non-metal dopants in graphene can prevent the surface diffusion of a single Pt atom.

We also investigated the electronic structure difference of $\text{Ca}_2\text{AlMnO}_5$, which is one of the promising oxygen sorption

materials, between before and after oxygen sorption. [2] We obtained the electron energy loss (EEL) spectra with scanning transmission electron microscopy (STEM) and DFT calculation. From comparison of these results, we clarified the pre-edge peak strength of O-K edge spectra depend on the oxygen sorption states.

In addition, we investigated the hydrogen absorption properties of Al(111) subsurfaces, the interface properties of hematite, and dielectric properties of $\alpha\text{-Al}_2\text{O}_3$.

References

- [1] S. Hasegawa, Y. Kunisada, N. Sakaguchi: submitted.
- [2] G. Saito, Y. Kunisada, K. Hayami, T. Nomura, N. Sakaguchi: *Chem. Mater.* 29 (2017) 648.
- [3] Y. Kunisada, N. Sakaguchi: *J. Jpn. Inst. Met. Mater.* 80 (2016) 570.
- [4] G. Saito, Y. Kunisada, T. Nomura, N. Sakaguchi, T. Akiyama: *Phys. Chem. Miner.* 43 (2016) 749.
- [5] N. Sakaguchi, L. Tanda, Y. Kunisada: *Ultramicroscopy* 169 (2016) 37.

Determination of geometric and electronic structures of organic crystals from first-principles

Susumu Yanagisawa

Department of Physics and Earth Sciences, University of the Ryukyus

1 Senbaru, Nishihara, Okinawa, Japan 903-0213

These years, there have been discussions on the possible band-like transport in the organic crystals, and the mechanism of the charge carrier transport in organic semiconductors is still under the intense debate. In order to predict the charge carrier transport properties, it is crucial to obtain theoretically the accurate crystal structure. The intermolecular distance and the molecular orientation angle have been proposed to impact the electronic properties [1]. In this study, by using oligoacene crystals as examples, we showed that the recent variant of the van der Waals density functional (vdW-DF)[2] is able to predict accurate crystal geometries and cohesive properties of organic crystals. We also demonstrated that by using the calculated crystal structure it is also possible to calculate the accurate electronic structure based on the *GW* approximation [3].

We first performed the structural optimizations and determined the stable structures for naphthalene, anthracene, and tetracene single crystals by using vdW-DF, as implemented in the Vienna ab-initio simulation package (VASP) [4]. In the present work, we carefully checked the convergence of the result

with respect to the number of \mathbf{k} -points, the cutoff energy, and the convergence threshold for the Hellmann-Feynman forces and stresses, presenting the converged results and comparison with the experimental values obtained at low temperatures. All the computations were done at the system B of ISSP supercomputer system with largest CPU cores of 432.

We performed the band structure calculation using the *GW* space-time code [5]. The code has been modified for parallel calculation with thousands of CPU cores. The *GW* calculations were based on the norm-conserving pseudopotentials and plane-wave basis set, and the starting wave functions were generated with the GGA-PBE exchange-correlation using the STATE code [6]. In addition to the one-shot *GW* (G_0W_0) calculation based on the PBE wave functions, we performed the partially self-consistent *GW* calculations in which the eigenvalues constructing the Green's functions replaced with the previous iteration (ev*GW*). The convergence of the calculated band gap (band width) with respect to the number of empty states, \mathbf{k} -point sampling, and plane-wave

cutoff was estimated to be within 0.05 (0.01) eV.

To elucidate how the molecular configuration affects the intermolecular transfer integrals, we analyze the electronic structures in detail by using the maximally localized Wannier function [7].

It was found that the theoretical cell lengths and volumes are in general underestimated. The calculated cell lengths and cell angle of naphthalene and anthracene were on average deviated by less than 0.7 % from the experimental diffraction data measured at 8-15 K. On the other hand, relative errors of those of tetracene were 1.0 % compared to the experimental values measured at 175 K. The result indicates that the calculated cell lengths and volumes, corresponding to those at 0 K, are close to the experimental values at low temperature. We also found that inclusion of the zero-point vibrational energy by the multi \mathbf{k} -point phonon calculation may remedy the underestimation.

The theoretical band gaps within G_0W_0 were slightly underestimated compared to the experimental values determined with the photoconductivity measurement, and they were improved by including the partial self-consistency.

The appreciable dispersion of the highest-occupied (HOMO) and lowest-unoccupied molecular orbital (LUMO) bands was

elucidated by the in-phase or out-of-phase stacking of the neighboring HOMOs or LUMOs, and the tight-binding approximation employing the nearest-neighbor transfer integrals described well the first-principles band structure. It was also found that only slight geometrical relaxation caused by the sliding of the molecule along the molecular long axis alters the signs of the transfer integrals between the herringbone-arranged molecules. The result highlights the subtle balance between the transfer integral or the band width and the molecular arrangement in the crystal unit cell.

References

- [1] V. Coropceanu et al.: Chem. Rev. **107** (2007) 926.
- [2] I. Hamada: Phys. Rev. B **89** (2014) 121103(R).
- [3] S. Yanagisawa and I. Hamada: J. Appl. Phys. **121** (2017) 045501.
- [4] G. Kresse and D. Joubert: Phys. Rev. B **59** (1999) 1758.
- [5] M. M. Rieger, L. Steinbeck, I. D. White, H. N. Rojas, and R. W. Godby: Comput. Phys. Commun. **117** (1999) 211.
- [6] Y. Morikawa, H. Ishii, and K. Seki: Phys. Rev. B **69** (2004) 041403(R).
- [7] N. Marzari, A. A. Mostofi, J. R. Yates, I. Souza, and D. Vanderbilt: Rev. Mod. Phys. **84** (2012) 1419.

First-principles meta-dynamics analysis of Catalyst Referred Etching method (analysis on dissociative adsorption of water molecule and etching reaction at interface between Pt and material surface)

Kouji INAGAKI

Graduate School of Engineering, Osaka University,

Yamada-oka 2-1, Suita, Osaka 565-0871

We investigated reaction mechanisms of chemical etching processes in a surface smoothing technique named Catalyst Referred Etching (CARE)[1], in which etching is invoked by approaching a catalyst (e.g. Pt) surface to material surface (e.g. wide band-gap semiconductors) in an etching solution (e.g. aqueous HF solution for SiC etching or pure water for GaN etching). In SiC-HF system, we have already obtained findings in the previous study with respect to SiC back-bond cleavage and simultaneous dissociative adsorption of HF molecule as the first step of etching process. The reaction barrier is clarified to be strongly lowered by the existence of Pt catalyst [2]. In this project, we analyzed H₂O splitting reaction on 3c-GaN(111) surface with respect to the distance between Pt catalyst and GaN. We find that a dissociative adsorption onto OH terminated kinked-GaN surface occurs in the presence of Pt catalyst (Fig. 1) with almost no barrier ($\sim 0.2\text{eV}$). By subsequent approach of Pt to GaN surface, Ga-N bond cleavage with H-terminating the cleaved N atom occurs with a small barrier ($\sim 0.8\text{eV}$), which is effectively smaller

than the barrier in no-Pt reaction (1.4eV). It is concluded that first H₂O dissociation with cleaving Ga-N bond is effectively facilitated by approach of Pt, i.e., the reaction barrier reduced from 1.4eV to 0.8eV.

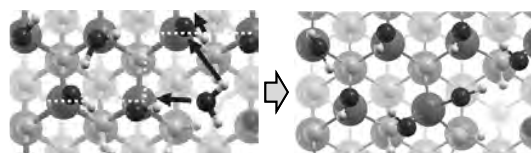


Fig. 1: H₂O dissociative adsorption at kink-site of GaN surface with Pt catalyst. OH adsorbs at kink-Ga and H adsorbs at O atom in OH termination.

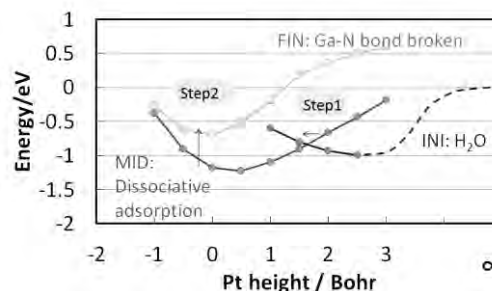


Fig. 2: Relative total energy change with respect to the position of Pt catalyst. Pt height origin is determined by the most stable Pt atom adsorption height. At Pt height 2 Bohr, H₂O dissociative adsorption (Fig.1). At around 0 to -1 Bohr, Ga-N bond break take place and N is terminated by H atom in OH termination.

References

- [1] H.Hara, et al., J.Electron.Mater. 35 (2006) L11.
- [2] P. V. Bui, et al. Curr. Appl. Phys., 12 (2012) S42.
- [3] P. V. Bui, et al. Appl Phys.Lett.107(2015)20160.

Protonic Activity on the Hydrated Surface of Acidic and Basic Oxide Catalyst for CO₂ Conversion Processes

Ryuhei Sato and Shu Yamaguchi

Department of Materials Engineering,

The University of Tokyo, Bunkyo-ku, Hongo, Tokyo 113-0032

Proton activity on oxide surface is paid considerable attention for the application to metal/oxide catalysts such as Cu/ZnO for methanol synthesis. The efficiency of methanol synthesis ($\text{CO}_2 + 6\text{H}^+ + 6\text{e}^- \rightarrow \text{CH}_3\text{OH} + \text{H}_2\text{O}$) highly depends not only on the Red-Ox property but also on the acid-base property on oxide surfaces. Therefore, in recent years, the acidity of hydroxyl groups on oxide surfaces has been studied, although there are few report about the effect of acidic molecule adsorption on surface acidity. Here, we studied the change in acidity by the adsorption of CO₂, HCOOH, and CH₃OH.

First, we analyzed the adsorption of CO₂, HCOOH, and CH₃OH on bare cubic ZrO₂ (110) surface by *ab initio* molecular dynamic (AIMD) simulation. Subsequently, by introducing H₂O molecules above ZrO₂ surface terminated by those species, hydration reactions are analyzed by AIMD simulation. All the simulations were performed by home-made code written by F. Shimojo et al. [1]. The GGA/PBE functional and PAW method were employed with L4cpu and L36cpu queues.

After 10,000-step (2.4 ps) simulation for

adsorption of each organic molecule on the bare surface, bidentate and polydentate carbonates, bidentate and monodentate formate, and methoxy groups are observed on the surface, the structure of which well agrees with that predicted from Fourier transform infrared spectroscopy measurement (FT-IR). These adsorbates except methoxy groups hardly interact with H₂O molecules, monodentate hydroxyl group (Zr-OH⁻), and chemisorbed H₂O molecules on the Zr ions (Zr-OH₂) after the hydration. Therefore, these adsorbates are very weak conjugate base and inert to the acid-base reactions. In addition, by analyzing the radial distribution function and bond overlap population (RDF and OVP) between O and H atoms in H₂O adsorbates, it is confirmed that the acidity of H₂O adsorbates on Zr ion sites, Zr-OH₂ and Zr-OH⁻, is constant regardless of the adsorption of organic molecules. pH at point of zero charge (pH_{PZC}) and acidity constant (pK_{a0}) for deprotonation reaction on O ion sites are estimated using $\text{pK}_{a1} - \text{pH}_{\text{PZC}, \text{H}_2\text{O}}$, pK_a for deprotonation reaction of Zr-OH₂ normalized by pH_{PZC} on hydrated cubic ZrO₂ surface without any organic molecules,

obtained from previous simulations[2]. Figure 1 shows the calculated change in pH_{PZC} as a function of the coverage of organic molecules on the surface. Note that the similar reduction of $\text{p}K_{\text{a}0}$ as a function of the coverage is observed in all hydration reactions on the surface terminated by carbonate and its derivatives, which suggests the reduction of basicity on surface oxide ions. It is also found that pH_{PZC} is reduced to the degree of 1.5 pH unit by CO_2 adsorption, which is comparable with the results obtained by an electro-kinetic measurement [3]. The extent of the decrease in pH_{PZC} by HCOOH and CH_3OH adsorption is much smaller, although HCOOH molecules themselves are stronger acid than CO_2 in aqueous solution. Therefore, further discussion on the difference between chemisorption of adsorbates on Brønsted and Lewis acid site is now under way to reveal the chemistry of surface acidity and basicity.

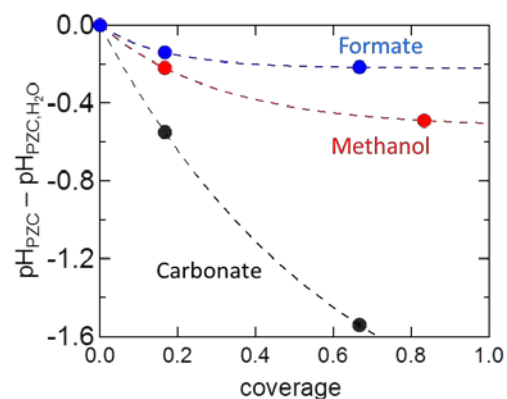


Figure 1. Estimated pH_{PZC} normalized by $\text{pH}_{\text{PZC,H}_2\text{O}}$, pH_{PZC} on the organic-molecule-free hydrated surface, as a function of organic molecule coverage.

References

- [1] F. Shimojo, R.K. Kalia, A. Nakano, P. Vashishta, *Comp. Phys. Comm.* **140** (2001) 303.
- [2] R. Sato, S. Ohkuma, Y. Shibuta, F. Shimojo, S. Yamaguchi: *J. Phys. Chem. C.* **199** (2015) 28925.
- [3] C. Su, D.L. Suarez *Clays and Clay Miner.*, **45** (1997) 814.

Ab initio study for nano catalysts based on abundant elements

Tetsuya TAKETSUGU

Faculty of Science, Hokkaido University

N10W8, Sapporo, Hokkaido 060-0810

Heterogeneous catalysts used in automotive gas exhausts control, water gas shifts, and fuel cells rely mostly on the precious metals (PMs) such as Pt, Rh, Pd. Due to their high cost and limited amounts, to reduce or even replace these metals is emergent issues in industry. To that end, we perform density functional theoretical (DFT) computations using ISSP supercomputers to understand the chemical mechanisms in conventional catalysts as well as to design novel catalysts with abundant elements. Specifically, our project focuses on the three-way catalysts (TWC) and fuel cells with water-gas shifts (WGS) and oxygen reduction reactions (ORR). In TWC, NO_x is reduced while CO and CH (hydrocarbons) are oxidized at the same time under the drastic temperature and oxygen concentration changes. With such extreme conditions, only Pt, Rh, and Pd turned out to be effective. To understand the reason as well as to clarify the possible chemical reaction pathways for TWC, we investigate the catalytic activities of these metals by using the slab model under the periodic boundary condition to model surfaces. Whereas to test the abundant elements, we focus on transition metals with 3d electrons (TM^{3d}) that are generally abundant and cost-effective. Although some of bulk TM^{3d} are known to inactive for TWC, we shed light on the nano-size effect, meaning we test nano-sized TM^{3d} such as clusters or islands on an oxide substrate. As for fuel cells, we focus on a hexagonal boron nitride (h-BN) sheet having a 2-dimensional

structure similar to graphene. h-BN itself is inert but a carbon doping alters its reactivity. In a previous study, it was found that carbon doped BN sheet work as catalysts [1].

For PM surfaces and supported nano-sized TM^{3d} systems, DFT computations with periodic boundary conditions were performed using the PBE functional with PAW basis sets as implemented in VASP. It should be noted that the calculations for some of the latter system require massive parallelization using about 100 nodes. We considered PM-surfaces of flat (111) and (100) and steps and edges. Until now, we have obtained optimized slab structures and molecule-adsorbed structures and some of reaction pathways. For supported nano-sized TM^{3d} systems, we have obtained optimized structures for one TM^{3d} atom doping with pristine and O-defective oxide substrates and some adsorption states of small molecules. For calculations including transition metals with localized d- or f- electrons, we used +U technique to account for the localized electrons. We have also tried hybrid functionals such as HSE06 but using those functionals are computationally too demanding to the present purpose. For computations on h-BN (7×7) surface using SIESTA, a charge density difference comparing the pristine and doped h-BN indicate the large area would be activated for oxidation reactions.

References

- [1] M. Gao, A. Lyalin, and T. Taketsugu, *J. Phys. Chem. C* **120**, 15993 (2016).

Accurate evaluation of electron-phonon coupling in sulfur-hydride superconductors

Ryosuke AKASHI

Department of Physics, University of Tokyo

Hongo, Bunkyo-ku, Tokyo 113-0033

In this project, we calculated the electron-phonon coupling strength responsible for the phonon-mediated superconductivity in sulfur hydride systems H_xS and also in another sulfide BiS_2 superconductor. These two superconducting compounds have attracted tremendous interest since their recent discovery [1–

3], and we have addressed their origins of the superconducting transition from the viewpoint of accurate first-principles simulation. In the theory of phonon-mediated superconducting mechanism [4, 5], an essential quantity for accurate estimation of the superconducting transition temperature (T_c) is the following Eliashberg function

$$\alpha^2 F(\omega) = \frac{1}{N(E_F)} \sum_{nn'\mathbf{k}\mathbf{q}\lambda} |g_{n\mathbf{k}+\mathbf{q}n'\mathbf{k}}^{\lambda\mathbf{q}}|^2 \delta(\omega - \omega_{\lambda\mathbf{q}}) \delta(\varepsilon_{n\mathbf{k}+\mathbf{q}} - E_F) \delta(\varepsilon_{n'\mathbf{k}} - E_F). \quad (1)$$

Here, E_F , $N(E_F)$, $g_{n\mathbf{k}+\mathbf{q}n'\mathbf{k}}^{\lambda\mathbf{q}}$, $\omega_{\lambda\mathbf{q}}$, $\varepsilon_{n\mathbf{k}}$, denotes the Fermi energy, electronic density of states at the Fermi level, electron-phonon coupling matrix element, phonon frequency and the electron one-particle energy eigenvalue in the normal state, respectively. For example, there is a practical approximate formula of T_c , called McMillan-Allen-Dynes formula [6, 7], derived from the Eliashberg equations [5]

$$T_c = \frac{\omega_{\text{ln}}}{1.2} \exp \left[-\frac{1.04(1+\lambda)}{\lambda - \mu^*(1+0.62\lambda)} \right], \quad (2)$$

where λ and ω_{ln} represent the electron-phonon coupling strength and typical frequency of phonons contributing to the electron pairing. Parameter μ^* represents the effective pair-breaking repulsion and called Coulomb pseudopotential [8]. The former coupling parameters are defined with $\alpha^2 F(\omega)$ as

$$\lambda = 2 \int d\omega \frac{\alpha^2 F(\omega)}{\omega}, \quad (3)$$

$$\omega_{\text{ln}} = \exp \left[\frac{2}{\lambda} \int d\omega \ln \omega \frac{\alpha^2 F(\omega)}{\omega} \right] \quad (4)$$

Although $\alpha^2 F(\omega)$ is thus essential for theoretical estimation of superconducting T_c , accurate calculation of this requires enormous computational cost; we used the system B (sekirei) for overcoming this difficulty.

The calculations of the phonon and electron-phonon coupling properties were carried out based on the density functional perturbation theory [9] as implemented with the plane-wave basis in QUANTUM ESPRESSO code package (5.0.3)(Ref. [10]). The Fermi-surface intergral was performed with the optimized tetrahedron method [11]. The GGA-PBE [12] and LDA-PZ [13] exchange-correlation potentials were used for the H_xS and BiS_2 systems, respectively. Parallelization was performed with respect to \mathbf{k} points (*-npool* option) as implemented in *ph.x* code. The calculations were mainly done in System B (sekirei). Typical computational time was, for example, $\lesssim 16$ hours per \mathbf{q} point with 9 nodes and *-npool 9*.

In the last year, we performed the calculations for $H_{13}S_5$ and $H_{31}S_{11}$ (see Ref. [14]):

We further calculated the coupling for more various compounds. These H_xS systems with $2 \leq x \leq 3$ are the new crystalline phases found by the author and coworkers, called ‘‘Magnéli’’ phases in analogy to the well-known Magnéli phases in transition-metal oxides [15]. We found that the electron-phonon coupling shows monotonic increase as the hydrogen ratio x is increased (Table I). Using a first-principles method to calculate T_c based on the density functional theory for superconductors (SCDFT [16, 17]), we showed that this increase yield gradual increase of T_c . Remarkably, this behavior explains the experimentally observed pressure-induced behavior of T_c , which was unprecedented in the previous theoretical studies. This achievement has been published in Physical Review Letters [18].

TABLE I. Sulfur hydride ‘‘Magnéli phases’’ at high-pressure: First-principles calculated electron-phonon coupling parameters and superconducting transition temperature.

	H_7S_3	$H_{10}S_4$	$H_{13}S_5$	$H_{31}S_{11}$
H-ratio	0.70	0.714	0.722	0.738
Pressure (GPa)	130	180	190	200
λ	0.936	1.162	1.303	1.478
ω_{ln} (K)	893	1218	1289	1355
T_c^{SCDFT} (K)	41	80	107	121

Also, we calculated the electron-phonon coupling in BiS_2 -layered superconductor $LaO_{0.5}F_{0.5}BiS_2$ (Ref. [2, 3]). Previous studies have shown that this system is possibly subject to lattice distortion and/or charge-order instability, sensitively depending on the environment [19–21]. We therefore adopted the supercell configuration to treat these possibilities. The size of supercell (20 atoms) and multiple number of orbitals (especially of La and Bi) render the calculation cost

enormous; namely, calculation of the electron-phonon coupling matrix element in Eq. (1) requires much time and therefore it becomes difficult to get their values on dense \mathbf{q} -point meshes. In order to accelerate the convergence of the calculation with respect to the \mathbf{q} -mesh, we applied the recently developed method of postprocessing rescaling [22]. The convergence of the calculations were also cross-checked with the results using the optimized tetrahedron method [11]. As shown in Fig. 1, the rescaled values show modest converging trend to the values calculated with the tetrahedron method. The good agreement between the results with the rescaling and optimized tetrahedron methods indicates the reliable convergence. First-principles study based on these data has been submitted to a journal [24].

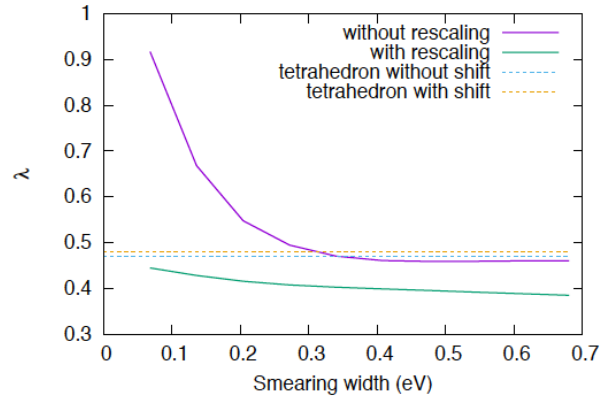


FIG. 1. Electron-phonon coupling in $LaO_{0.5}F_{0.5}BiS_2$ calculated from the first principles. Solid curves represent the calculated values of λ (Eq.(3)) using the Gaussian smearing approximation for the delta functions [23] with and without the rescaling method [22]. This calculation was carried out with the $4 \times 4 \times 2$ \mathbf{q} point mesh. The rescaled values show modest converging trend to the values calculated with the tetrahedron method using the $4 \times 4 \times 2$ \mathbf{q} point meshes with and without a half shift (dashed lines).

-
- [1] A. P. Drozdov, M. I. Erements, and I. A. Troyan, V. Ksenofontov, and S. I. Shylin, *Nature* (London) **525**, 73 (2015).
- [2] Y. Mizuguchi, H. Fujihisa, Y. Gotoh, K. Suzuki, H. Usui, K. Kuroki, S. Demura, Y. Takano, H. Izawa, and O. Miura, *Phys. Rev. B* **86**, 220510 (2012).
- [3] Y. Mizuguchi, S. Demura, K. Deguchi, Y. Takano, H. Fujihisa, Y. Gotoh, H. Izawa, and O. Miura, *J. Phys. Soc. Jpn.* **81**, 114725 (2012).
- [4] A. B. Migdal, *Sov. Phys. JETP* **7**, 996 (1958).
- [5] G. M. Eliashberg, *Sov. Phys. JETP* **11**, 696 (1960); D. J. Scalapino, in *Superconductivity* edited by R. D. Parks, (Marcel Dekker, New York, 1969) VOLUME 1; J. R. Schrieffer, *Theory of superconductivity; Revised Printing*, (Westview Press, Colorado, 1971).
- [6] W. L. McMillan, *Phys. Rev.* **167**, 331 (1968).
- [7] P. B. Allen and R. C. Dynes, *Phys. Rev. B* **12**, 905 (1975).
- [8] P. Morel and P. W. Anderson, *Phys. Rev.* **125**, 1263 (1962).
- [9] S. Baroni, S. de Gironcoli, A. Dal Corso, and P. Giannozzi, *Rev. Mod. Phys.* **73**, 515 (2001).
- [10] P. Giannozzi *et al.*, *J. Phys.: Condens. Matter* **21**, 395502 (2009); <http://www.quantum-espresso.org/>.
- [11] M. Kawamura, Y. Gohda, and S. Tsuneyuki, *Phys. Rev. B* **89**, 094515 (2014).
- [12] J. P. Perdew, K. Burke, and M. Ernzerhof, *Phys. Rev. Lett.* **77**, 3865 (1996).
- [13] J. P. Perdew and A. Zunger, *Phys. Rev. B* **23**, 5048 (1981).
- [14] R. Akashi, in *Activity report 2015* (Supercomputer Center, Institute for Solid State Physics, 2016).
- [15] A. Magnéli, *Acta Cryst.* **6**, 495 (1953).
- [16] M. Lüders, M. A. L. Marques, N. N. Lathiotakis, A. Floris, G. Profeta, L. Fast, A. Continenza, S. Massidda, and E. K. U. Gross, *Phys. Rev. B* **72**, 024545 (2005).
- [17] M. A. L. Marques, M. Lüders, N. N. Lathiotakis, G. Profeta, A. Floris, L. Fast, A. Continenza, E. K. U. Gross, and S. Massidda, *Phys. Rev. B* **72**, 024546 (2005).
- [18] R. Akashi, W. Sano, R. Arita, and S. Tsuneyuki, *Phys. Rev. Lett.* **117**, 075503 (2016)
- [19] T. Yildirim, *Phys. Rev. B* **87**, 020506(R) (2013).
- [20] X. Wan, H. C. Ding, S. Y. Savrasov, and C. G. Duan, *Phys. Rev. B* **87**, 115124 (2013).
- [21] T. Tomita, M. Ebata, H. Soeda, H. Takahashi, H. Fujihisa, Y. Gotoh, Y. Mizuguchi, H. Izawa, O. Miura, S. Demura, K. Deguchi, and Y. Takano, *J. Phys. Soc. Jpn.* **83**, 063704 (2014).
- [22] T. Koretsune and R. Arita, arXiv:1610.09441.
- [23] M. Methfessel and A. T. Paxton, *Phys. Rev. B* **40**, 3616 (1989).
- [24] C. Morice, R. Akashi, T. Koretsune, S. S. Saxena, and R. Arita, arXiv:1701.02909.

Microscopic Structure and Dynamics of Solutions Faced to Solid Materials Using First-Principles and Classical Molecular Dynamics

Ken-ichi FUKUI

*Department of Materials Engineering Science, Graduate School of Engineering Science,
Osaka University, Machikaneyama, Toyonaka, Osaka 560-8531*

Microscopic structure of the electric double layer (EDL) formed at aqueous solution / electrode interfaces is important for fundamental understanding of the electrochemical processes occur at the electrodes. It is essential to model EDL focusing on orderings and mobility of water and solute ions. Previous investigations showed that several hydration layers were formed at the interface and density profiles of water changed depending on the electrode potential [1], and the stiffness of such hydration layers also depended on the electrolyte ion species as well as the potential [2]. To evaluate microscopic dynamics of water and ions and their networking in the EDL theoretically, we have investigated the various aqueous solution / graphite electrode interfaces by molecular dynamics (MD) simulation.

Each simulation cell contains two graphite electrodes and 0.5 M sodium halide aqueous solution between them (ca. $5 \times 5 \times 9 \text{ nm}^3$) (Fig.1). Electrode potential is applied by assigning uniform electric charge on each surface graphite carbon atom (1.83, 3.66, 5.49, 7.32 $\mu\text{C cm}^{-2}$, which corresponds to 0.34, 0.72, 1.16, 1.61 V vs. pzc potential by solving the Poisson's equation).

Density profiles of water molecules (H and O atom) (Fig.1) show that hydration layers are formed at the graphite electrode interface independent of electrolytes. For the case of hydrophobic HOPG without apparent charge at the pzc potential, two stable alignments are known at the 1st layer ($0 \sim 5 \text{ \AA}$): one is the parallel alignment and the other is the one H up alignment with some preference to the former one. Fig. 1 clearly shows that hydrophobic F⁻ ion more favors the interface: it is closely related to its

weaker coordination to water molecules.

We also analyzed mobility of a water molecule in the 1st layer by diffusion coefficient (Fig.2) as an index of effective hydrogen bonding networks. By applying positive potential to (positive charge on) HOPG, portion of H-up water molecules increases, which also favors the coordination to hydrophilic halide (F⁻). Thus, more positive electrode potential and decrease water mobility in the 1st layer.

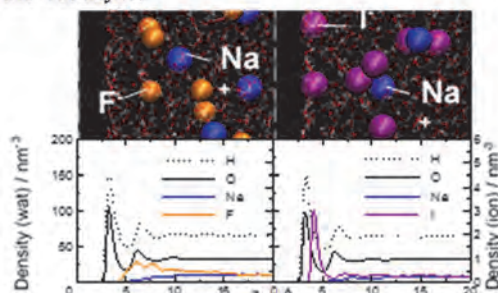


Fig. 1: Snapshots and density profiles of electrolytes at positively charged HOPG surface. ($+5.49 \mu\text{C cm}^{-2}$, left : NaFaq / right : NaIaq).

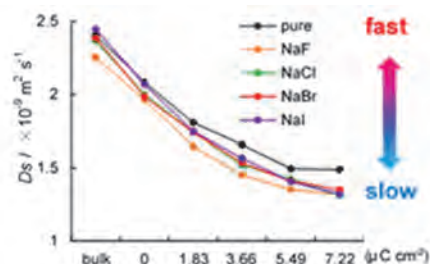


Fig. 2: Diffusion coefficient of water in the 1st layer depending on electrolytes and potential.

References

- [1] M. Toney, et al., *Nature* **31**, 444 (1994).
- [2] T. Utsunomiya, Y. Yokota, T. Enoki, K. Fukui, *Chem Commun.* **50**, 15337 (2014).

Ab initio molecular dynamics simulation of graphene/water interfaces

Tatsuhiko OHTO

Graduate School of Engineering Science,

Osaka University, 1-3 Machikaneyama, Toyonaka, Osaka 560-8531

Ab initio MD (AIMD) is a powerful tool to describe heterogeneous systems such as the water/solid interface. Although AIMD is computationally expensive, it describes electronic states beyond classical force fields,[1] which is important for interfaces. We calculated graphene/water interfaces with AIMD to reveal the interfacial structure of water. We accumulated 100 ps trajectories by using the CP2K code [2]. The analysis is ongoing together with experiments.

In addition to the simulation of graphene/water interfaces, we studied the interfacial structure of room temperature ionic liquids (RTILs).[3] RTIL interfaces controls many of the unique properties of RTILs, such as the high capacitance of RTILs and the efficiency of charge transport between RTILs and electrodes. RTILs have been experimentally shown to exhibit interfacial molecular layering structures over a 10 Å length scale. However, the driving force behind the formation of these layered structures has not been resolved. Here, we report *ab initio* molecular dynamics simulations of imidazolium RTIL/air interfaces

along with force field molecular dynamics simulations. We find that the $\pi^+-\pi^+$ interaction of imidazolium cations enhances the layering structure of RTILs, despite the electrostatic repulsion.

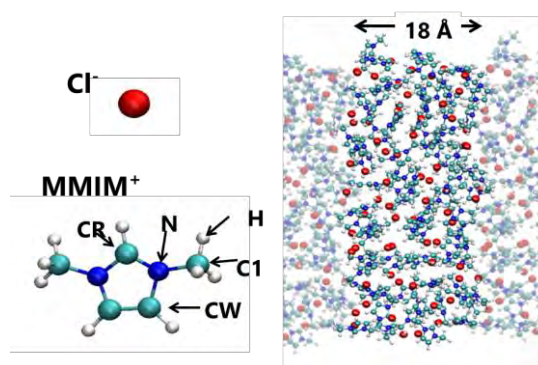


Fig. 1: Structures of RTIL and the RTIL-air interface.

References

- [1] T. Ohto et al. *Phys. Chem. Chem. Phys.* **19**, 6909 (2017).
- [2] The CP2K developers group, <http://cp2k.berlios.de/>
- [3] T. Fujie et al. *Phys. Chem. Chem. Phys.* **19**, 2805 (2017).

First-principles calculation of anharmonic effects of phonons and related properties in solids

Terumasa TADANO

*International Center for Young Scientists, National Institute for Material Science
Sengen, Tsukuba, Ibaraki 305-0047*

Intermetallic clathrates are promising materials for thermoelectric applications because of their unusually-low lattice thermal conductivity (LTC) values [1]. Our previous computational study on a type-I clathrate $\text{Ba}_8\text{Ga}_{16}\text{Ge}_{30}$ (BGG) showed that the low LTC values can be attributed to the increased Umklapp scattering of heat-carrying acoustic phonons induced by rattling guest atoms [2]. While this study clearly unveils the role of three-phonon scattering processes in BGG, the effect of the quartic anharmonicity is still unclear, which is believed to be significant due to large atomic displacements of rattlers.

To elucidate the actual role of the quartic anharmonicity in BGG, we have performed the self-consistent phonon (SCP) calculations in which the following equations were solved self-consistently [3]:

$$\Omega_{\mathbf{q}\nu}^2 = \omega_{\mathbf{q}\nu}^2 + 2\Omega_{\mathbf{q}\nu}I_{\mathbf{q}\nu},$$

$$I_{\mathbf{q}\nu} = \sum_{\mathbf{q}'\nu'} \frac{\Phi(\mathbf{q}\nu; -\mathbf{q}\nu; \mathbf{q}'\nu'; -\mathbf{q}'\nu')}{4\Omega_{\mathbf{q}\nu}} \langle Q_{\mathbf{q}'\nu'}^* Q_{\mathbf{q}'\nu'} \rangle$$

Here, $\omega_{\mathbf{q}\nu}$ is the phonon frequency within the harmonic approximation, $\Omega_{\mathbf{q}\nu}$ is the temperature-dependent phonon frequency that includes the effect of the quartic anharmonicity in the mean-field level, $\Phi(\mathbf{q}\nu; -\mathbf{q}\nu; \mathbf{q}'\nu'; -\mathbf{q}'\nu')$ is the reciprocal representation of quartic force constants, and $\langle Q_{\mathbf{q}'\nu'}^* Q_{\mathbf{q}'\nu'} \rangle$ is the temperature-dependent displacement factor of the normal coordinate $Q_{\mathbf{q}\nu}$. Solving the SCP equation for BGG was a great numerical challenge because of a large number of phonon modes, i.e.

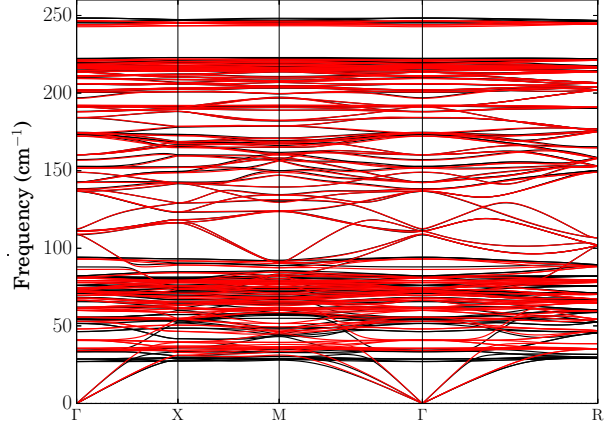


Figure 1: Anharmonic phonon dispersion of BGG at 300 K (red) compared with the harmonic dispersion curves (black)

$N_\nu = 162$. To make the computation feasible, we have developed an MPI-based code for calculating all elements of $\Phi(\mathbf{q}\nu; -\mathbf{q}\nu; \mathbf{q}'\nu'; -\mathbf{q}'\nu')$ in parallel.

Figure 1 shows the anharmonic phonon dispersion of BGG calculated at 300 K. As can be seen in the figure, the frequency renormalization by the quartic anharmonicity is almost negligible except for the low-lying rattling modes around 30 cm^{-1} , for which the phonon frequency is slightly increased. We have also calculated LTC of BGG by solving the Boltzmann transport equation (BTE) using the SCP lattice dynamics wavefunctions and found that the small change in the rattling frequencies considerably affects the LTC values as shown in Fig. 2. Interestingly, the quartic anharmonicity reduces the scattering

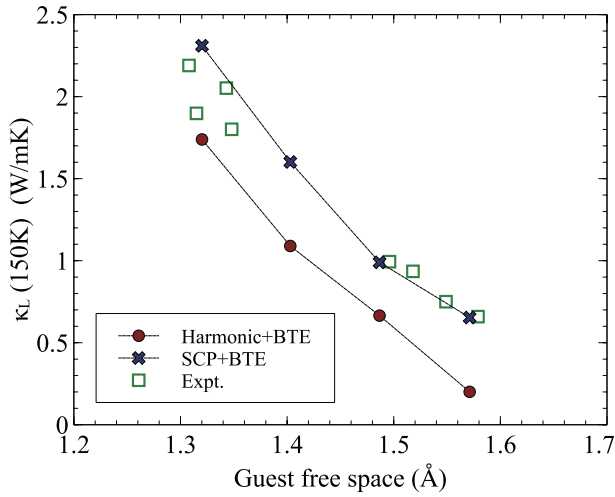


Figure 2: Correlation between the guest-free-space of the rattling atoms and the lattice thermal conductivity in BGG and other Ge clathrates. The experimental values are adapted from Ref. [4].

channel of the three-phonon interactions and therefore increases the LTC values. Moreover, we have found that the quartic anharmonicity is essential for explaining the observed correlation between the guest-free-space of the rattling atoms and the LTC values as shown in the figure [5].

References

- [1] T. Takabatake *et al.*: Rev. Mod. Phys. **86** (2014) 669.
- [2] T. Tadano, Y. Gohda, and S. Tsuneyuki: Phys. Rev. Lett. **114** (2015) 095501.
- [3] T. Tadano and S. Tsuneyuki: Phys. Rev. B **92** (2015) 054301.
- [4] K. Suekuni *et al.*: Phys. Rev. B **77** (2008) 235119.
- [5] T. Tadano and S. Tsuneyuki, in preparation.

Atomistic simulation of nonlinear optical response in solids

Yasushi SHINOHARA

Photon Science Center;

The University of Tokyo, Hongo, Bunkyo-ku, Tokyo 113-8656

Interactions between light and electrons in solids is one of the most active fields in optical science, in which the electronic motion in attosecond scale is encoded in optical responses. We have developed an atomistic simulation method for describing ultrafast electronic response triggered by intense and short light field, using information derived by density-functional theory (DFT).

We have developed a theoretical framework temporally evolving one-body density matrix without interaction between electrons but with coupling to a time-dependent electric field based on the velocity gauge. Matrix elements of one-body Hamiltonian and momentum operator are taken from orbitals at self-consistent-solution of DFT with the local-density approximation (LDA), by all-electron LAPW code, Elk [1]. Since number of active bands are around a few hundreds, instantaneous Hamiltonian is easily diagonalizable by LAPACK routines. Time-propagation of the equation of motion is performed by an exponential propagator relying on explicit diagonalization on each time-step, to realize efficient temporal integration.

We apply the framework to an unexpected

problem appeared in high-order harmonic generation (HHG) experiments in ϵ GaSe crystal [2]. We perform a calculation such that 30 thousand time-step, $64 \times 64 \times 12$ k-point mesh, and 103 bands as active space, covering 39 eV frequency ranges. To correct underestimation of the band gap due to LDA, scissors operator is introduced downshifting all valence bands by the amount of 1.2 eV to obtain experimental band gap 2.0 eV. Our simulation successfully captures whole part of experimental outcomes including the unexpected behavior. By analysis based on intensity dependence, we pin down the physical interpretation for the unexpected signal as higher-order nonlinear process showing up because of significantly nonlinear response.

References

- [1] <http://elk.sourceforge.net/>
- [2] Keisuke Kaneshima, Yasushi Shinohara, Kengo Takeuchi, Nobuhisa Ishii, Kotaro Imasaka, Tomohiro Kaji, Satoshi Ashihara, Kenichi L. Ishikawa, and Jiro Itatani, in preparation.

First-Principles Molecular-Dynamics Study of Structural and Electronic Properties of Covalent Glasses under Pressure

Fuyuki SHIMOJO, Akihide KOURA, Masaaki MISAWA, and Emina RYUO

Department of Physics, Kumamoto University, Kumamoto 860-8555

SiO₂ glass has been well known to be an archetypal three-dimensional network-forming glass and a material of great interest in various research fields. In particular, numerous experimental and theoretical studies on permanent densification have been carried out since its discovery in the 1950s [1]. However, the microscopic mechanism of permanent densification has not been clarified yet.

To clarify the microscopic structure of densified SiO₂ glass, we have conducted first-principles molecular-dynamics simulations on the decompression process of SiO₂ glass in its relaxed state from high pressures up to 40 GPa. When decompressed from high pressures above at least 15 GPa, the density and structure always converge to those of densified glass, while the coordination number of Si decreases to four rapidly. This is in good agreement with previous experimental studies and strongly suggests that densified glass behaves as a high-pressure polymorph of SiO₂ glass.

In comparison of ordinary glass, the coordination number of densified glass is almost the same, i.e. 4, which indicates that the glass consists of SiO₄ tetrahedra. However, the

ring size distribution shows that the network of densified glass is formed from smaller size rings than ordinary glass. This result suggests that permanent densification is caused by the reconstruction of the network structure to a smaller one. Also, the O-Si-O angle distribution shows that SiO₄ tetrahedra of densified glass are deformed.

The difference in the bonding properties between densified and ordinary glasses is estimated with a population-analysis method. It is suggested that the Si-O bond becomes less covalent due to the rearrangement of network, which is in remarkable agreement with previous experimental studies [2].

It is concluded from this study that fully densified glass recovered from a pressure above 15 GPa has a small network structure consisting of deformed SiO₄ tetrahedra with less covalent Si-O bonds.

References

- [1] P. W. Bridgman and I. Šimon: *J. Appl. Phys.* **24**, 405 (1953).
- [2] D. Wakabayashi, N. Funamori, and T. Sato: *Phys. Rev. B* **91**, 014106 (2015).

Large scale ab initio calculations on the fundamental processes of solar energy convergence devices and on designing principles for new materials

Koichi YAMASHITA

Department of Chemical System Engineering, School of Engineering,

The University of Tokyo, 7-3-1, Hongo, Bunkyo-ku, Tokyo 113-8656

Recently, perovskite oxides and oxynitrides have been attracting wide attention since they are promising candidates for highly efficient water splitting photocatalysts. However, their activity still remains low, and further investigations such as theoretical calculations on these materials have not been fully done yet. Here, we investigated several perovskite oxides and oxynitrides which have been actively studied to achieve visible light responsive overall water splitting, or studied due to their novel features such as metallic properties.

First, we have investigated CaTaO_2N , an oxynitride photocatalyst which have succeeded in overall water splitting under visible light irradiation [1]. Here, we focused on the impacts of the atomic arrangement of O^{2-} and N^{3-} (= anion orderings) on its band structure. Bandgaps, carrier effective masses, and band edge positions of CaTaO_2N with various anion orderings were calculated using density functional theory (DFT), which is implemented in VASP code. As a result, we found that anion orderings significantly impacts on their valence band structures due to the different orbital

overlap between N 2p and Ta 5d bands (Fig. 1).

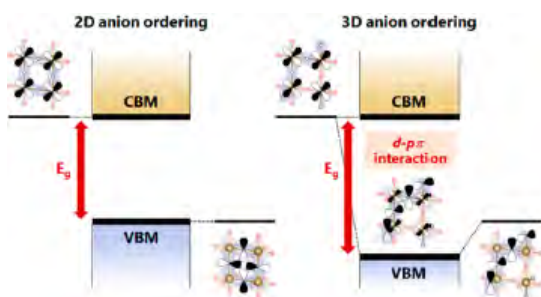


Fig. 1: Schematic diagram of the impact of anion orderings on the valence band structures of CaTaO_2N [2].

Second, we have studied on SrNbO_3 , a novel metallic photocatalyst with d^1 electronic structure [3], which was also reported to generate both H_2 and O_2 individually under sacrificial reagent. However, there have been controversial arguments on the photoexcitation path of SrNbO_3 among three relevant bands, a fully occupied band (B_{-1}), a partially empty conduction band (CB), and a higher level unoccupied band (B_1). Here, by means of DFT based calculations on the imaginary part of its dielectric function, we revealed that photoexcitation around its optical gap 1.9 eV is

constituted of $CB \rightarrow B_1$ transitions from the imaginary part of dielectric function (Fig. 2).

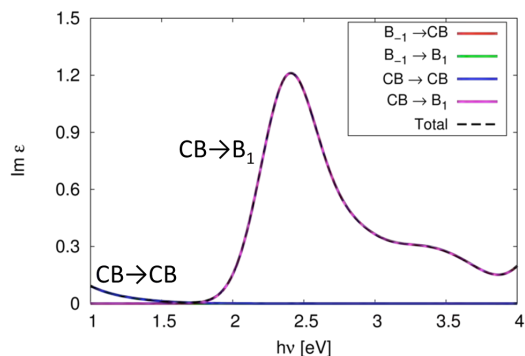


Fig. 2: Calculated imaginary part of dielectric function of each band of $SrNbO_3$.

Third, we have investigated $BaTaO_2N$, an oxynitride photocatalyst which can generate H_2 and O_2 individually with sacrificial reagent under visible light up to 660 nm [4]. In this study, we mainly focused on its carrier lifetime, since its band edge position is already suitable for water splitting. By means of electron-phonon coupling calculation, which is done by

the combination of QUANTUM ESPRESSO and YAMBO codes, we found that the carrier lifetime of $BaTaO_2N$ is about 1~10 fs, which is shorter than those of other semiconductors[5], and thus their electronic structures around the band edges need to be modified to retard the relaxation of the carriers.

References

- [1] J. Xu, C. Pan, T. Takata, K. Domen: Chem. Commun. **51** (2015) 7191.
- [2] A. Kubo, G. Giacomo, K. Yamashita: Chem. Mater. **29** (2017) 539.
- [3] X. Xu, C. Randorn, P. Efstathiou, and J. T. S. Irvine: Nat. Mater. **11**, 595 (2012)
- [4] M. Hojamberdiev, K. Yubuta, J. J. M. Vequizo, A. Yamakata, S. Oishi, K. Domen, K. Teshima: Cryst. Growth Des. **15** (2015) 466.
- [5] H. Kawai, G. Giorgi, A. Marini, and K. Yamashita: Nano Lett. **15**(5) (2015) 3103.

First-principles analysis of the dielectric response of defective interfaces

Shusuke Kasamatsu

Institute for Solid State Physics,

The University of Tokyo, Kashiwa-no-ha, Kashiwa, Chiba 277-8581

Surfaces of and interfaces between materials are sources of various functionalities in nanoelectronics and energy conversion devices. Control of surface and interface properties, which can sometimes be enormously different from bulk, is a key issue for device performance and durability. However, progress in this regard is hindered by lack of knowledge of the microscopic mechanisms for modifications of properties such as permittivity, conductivity, and reactivity at surfaces and interfaces. This year, we focused on how ion vacancies near metal/oxide interfaces affect the dielectric constant. We employ the orbital-separation approach [1,2] that we implemented in VASP code [3] for consideration of the dielectric response of metal/insulator/metal capacitors under bias.

In this work, we considered hydroxyapatite ($\text{Ca}_{10}(\text{PO}_4)_6(\text{OH})_2$; HAp), which comprises up to 50% of human bone and is a well-studied biomaterial for medical use. It is also an intriguing material in that it exhibits proton conductivity [4], as well as ferroelectricity at the nanoscale [5]. Figure 1 shows the Cu/HAp/Cu model considered in this work and its inverse permittivity profiles with one OH^- ion vacancy

at the positions indicated by arrows. We find that the position of the defects significantly affects the permittivity profile. However, it is difficult to understand the underlying mechanism due to rather large relaxation of the lattice induced by introduction of a single vacancy.

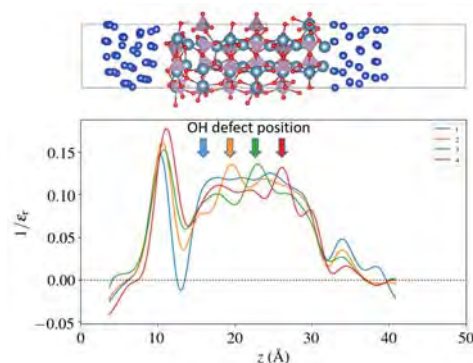


Figure 1 Cu/HAp/Cu model and the calculated inverse permittivity profile with OH^- vacancies.

References

- [1] S. Kasamatsu et al., Phys. Rev. B **84** (2011) 085120.
- [2] S. Kasamatsu et al., Phys. Rev. B **92** (2015) 115124.
- [3] G. Kresse et al., Phys. Rev. B **54** (1996) 11169.
- [4] M. Yashima et al., J. Phys. Chem. C **118** (2014) 5180.
- [5] S. B. Lang, Phase Transitions **89** (2016) 678.

Theory of molecular Rydberg states by light-mass impurities in semiconductors: tunneling current and strong luminescence properties

Takashi NAKAYAMA

Department of Physics, Chiba University

1-33 Yayoi, Inage, Chiba 263-8522

Tunneling field-effect transistor (TFET) is one of the promising candidates for replacing conventional Si-MOSFETs and realizing energy-saving future devices. However, the current is low for Si-TFETs because the tunneling corresponds to weak indirect transitions between valence and conduction bands. Recent experiments showed that the tunneling current is remarkably enhanced by the codoping of Al and N impurities. However, it has not been clarified why such codoping increases the current. One purpose of the present project is to clarify what electronic structures are realized by various cation+anion pairs and answer this question using the first-principles calculation. On the other hand, it was also found in recent experiments that N or O-atom doping into III-V and II-VI semiconductors promotes strong optical transitions useful for solar-cell applications. The other purpose is to clarify why so strong transition occurs in N/O-doped III-V/II-VI semiconductors.

We first doped III+N and III+O pairs in a large unit cell made of 521/1024 Si atoms as shown in Fig.1(a) and studied which type of pair structure is the most stable using the formation energy. We found that the nearest-neighboring substitutional pair is the most stable for Al+N, Ga+N, and In+N dopings. This is because both III and N atoms have four-coordination covalent bonds as shown in Fig.1(b) and there is no electron-occupied state in the band gap of Si as shown in Fig.2(a). In cases of B+N, Be+O, and Mg+O dopings, on the other hand, the substitutional+interstitial pair with a coordination number of three shown in Fig.1(c) is the most stable. This occurs due to the small atomic radius of these dopants and the lower energies of

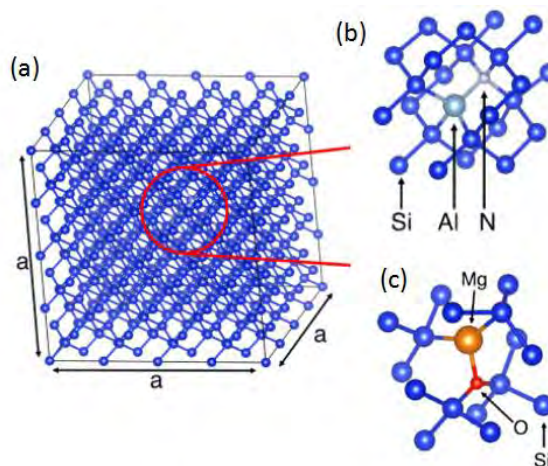


Fig.1. (a) Bulk Si₅₁₂ unit cell adopted in the present calculation. The most stable configurations of (b) Al+N and (c) Mg+O pairs embedded in Si.

N-2p and O-2p dangling bonds.

Then, we consider what electronic structures are produced by these pair dopants. Figures 2(a) and 2(b) show band structures of Al+N and Mg+O doped Si. In both figures, there appear electronic states in the band gap of Si. The electron-unoccupied state around 0.5 eV in the band gap of Al+N doped Si is mainly made of a N-3s orbital that is strongly hybridized with the conduction-band states of Si and is weakly localized around N with a localization length of around 20Å as shown in Fig. 2(c). In case of Mg+O dopant, on the other hand, the electron occupied state appears around 0.2 eV above the top of the valence bands of Si. This state is mainly made of a Mg-3s orbital that is slightly hybridized with the valence bands of Si. These band-gap states can increase the band-to-band transitions.

Next, we consider the tunneling-current feature

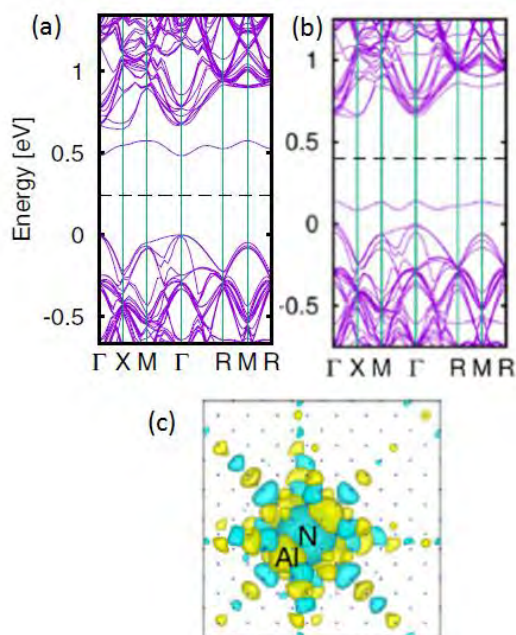


Fig.2. Calculated band structures of (a) Al+N and (b) Mg+O doped Si₅₁₂. Dashed line corresponds to the boundary between electron occupied and unoccupied bands. (c) Wavefunction of N-related unoccupied state that appears in the band gap of Al+N doped Si. Small dots indicate the positions of Si atoms.

when the Al+N pairs are doped in Si p-i-n device structures. Figure 3(a) shows the calculated tunneling probability as a function of tunneling length L between p and n-type Si layers, where we used calculated electronic states and assumed the constant applied voltage of 3.0 volt. From this figure, we know that the probability increases with decreasing L and that the probability is much larger for Al+N doped case compared to the band-to-band transition (BTBT) without doping. This is because the weakly localized electronic states shown in Fig.2(c) act as stepping stones for the tunneling transitions between the p- and n-Si layers.

Finally, we consider optical transition when N atom is doped in InP. Figure 3(b) shows calculated photo-absorption spectra as a function of photon energy. We can see that the absorption is markedly enhanced around/below the direct band gap of InP. This occurs due to the weakly localized N-orbital states that are hybridized with the conduction bands of host InP.

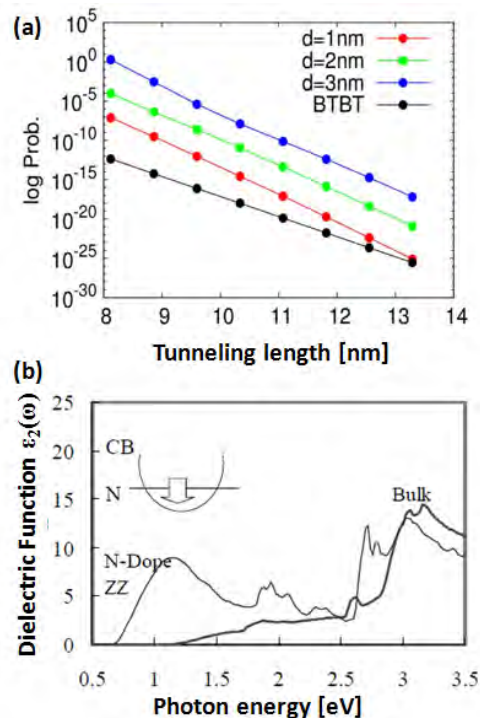


Fig.3. (a) Calculated tunneling probability between valence and conduction bands at Si p/n junction, as a function of p-i-n junction length L . BTBT corresponds to transition without dopants, while the others to those with Al+N dopants. (b) Photo-absorption spectra of N-doped InP as a function of photon energy. Inset shows schematic band structure.

From these calculations, we can conclude that all these unique conductive and optical properties of N/O doped systems originate from the large electron negativity of N/O atoms. In fact, when we consider other V-family dopants such as P and As with III atoms, we have no electronic states in the band gaps of semiconductors.

All these calculations were performed using the xTAPP and VASP codes. In order to realize calculations for the present impurity-doped systems, because the system is made of a large number of atoms (500-1000 atoms), the advanced computing facility having higher-speed CPU (more than 100G Flops), larger-size memory (around 100GB), larger-size storage (more than 1.0TB), and a multi-task operation is indispensable. These conditions are realized only by the supercomputing systems of the ISSP.

Ab initio calculation for superconducting parameters

Kazuma NAKAMURA

*Quantum Physics Section, Kyushu Institute of Technology
1-1 Sensui-cho, Tobata, Kitakyushu, Fukuoka, 804-8550*

We estimated superconducting transition temperature T_c of weak-coupling material Al and strong-coupling one Nb from first principles via the McMillan-Allen-Dynes formula as

$$T_c = \frac{\omega_{\log}}{1.2} \exp \left[-\frac{1.04(1 + \lambda)}{\lambda - \mu^*(1 + 0.62\lambda)} \right] \quad (1)$$

where ω_{\log} is the characteristic phonon frequency, λ is the electron-phonon coupling, and μ^* is the Coulomb pseudo potential. The program code for the parameter derivation was made originally.

First-principles calculations were performed using Tokyo Ab-initio Program Package (xTAPP) with plane-wave basis sets, where norm-conserving pseudopotentials and the generalized gradient approximation of the exchange-correlation potential with partial core correction were employed. The cutoff energies for the wave function and charge densities are 36 and 144 Ry for Al and 64 and 256 Ry for Nb, respectively, and $21 \times 21 \times 21$ k -point sampling was employed. The integral over the Brillouin zone was evaluated by the Methfessel-Paxton method with a broadening of 0.27 eV for Al and 0.81 eV for Nb. The density of states at the Fermi energy was estimated to be 0.185/eV/spin for Al and 0.837/eV/spin for Nb, which are consistent with the past estimate.

Phonon calculations were performed with the help of PHONOPY with the supercell approach. The $4 \times 4 \times 4$ and $8 \times 8 \times 8$ supercells were employed for Al and Nb, respectively. The electron-phonon coupling λ was evaluated with the frozen-phonon approximation

and calculated for the $2 \times 2 \times 2$ q phonon modes and the $21 \times 21 \times 21$ k wave functions. The Coulomb pseudo potential μ^* was evaluated within the random-phase approximation using the *ab initio* many-body perturbation code RESPACK.

Figure 1 displays *ab initio* phonon dispersion for Al and Nb, which are compared with experimental data (blue dots) [1, 2]. The Debye frequency was estimated as 448.73 K for Al and 298.69 K for Nb.

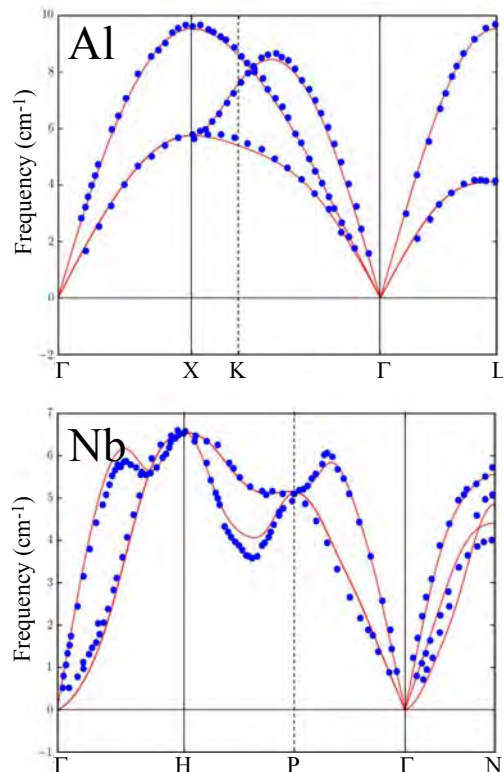


Figure 1: Calculated *ab initio* phonon dispersion of Al and Nb, where blue dots denotes experimental data taken from Ref. [1] for Al and Ref. [2] for Nb.

Table 1 compare our calculated superconducting parameters ($\omega_{\log}, \lambda, \mu^*, T_c$) with other theoretical [3, 4, 5, 6, 7] and experimental values [8, 9]. Our code gives reasonable agreements with the past data. We note that the μ^* of Ref. [4] is set to reproduce the experimental T_c .

Table 1: Calculated superconducting parameters of Al and Nb.

Al	ω_{\log} (K)	λ	μ^*	T_c (K)
present	248	0.46	0.10	2.0
Ref. [3]	308	0.42	0.11	1.4
Ref. [4]	270	0.44	0.12	1.2
Ref. [5]	-	0.45	-	-
Ref. [6]	-	0.45	-	-
Ref. [7]	-	-	0.10	-
Expt.	-	0.42 [8]	-	1.2 [9]

Nb	ω_{\log} (K)	λ	μ^*	T_c (K)
present	199	1.36	0.14	18.2
Ref. [3]	164	1.31	0.13	14.5
Ref. [4]	185	1.26	0.21	10.5
Ref. [5]	-	1.33	-	-
Ref. [7]	-	-	0.13	-
Expt.	-	1.22 [8]	-	9.3 [9]

References

- [1] R. Stedman, G. Nilsson, Phys. Rev. **145**, 492 (1966).
- [2] M. Holt, P. Czoschke, H. Hong, P. Zschack, H. K. Birnbaum, T.-C. Chiang, Phys. Rev. B **66**, 064303 (2002).
- [3] R. Akashi, K. Nakamura, R. Arita, M. Imada, Phys. Rev. B **86**, 054513 (2012).
- [4] S. Y. Savrasov, D. Y. Savrasov, Phys. Rev. B **54**, 16487 (1996).
- [5] R. Bauer, A. Schmid, P. Pavone, D. Strauch, Phys. Rev. B **57**, 11276 (1998).
- [6] M. M. Dacorogna, M. L. Cohen, P. K. Lam, Phys. Rev. Lett. **55**, 837 (1985); P. K. Lam, M. M. Dacorogna, M. L. Cohen, Phys. Rev. B **34**, 15065 (1998).
- [7] K.-H. Lee, K. Chang, M. L. Cohen, Phys. Rev. B **52**, 1425 (1995); K.-H. Lee, K. Chang, Phys. Rev. B **54**, 1419 (1996).
- [8] For a review, see, e.g., E. L. Wolf, in *Principles of Electronic Tunneling Spectroscopy* (Oxford University Press, New York, 1985).
- [9] N. W. Ashcroft and N. D. Mermin, Solid State Physics (Thomson Learning, Singapore, 1976).

Large-scale device-material research by massively parallel electronic structure calculation and data science

Takeo Hoshi and Hiroto Imachi (*)

Department of Applied Mathematics and Physics, Tottori University,

4-101 Koyama-Minami, Tottori 680-8550, Japan;

(*) Present affiliation: *Preferred Networks, Inc.*

The present project was carried out for the joint research between electronic structure calculations and data science. Mathematical studies and first principle studies were also carried out. The main collaborators are Yusaku Yamamoto (U. Elec. Comm.) and Kentaro Kinoshita (Tokyo U. Sci.).

The large-scale electronic-state and transport calculations were carried out for flexible organic devices. [1-4] Our parallel electronic structure calculation code ELSESES (<http://www.elses.jp>) was used for 10^8 -atom condensed polymers and presents a transport mechanism through the dynamical small polymer networks. Quantum transport was carried out by the wavepacket dynamics for hole. The calculations are realized with *ab initio* based tight-binding formulations.

Figure 1 shows a preliminary result for our machine learning research [3,4]. A classification analysis of the disordered polymer structures with the k-means clustering method, a typical data scientific analysis method. The analysis will be used as a prescreening procedure of real transport simulations. A part of the research was

realized by the collaboration with Weichung Wang (National Taiwan U.).

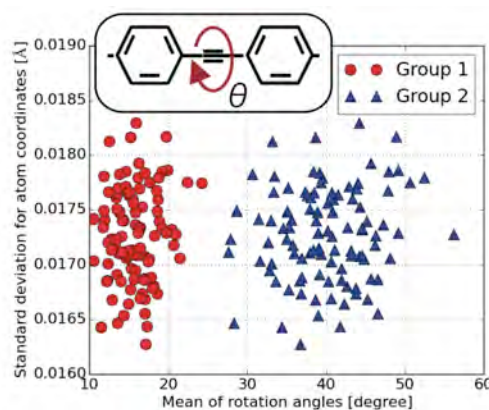


Fig. 1 A data scientific analysis (classification problem) for disordered organic polymer structures.

As mathematical studies, we analyzed convergence properties of the serial block Jacobi method for the symmetric eigenvalue problems and proved its quadratic convergence [5]. We also implemented the block Jacobi method on the system B at ISSP and showed that it is faster than ScaLAPACK under certain conditions. [6]

First principle calculations with experiments were carried out for Resistive Random Access Memory (ReRAM). [7,8] Practical use of ReRAM depends on thorough

understanding of the resistive switching (RS) mechanism in transition metal oxides (TMOs). We discuss what determines resistance values in a Pt/polycrystalline TMOs (NiO, CoO, MgO)/Pt ReRAM structures by using both experiments and first-principles calculations with a first-principles calculation program PHASE/0. Electrical measurements suggest that the RS is caused in the grain boundaries of TMO films. First-principles calculations indicate that slight displacements of atoms with a small energy change of 0.04 eV per atom on the surfaces exposed in the grain boundaries can drastically change conductivities. We newly propose the tiling model, in which grain surfaces are composed by insulating and conductive micro surface structures, and the surface resistances are determined by the tiling patterns. The research was collaborated with Satoru Kishida (Tottori U), Takahiro Yamasaki, and Takahisa Ohno (NIMS).

References

- [1] H. Imachi, S. Yokoyama, T. Kaji, Y. Abe, T. Tada, T. Hoshi, ‘One-hundred-nm-scale electronic structure and transport calculations of organic polymers on the K computer’, AIP Conf. Proc. 1790, 020010, 4pp. (2016)
- [2] T. Hoshi, H. Imachi, K. Kumahata, M. Terai, K. Miyamoto, K. Minami and F. Shoji, ‘Extremely scalable algorithm for 10^8 -atom quantum material simulation on the full system of the K computer’, Proc. ScalA16 in SC16, pp.33-40, (2016).
- [3] H. Imachi, Y. M. Tsai, T. Hoshi, W. Wang, ‘A data scientific research on organic polymer device materials’, in *The 19th Asian Workshop on First-Principles Electronic Structure Calculations*, National Chiao Tung University, Hsinchu, Taiwan, 31. Oct.- 2. Nov. (2016).
- [4] H. Imachi, ‘Numerical methods for large-scale quantum material simulations’, D. Thesis, Tottori University, 17. Jan. (2017).
- [5] S. Kudo, Y. Yamamoto, M. Becka, M. Vajtersic, ‘Performance analysis and optimization of the parallel one-sided block Jacobi SVD algorithm with dynamic ordering and variable blocking’, *Concurrency and Computation: Practice and Experience*, to appear (DOI : 10.1002/cpe.4059)
- [6] G. Oksa, Y. Yamamoto, M. Vajtersic, ‘Asymptotic quadratic convergence of the serial block-Jacobi EVD algorithm for Hermitian matrices’, *Numerische Mathematik*, to appear (DOI : 10.1007/s00211-016-0863-5).
- [7] T. Moriyama, T. Yamasaki, S. Hida, T. Ohno, S. Kishida, and K. Kinoshita, ‘Switching mechanism in resistive random access memory by first-principles calculation using practical model based on experimental results’, *Jpn. J. Appl. Phys.*, Accepted.
- [8] T. Moriyama, T. Yamasaki, T. Ohno, S. Kishida, and K. Kinoshita, ‘Resistance given by tiling grain surface with micro surface structures in polycrystalline metal oxide’, *J. Appl. Phys.* Vol. 120, 215302 (2016)

Search for magnet and spintronics materials based on materials informatics

Tomoki YAMASHITA

*Center for Materials Research by Information Integration, National Institute for Materials Science
Sengen, Tsukuba, Ibaraki 305-0047*

Sm-Co and Nd-Fe-B intermetallic compounds are known for high-performance rare-earth permanent magnets which are one of the key materials in magnetic and energy conversion devices. For material search of permanent magnets, developments of basic methods with data-driven approaches have been highly desired because of the rapid growth of supercomputer performances. One of difficulties in finding new permanent magnet materials is how to predict the complex crystal structures. For example, the best magnet, $\text{Nd}_2\text{Fe}_{14}\text{B}$, contains 68 atoms in the unit cell. This system is quite difficult to predict the crystal structure because number of configuration explosively increases as atoms increase. In this study, we have developed and investigated methods of crystal structure predictions to overcome those difficulties. First, random search algorithm in combination with structure optimization technique using first-principles calculations was employed. Furthermore, Bayesian optimization method was added to accelerate crystal searches.

Crystal structure prediction simulations were tested for Y_2Co_{17} by using both random search algorithm and Bayesian optimization. In the random search simulations, we randomly generated several hundreds of crystal structures. For the generated structures, total energy calculations and structure optimization were carried out using the density functional theory with the projector-augmented wave method [1], as implemented in the VASP

code [2]. We carried out several random search simulations using supercomputer system at ISSP. Total number of calculated structures was several thousands. We checked efficiency of Bayesian optimization by using the structure and energy data set obtained by random search simulations. Our simulations with Bayesian optimization show highly efficient results compared to the random search algorithm. We succeeded developing a new algorithm for crystal structure prediction.

References

- [1] P.E. Blöchl: Phys. Rev. B **50** (1994) 17953.
- [2] G. Kresse and J. Furthmüller: Phys. Rev. B **54** (1996) 11169.

Theoretical study on electrode materials for sodium ion batteries

Atsuo YAMADA

*Department of Chemical System Engineering,
The University of Tokyo, Hongo, Bunkyo-ku, Tokyo 113-8656*

Sodium ion batteries have received much attention in recent years due to its abundance and potential low cost, which may offer large scale applications such as smart grids and electric vehicles. With a purpose of developing electrode materials, we have studied (i) intrinsic electrochemical properties of $\text{Na}_2\text{Fe}_2\text{Si}_2\text{O}_7$ and (ii) reaction mechanism of the hard carbon.

A sodium pyrosilicate $\text{Na}_2\text{Fe}_2\text{Si}_2\text{O}_7$ is an appealing cathode materials which was successfully synthesized in our group. However, very limited reversible capacity was observed at present. Towards practical utilizations, we applied density functional theory calculations to elucidate the intrinsic bulk properties of $\text{Na}_2\text{Fe}_2\text{Si}_2\text{O}_7$ such as volume change, voltage, electronic structure, and charge carrier transport. From our calculations, volumetric change during charging-discharging process, Na-ion migration energy, and polaron migration energy are found to be reasonable for active electrochemical intercalations at room temperature. Therefore, the origin of limited reversible capacity remains to be determined,

and further work is necessary to activate this intriguing cathode material.

Hard carbon is one of the most promising anode material for the sodium-ion battery owing to its large reversible capacity. However, the reaction mechanism has not been fully elucidated. We built several models of hard carbon with a graphene sheet that have typical point defects (MV, DV, SW). Then the sodiation and lithiation potential of the alkali adatom on the defective graphene was calculated. As a result, it was found that the adsorption potential of alkali ions was increased to positive values by introduction of defects. In particular, MV and DV enhanced adsorption, and its effects were not dependent on alkali species. Consequently, it was revealed that charge-discharge reaction at high potential of hard carbon is caused by adsorption / desorption of alkali ions to defects.

All the calculations were performed using VASP code. The GGA/PBE functional and PAW method were employed for all the calculations. We used F4cpu, F18acc and F36cpu queues.

Spontaneous Distortion via Quantum-well Induced Ferromagnetism in Pd(100) Ultrathin Films

Shunsuke SAKURAGI,¹ Hiroyuki KAGESHIMA,² and Tetsuya SATO^{1,*}

¹*Department of Applied Physics and Physico-Informatics,
Keio University, Hiyoshi, Yokohama 223-0061*

²*Interdisciplinary Graduate School of Science and Engineering,
Shimane University, Nishikawatsu-cho, Matsue 690-8504*

Recently, we found the appearance of ferromagnetism in the ultrathin film of Pd(100) periodically depending on the film thickness [1]. The period was consistent with the first-principles calculation, which predicted the appearance of ferromagnetism based on d -electron quantum-well states in Pd(100). From the surface x-ray diffraction experiments, we have shown the appearance of ferromagnetism in Pd(100) films promotes the atomically flat film growth which is accompanied by spontaneous lattice expansion. In order to clarify the origin of the correlation between magnetism and crystal structure, we performed the density functional calculation [2].

The PHASE/0 program using the PAW method to the spin-polarized local density approximation reported was used. The values of lattice constant converged to 3.84 Å for fcc bulk Pd, and we used this value for film shaped Pd(100). To evaluate the magnetism of Pd(100) ultrathin films, the slab of Vacuum(2 monolayers)/Pd(N monolayers)/Vacuum(3 monolayers), $56 \times 56 \times 1$ k -points, and 36 Ry of cut off energy were used. Based on this, we calculated the difference of total energies between paramagnetic and ferromagnetic states where the spin polarization is fixed to a certain value in freestanding Pd(100).

Based on the density functional calculation, we discovered that when the ferromagnetism

was appeared in Pd(100) ultrathin films due to increase of the density of states near the Fermi energy induced by quantum-well states, Pd films expanded the lattice constant in order to suppress the increase in kinetic energy of electrons accompanied by occurring of the exchange splitting. This finding reveals an effect that the transition metal spontaneously regulates the electronic states; i.e., inverse mechanism of Stoner's theory, in order to stabilize ferromagnetic state. This energy gain due to stabilizing of ferromagnetic state reduces the surface energy of Pd(100) films, and makes the film flat and uniform structure. This mechanism can explain our surface x-ray diffraction experiments, and indicates the existence of closely relationship between magnetism, crystal structure, and quantum-well states which are the specific electronic states of confined electrons in nanoscale films. This finding gives us the key to understanding the origin of ferromagnetism in nano-film shaped metals, and thus, this indicates the possibility of creating a nano-material with a desired magnetism by processing nonmagnetic metals artificially.

References

- [1] S. Sakuragi *et al.*: Phys. Rev. B **90** (2014) 054411.
- [2] S. Sakuragi, H. Tajiri, H. Kageshima, and T. Sato: arXiv:1612.06216.

Structural analysis of titanium dioxide by first-principles calculation

Kanakano YOSHIZAWA

*Research Organization for Information Science and Technology,
Kobe, Hyogo 650-0047*

Titanium dioxide (TiO_2) has attracted an increasing amount of attention in recent years due to its numerous technological applications. TiO_2 is a widely used photocatalytic material with many potential application in electronics, optoelectronics, and photovoltaics. It is well-known that TiO_2 can lose oxygen, resulting in the formation of both bulk and surface vacancies. Impurity hydrogen (H) and oxygen vacancy (V_O) affect electronic properties of TiO_2 and we study the effect of H doping of it.

Therefore, we pay attention to the effect of H doping of TiO_2 , and there are excess electrons accompanying H or V_O . It is known that the electrons can localize at Ti 3d orbitals, forming Ti^{3+} ions [1, 2]. The trapped electrons form small polarons that consist of the electrons coupled to the distortion of the lattice around the Ti^{3+} ions.

We examine the electronic structure of H in rutile TiO_2 by using DFT calculation. We calculated using VASP package [3] on System B and C in ISSP. The large scale calculation was carried in 216-atom supercell with HSE hybrid functional in DFT. The spin density for a localized electron in Ti site is shown in

Figure. It is verified that the excess electrons are described as localized small polaron by DFT calculation.

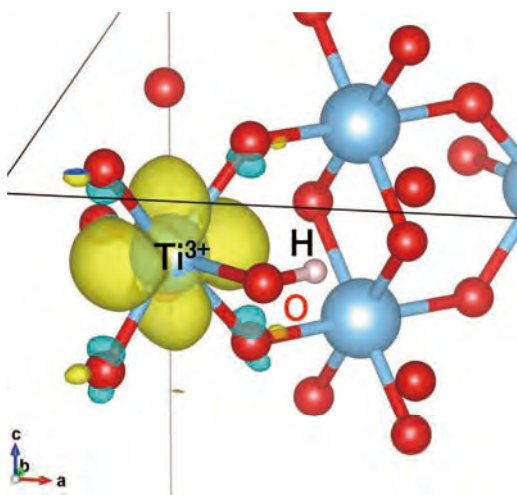


Figure: Spin density of a localized electron (small polaron) in Ti, forming Ti^{3+} ions in rutile TiO_2 by DFT calculation.

References

- [1] A. Janotti, C. Franchini, J. B. Varley, G. Kresse, and C.G. Van de Walle, *Phys. Status Solidi RRL* **7**, 199 (2013).
- [2] F. Filippone, G. Mattioli, P. Alippi, and A. Amore Bonapasta, *Phys. Rev. B* **80**, 245203 (2009).
- [3] <http://www.vasp.at>.

First-Principles Calculations of Electron and Spin Device Materials

Hiroyoshi MOMIDA, Motoyuki HAMAGUCHI, Hiroshi KATSUMOTO

Institute of Scientific and Industrial Research, Osaka University

8-1 Mihogaoka, Ibaraki, Osaka 567-0047

We have studied electronic properties of future electron and spin device materials using the first-principles method. In the fiscal year 2016, we have mainly investigate piezoelectric properties of wurtzite materials [1] using the supercomputer systems. We have also studied electronic structures of layered topological materials which consist of Bi_2Se_3 and PbSe layers [2]. In this project, the first-principles calculations were performed by using the HiLAPW code. The calculations are based on the density functional theory with the all-electron full-potential linearized augmented plane wave method.

Piezoelectricity of wurtzite materials

We perform the first-principles calculations of the piezoelectric constants of $w\text{-Sc}_x\text{Al}_{1-x}\text{N}$ in all the ranges of x . We find that piezoelectric e constants (e_{33}) of the $w\text{-Sc}_x\text{Al}_{1-x}\text{N}$ materials can be significantly enhanced as x increases from 0 to 0.75. In addition to the e_{33} enhancement, the elastic constant (C_{33}) softening due to the Sc substitution can contribute to the piezoelectric d constant (d_{33}) enhancement in the x ranges up to about 0.75. The wurtzite-type $\text{Sc}_x\text{Al}_{1-x}\text{N}$ materials have been experimentally obtained for x less than about 0.43, and our results predict that wurtzite-type $\text{Sc}_x\text{Al}_{1-x}\text{N}$ with higher x have a strong potential to further enhance the piezoelectric constants. Such higher piezoelectric $\text{Sc}_x\text{Al}_{1-x}\text{N}$ could be experimentally realized if we could stabilize the wurtzite-type phases at the high x range against the cubic-type phases, for exam-

ple, by doping an additional third element. We also study the element dependences on piezoelectricity in $w\text{-}A_{0.5}B_{0.5}\text{N}$ ($A = \text{Sc}, \text{Y}, \text{La}$ and $B = \text{Al}, \text{Ga}, \text{In}$). The result shows that Sc, Y, and La have the strongest effect on the enhancement of piezoelectric d constants in AlN , GaN , and InN , respectively. The calculated results are partly published in the journal [1].

Topological states in layered materials

Recently, interesting electronic structures of $(\text{PbSe})_5(\text{Bi}_2\text{Se}_3)_6$, which forms a natural heterostructure consisting of a topological insulator and an ordinary insulator, have been experimentally studied by the angle-resolved photoemission spectroscopy [3]. We have theoretically studied electronic band structures of $(\text{PbSe})_5(\text{Bi}_2\text{Se}_3)_6$, showing this material can have topological interface states in the bulk [2].

We partially used the system to clarify Li-ion battery reaction mechanism in transition-metal oxide cathodes and spectroscopic properties of circular dichroism in chiral materials, and the computations were partly done by Motoyuki Hamaguchi and Hiroshi Katsumoto in collaboration with Tamio Oguchi.

References

- [1] H. Momida, A. Teshigahara, and T. Oguchi: *AIP Advances* **6** (2016) 065006.
- [2] H. Momida *et al.*: in preparation.
- [3] K. Nakayama *et al.*: *Phys. Rev. Lett.* **109** (2012) 236804.

The effect of Cu addition to Nd-Fe-B magnets studied by first-principles calculations

Yasutomi TATETSU

The University of Tokyo, Hongo, Bunkyo, Tokyo 113-0033

Nd-Fe-B sintered magnets are used in various kinds of applications, mostly in motors since they have the largest $(BH)_{\max}$ among other permanent magnets. However, the magnetic instability, especially the coercivity decrease at high temperatures, is a critical issue in order to keep its good performance. Controlling the grain boundary phase by annealing processes or doping some elements is the most effective way in terms of improving the coercivity of Nd-Fe-B magnets.

We performed first-principles calculations for the Cu-doped $\text{Nd}_2\text{Fe}_{14}\text{B}/\text{Nd}_4\text{O}$ systems using a computational code OpenMX [1] in order to understand these electronic and magnetic structures. We chose Nd_4O as the subphase, which existence around the grain boundaries is confirmed by the experimental and theoretical studies [2, 3]. One Cu atom is existing around the interface of the grain-boundary-model structures. By calculating the formation energies of these model structures, we found that the models with Cu existing at the interstitial space and Fe site at the interface are energetically stable compared to the non-Cu-doped model structure. Especially, in the model with Cu at the Fe site at the interface, the magnetic anisotropy K_1 of Nd near Cu at the

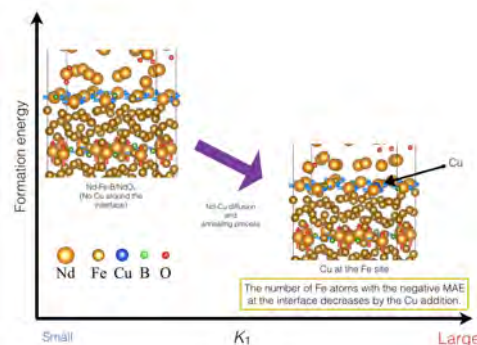


Figure: Schematic image of the relationship between the formation energy and the magnetic anisotropy of Nd at the interface based on our theoretical study. interface is improved due to Cu, which is in good agreement with experimental results (see Figure) [4]. We conclude that adding Cu to Nd-Fe-B magnets works effectively in terms of improving the magnetic anisotropy K_1 of Nd atoms at the interface of Nd-Fe-B magnets since the magnetic anisotropy of Nd is strongly related to the coercivity of Nd-Fe-B magnets [5].

References

- [1] <http://www.openmx-square.org>
- [2] T. Fukagawa and S. Hirosawa, J. Appl. Phys. **104**, 013911 (2008).
- [3] H. Misawa, Dr. Thesis, Faculty of Science, The University of Tokyo, Tokyo, (2015).
- [4] H. Sepehri-Amin *et al.*, Acta Mater. **60**, 819 (2012).
- [5] Y. Tatetsu, S. Tsuneyuki, and Y. Gohda, Phys. Rev. Appl. **6**, 064029 (2016).

Development and application of the large-scale GW calculation code

Ikutaro HAMADA

*Center for Green Research on Energy and Environment Materials ,
National Institute for Materials Science, 1-1 Namiki, Tsukuba 305-0044*

The electronic structure method based on density functional theory (DFT) has been used to study a wide range of materials, including bulk insulators, semiconductors, metals, and interfaces, and proven accurate and useful for in the researches of chemistry, physics, and materials science. However, DFT within the local density and generalized gradient approximation is known to suffer from several drawbacks, such as the band-gap underestimation. To get rid of the shortcomings of semilocal DFT, many-body perturbation theory within the GW approximation has been used to calculate more accurate electronic structure. Despite the theoretical and methodological development, the applicability of the GW method is limited, because of its complexity.

To overcome the limitation and apply the GW method to calculate accurate electronic structure of large-scale systems such as nanoparticles, aqueous solutions, and interfaces, an efficient method has been developed: The method uses the eigenpotential of static dielectric matrix as an efficient basis set for the polarizability, and the Lanczos method is used

to compute the frequency dependent polarizability of Green's function. The latter allows one to perform efficient frequency integration to calculate the electron self-energy, and to avoid the plasmon-pole approximation. The above algorithms are implemented in the WEST code [1].

In this work, we extend the applicability of the WEST code. We have introduced the spin-orbit coupling to WEST in a nonperturbative way, and accurate calculations of electronic properties of molecules and materials containing heavy elements are possible [2]. We also introduced general k-points WEST for efficient and accurate calculations of solids. A systematic benchmark calculations are under progress [3].

References

- [1] M. Govoni and G. Galli, *J. Chem. Theory Comput.* 11, 2680-2696 (2016).
- [2] P. Scherpelz, M. Govoni, I. Hamada, and G. Galli, *J. Chem. Theory Comput.* 12, 3523 (2016).
- [3] I. Hamada, M. Govoni, and G. Galli (in preparation)

Ab initio molecular dynamics study of static structure of glasses

Akihide KOURA

Student Affairs Department,

Kumamoto University, Kurokami, Kumamoto, Kumamoto 860-8555

We have studied static structure, electronic and dynamic properties of liquid, crystal, and glassy systems. In this project, we focused on the static structure of network forming glasses under pressure by using *ab initio* molecular dynamics simulations.

We have studied the static structure of ternary silver germanium triselenide ($\text{Ag}_x(\text{GeSe}_3)_{1-x}$) glass ($x = 0.15, 0.33, 0.5$). At $x \geq 0.33$, these glasses show properties of super ionic conductor, in which silver atoms migrate inside the GeSe_3 network glass. It is suggested experimentally that silver atoms make chain-like fragments at the concentration $x = 0.5$ [1], however, stable sites of silver atoms are still unclear. Our simulations confirmed that silver atoms replace germanium atoms. Furthermore, three-body bond angle distributions for Ge-Se-A ($A=\text{Ge}, \text{Ag}$) and Se-A-Se are wider than those without silver atoms. Ag-Ag fragments consisting of weak covalent bonds are confirmed not only at the concentration $x = 0.5$ but also $x = 0.33$ and 0.15 . However, in the present simulation, only 6 silver atoms exist in the system at $x = 0.15$, so

we need to enlarge the system to remove the problem of size dependence.

We have also studied the pressure dependence of the static structure of liquid GeTe [2]. The pressure and temperature ranges are from 0 to 250 GPa and 1000 to 4000 K, respectively. Liquid GeTe has a semiconducting property at ambient condition. With increasing pressure, the semiconductor-metallic transition occurs at approximately 12 GPa. At ambient and low pressure range up to 12 GPa, there exists Peierls-type distortion, where atoms are threefold-coordinated, even in the liquid state. However, the distortion disappears at about 12 GPa, and coordination numbers (CN) increases with increasing pressure. Finally, CN reaches 13.7 at approximately 250 GPa, which is quite similar to that of CsCl-type bcc crystalline state with taking the second neighbor into account.

References

- [1] K. Ohara, *et al.*: J. Phys. Soc. Jpn. **79** (2010) Suppl. A, 141.
- [2] A. Koura and F. Shimojo: submitted to LAM-16 conference proceedings.

First-Principles Molecular Dynamics Study of Biomolecule Synthesis Induced by Meteorite Impacts on Primitive Ocean

Kohei Shimamura

Graduate School of System Informatics,

Kobe University, 1-1 Rokkodai, Nada-ku, Kobe 657-8501

Whereas recent experimental simulations suggested that meteorite impacts on primitive ocean could provide a large amount of various biomolecules such as proteinogenic amino acids, the production process has not been well understood. To address this issue from the atomistic viewpoint, we have performed first-principles molecular dynamics in combination with multi-scale shock technique (MSST) simulations, where the MSST method was used to reproduce the behavior of moving atoms in shock waves. Since impact velocities of meteorites generally exceed the sound speed, a shock waves are generated.

In this study, in particular, we focused on investigation of how the production of ammonia, which is important nitrogen source for most biomolecules, is produced by the meteorite impacts [1-2]. We firstly prepared a calculation model consisting of nitrogen, water, and metallic iron contained in the meteorite, which imitated the environment of the early Earth. We applied a shock wave to this model to reproduce a meteorite impact and investigate the detailed production reaction pathways using population analysis.

We found that meteorite impacts of meteorites could drive three ammonia production mechanisms. The two are associative and dissociative mechanisms of nitrogen on the iron surface. The former and the latter are the mechanisms as seen in the catalysis of nitrogenase enzyme and in the Haber-Bosch process, respectively, both of which are currently supplying a large amount of ammonia to life. Meanwhile, in the remaining one mechanism, ammonia was produced away from the iron surface by reduction of nitrogen through the formation of hydrazine. Hydrazine has been regarded as an important precursor in the electrocatalytic synthesis of ammonia.

The emergence of such multiple production mechanisms capable of providing a large amount of ammonia induced by the meteorite impacts would have played a key role in the origin of life on Earth.

References

- [1] K. Shimamura, F. Shimojo, A. Nakano, and S. Tanaka: *Sci. Rep.* **6** (2016) 38953.
- [2] K. Shimamura, F. Shimojo, A. Nakano, and S. Tanaka: *Phys. Chem. Chem. Phys.* accepted.

Search and realization of novel electronic properties of solid surfaces and small particles

Takeshi INAOKA

*Department of Physics and Earth Sciences, Faculty of Science,
University of the Ryukyus, 1 Senbaru, Nishihara, Okinawa 903-0213*

In first-principles calculations of semiconductor surfaces, we usually assume a periodic array of slabs, and describe the electronic structure in terms of a plane-wave basis set. Recent remarkable progress of supercomputers has realized those large-scale slab calculations which can adequately treat surface-resonance states extending deeply into the substrate. On the other hand, strain engineering is expected to achieve higher operation performance of Si devices through modification of the band structure, since the conventional downsizing approach is showing its limitations. Using the program package 'Vienna Ab initio Simulation Package' (VASP) [1,2], we analyzed the strain effect on the electronic structure of the Si(001)-2x1 surface.

Presence of a dynamic dipole moment in the gap between the scanning tunneling microscope (STM) tip and the substrate produces a giant dynamic dipole moment through formation of the localized surface plasmons (LSPLs). It is reported that vibration-induced structures appear around the cutoff energy in the light-emission spectra from this enhanced dipole. Assuming a dynamic dipole moment in the STM gap, we examined the effect of phonon vibration of an admolecule on the LSPLs, and consequently on the enhanced total dipole moment.

(1) Compressive strain effect on the electronic structure of the Si(001)-2x1 surface [3]

Last year, we investigated the biaxial strain effect on the electronic structure of the Si(001)-2x1 surface. This year, we have examined the effect of uniaxial compressive strain in the $[\bar{1}10]$ (fundamental period) direction and in the $[110]$ (twofold period) direction. We assumed a 30 atomic-layer slab, and

terminated dangling bonds on the other side by hydrogen atoms. We considered normal tensility and internal strain in structure optimization under the normal-stress free condition.

As an example of the results, figure 1 shows the valence-band dispersion on the $\bar{\Gamma}-\bar{J}'$ line of the surface Brillouin zone when 2% uniaxial compression is applied in the $[\bar{1}10]$ direction. The $\bar{\Gamma}-\bar{J}'$ line corresponds to the compression direction. In this strain direction, a small-effective-mass band protrudes at the valence-band top. The dispersion of this protruding band agrees with that of the bulk band when the same strain is applied. This indicates that this band originates from the valence band of the semi-infinite system. The red circles represent the surface or surface-resonance states which can be identified

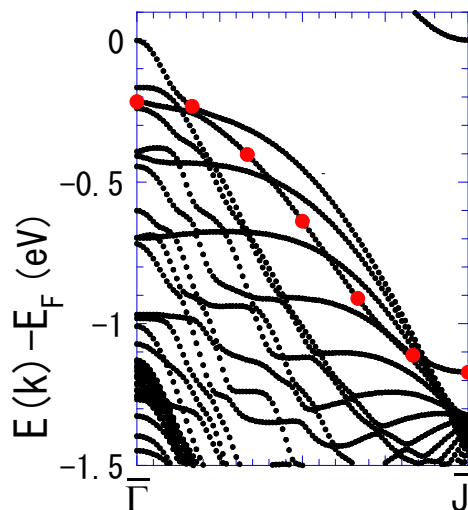


Fig. 1 Valence-band dispersion of the Si(001)-2x1 surface on the $\bar{\Gamma}-\bar{J}'$ line of the surface Brillouin zone under 2% uniaxial compressive strain in the $[\bar{1}10]$ direction. The red circles represent surface or surface-resonance states.

by analyzing the charge-density distribution of each state. These states are found to penetrate into the valence band of the semi-infinite system except near the \bar{J} point. The protruding dispersion in the strain direction is the same for uniaxial compression in the $[110]$ direction.

In each of these strain directions, the wave function at the top of this protruding band is connected closely in the strain direction, and this strong coupling is correlated with the energy increase of this valence-top state due to the compression. When the uniaxial compression is applied in the axis direction of the asymmetric surface dimer, buckling in the dimer becomes stable, which leads to the energy lowering of the surface (resonance) states relative to the valence band of the semi-infinite system.

(2) STM-enhanced dynamic dipole moments coupled with adsorbate vibration at substrate or tip surfaces [4]

We investigated the effect of phonon vibration of an admolecule in the STM gap on the enhanced total dipole for three models. In the model A, we considered the vibration of the dynamic point dipole near the substrate surface. In the models B and C, we assumed that the dipole arises from a tunneling current between an admolecule

and the substrate or tip surface. In the model B (C), the admolecule is at the substrate (tip) surface. In any of the three models, the phonon vibration of an admolecule in the gap produces a series of the resonance modes, each of which is shifted in energy from the corresponding mode involving no phonon by a multiple of the phonon energy $\hbar\omega_p$. If we pay attention to the intensity ratio of the phonon-shift resonance to that of the no-shift resonance as an indicator of detectability of the shifted resonance, the phonon effect is most remarkable in the model C, because the vibration of the admolecule is closest to the tip.

Presence of a dynamic dipole p_0 of angular frequency ω in the gap gives rise to an enhanced dipole $p_0 F_k(\omega)$ with angular frequency $\omega + k\omega_p$ ($k=0, \pm 1, \pm 2$) including phonon shifts. Figure 2 exhibits the ω dependence of $|F_k(\omega)|$ in the model C for $k=0$ and ± 1 when the tip and substrate are made of silver. The gap distance D , the tip curvature radius R , the height of the admolecule position h_0 , the phonon energy $\hbar\omega_p$, and the phonon vibration amplitude a_p are taken to be $D=10$ Å, $R=200$ Å, $h_0=7$ Å, $\hbar\omega_p=0.1$ eV, and $a_p=1$ Å, respectively. The dynamic dipole in the gap induces the LSPLs, which leads to a strongly enhanced total dipole. The resonance-peak energy of $k=1$ (-1) is lower than (higher) than the corresponding peak energy of $k=0$ by $\hbar\omega_p$. The resonance intensity of the phonon-shifted peak is considerable in this model, because the phonon vibration of the admolecule is close to the tip.

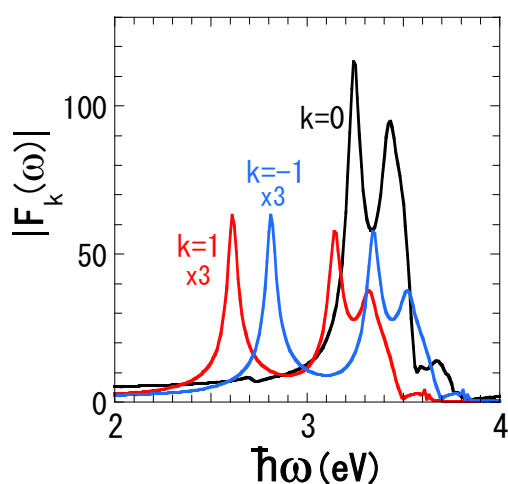


Fig. 2 ω dependence of the dipole enhancement $|F_k(\omega)|$ for $k=0$ and ± 1 in the model C where an admolecule at the tip surface vibrates with $\hbar\omega_p=0.1$ eV.

References

- [1] G. Kresse and J. Hafner: Phys. Rev. B **47** (1993) 558–561.
- [2] G. Kresse and J. Furthmüller: Comput. Mat. Sci. **6** (1996) 15–50.
- [3] T. Inaoka, S. N. Takeda, and T. Shirasawa: to be prepared.
- [4] T. Inaoka and Y. Uehara: submitted to J. Appl. Phys.

Hybrid *ab initio* QM/MM calculations of biological systems

Masaru TATENO

Graduate School of Life Science, University of Hyogo

To theoretically analyze the electronic structures that are relevant to the functional mechanisms of crucial biological macromolecular systems, we employed *ab initio* quantum mechanics (QM) calculations that are coupled to molecular mechanics (MM) classical calculations, with respect to the entire structures of the systems solvated with the explicit water. In our hybrid *ab initio* QM/MM calculations, our interface program is employed to connect highly-parallelized engines, gamess and amber, for the QM and MM calculations, respectively.

This FY, we analyzed the detailed electronic structural changes in the enzymatic reaction of a novel biological catalyst, and the analysis revealed the dynamical properties in the electronic structure. Interestingly, our findings are likely to be characteristic to biological macromolecular catalytic systems.

Here, our previous works should be introduced briefly: Our previous hybrid *ab initio* QM/MM MD simulations of leucyl-tRNA synthetase (LeuRS) complexed with the cognate tRNA that was mis-aminoacylated (threonyl) revealed that unexpectedly, the reaction of an “RNA-protein complex” is a “ribozymal” (RNA enzyme) self-cleavage reaction (not via a “protein enzyme”), but one in which the protein also plays a critical role. This was a novel catalyst, which operates via cooperation of the

“RNA enzyme” (the mis-aminoacylated threonyl-tRNA^{Leu}) and protein (LeuRS), and thus was referred to as “hybrid ribozyme/protein catalyst”.

In the present study, we investigated the dynamical changes that occur in the electronic structure of the catalytic site during the reaction, and observe dramatic rearrangements of functional importance in the molecular orbitals (MOs). The following two changes are particularly noteworthy.

One concerns the MO that contains a contribution from the nucleophile (a water molecule). It initially has a much lower energy than the HOMO, but it is activated as the reaction proceeds until it becomes the reactive HOMO. The other involves the reactive LUMO of anti-bonding character that emerges in the bond rupture that leads to products.

We term these processes dynamical induction of the reactive HOMO (DIRH) and LUMO (DIRL), respectively. In the complex environment of a biological macromolecule, the reactive HOMO and LUMO are likely to be hidden, and so these systems must implement DIRH and DIRL mechanisms that expose them. Thus, we conjecture that this is a characteristic feature that is specific to biological systems.

LeuRS is also a member of an enzyme family composed of aminoacyl-tRNA synthet-

ases (aaRSs). Eukaryotic aaRSs form a huge supercomplex composed of 20 types of aaRSs, each of which is corresponding to each of 20 amino acids, and thereby constitute a complicated reaction network. In general, most biological systems involve such biochemical reaction networks.

Analysis of such biochemical reaction networks has been a crucial target in various interdisciplinary fields, such as biophysics, complex systems, biochemistry, cell biology, etc., for a long time. Notably, theoretical analyses as well as experimental approaches have recently been important increasingly as a crucial issue of systems biology and bioinformatics, to understand the relationships between cellular responses/phenotypes and molecular mechanisms in detail.

This FY, we also analyzed the kinetics of biochemical reaction network systems. For this aim, we first decomposed cellular biochemical reaction cascades into building blocks, and investigated the mathematical features (e.g. the stability of the systems) of such elementary reaction units and their combinations, which are actually involved in real signal transduction cascades.

More specifically, in our present analysis, we focused on effects of the presence and absence of a positive feedback loop (PFL) that is combined with the above-mentioned elementary reaction cycles, by theoretically exploring the mathematical stability. As a consequence, we have discovered all the conceivable transitions, including the transition from the bistability (b) to the monostability (m) (i.e., the $b \rightarrow m$ transition), as well as the $m \rightarrow b$ transition, that were induced by the PFL,

depending on the parameter values.

Since in the previous works, the PFL reportedly induced only the latter, i.e., the $m \rightarrow b$ transition, this analysis is the first report to address the $b \rightarrow m$ transition induced by the PFL. Employing the resultant data, we also analyzed the detailed mechanisms of the $b \rightarrow m$ transition. As a result, the origin of the $b \rightarrow m$ transition was identified to be the significantly lower Michaelis-Menten constant in the PFL.

Moreover, based on the resultant data, we propose possible biological systems (e.g. iPS cell) where this type of transition may be induced, and discuss functional roles of the $b \rightarrow m$ transition, based on the mechanism that we theoretically elucidated. In this manner, this analysis also provides a new perspective in systems biology and complex systems, and a novel viewpoint to understand experimental data concerning the signal transduction network cascades, etc.

Further achievements of this FY are also cited as [3-5].

References

- [1] J. Kang, H. Kino, M. J. Field, and M. Tateno: *J. Phys. Soc. Jpn.* **86** (2017) 044801.
- [2] J. Kang and M. Tateno: *J. Phys. Soc. Jpn.* in press.
- [3] A. Sugimoto, J. Kang, T. Sumi, and M. Tateno: *J. Phys. Soc. Jpn.* in press.
- [4] J. Kang, K. Yamasaki, K. Sano, K. Tsutsui, K. M. Tsutsui, and M. Tateno: *J. Phys. Soc. Jpn.* **86** (2017) 014802.
- [5] S. Shimada, K. Shinzawa-Itoh, J. Baba, S. Aoe, A. Shimada, E. Yamashita, J. Kang, M. Tateno, S. Yoshikawa and T. Tsukihara: *EMBO J.*, **86** (2017) 291-300.

Novel Structures of Liquid Metal under Ultrahigh Pressures: ab initio Molecular-Dynamics Simulations

Satoshi OHMURA

Research Center for Condensed Matter Physics,,

Hiroshima Institute of Technology Saeki-ku, Hiroshima, 731-5143

We have studied static and dynamical properties of liquid metal and liquid semiconductor under extreme conditions (high pressure and high temperature) by *ab initio* molecular dynamics (MD) simulations. This year, we focused on liquid sodium under ultrahigh pressure and pressure induced metallization of liquid sulfur.

In the simulation, the electronic state was calculated using the projected augmented wave (PAW) method within the framework of density functional theory (DFT), in which the generalized gradient approximation was used.

From this simulation, it was found that liquid Na has asymmetric structure under ultra-high pressure at about a few hundred gigapascal. For liquid sodium, previous theoretical study suggested that pressure induced structural and electronic transition occur, analogous those observed in solid sodium. The relationship between this transition and the new structure observed in this study is currently under investigation.

We also performed *ab initio* MD simulation for liquid sulfur to investigate mechanisms of

pressure induced metallization in liquid semiconductor. It is well known that, at a temperature near the melting point, liquid sulfur is molecular liquid which consists of eight membered-ring molecules. When pressure increases, the ring breaks and forms chain and finally metallization occurs by breaking the chain. In this study, our *ab initio* MD simulations clarified the details of mechanism of the ring breakage and metallization under high pressure.

In addition to these liquids, we investigated charge dynamics in I-containing organic molecules under X-ray free electron laser (X-FEL) irradiation by a nonadiabatic quantum-mechanical MD simulation that incorporates electronic transitions through a surface-hopping approach. From the result of this simulation, it was found that holes generated in I by the X-FEL irradiation transfer from the iodine to the molecular counterpart in ~ 5 fs [1].

References

- [1] K. Nagaya, K. Motomura, E. Kukuk, Y. Takahashi, K. Yamazaki, S. Ohmura *et al.*, *Farad, discuss.* **194** (2016) 53

Exploring active sites of "Real" model catalysis via first principle calculations

Wataru Mizukami

*Department of Advanced Materials Science and Engineering, Faculty of Engineering Sciences
Kyushu University, 6-1 Kasuga-Park, Fukuoka, 816-8580, Japan*

Bimetallic nanoparticles have been attracted a lot of attention as potentially tunable catalysts such as for exhaust emission control or fuel cells. This year we studied electronic structures of bimetallic nanoparticles consisting of Pt and Rh/Pd using *ab initio* density functional theory (DFT). We employed the Vienna Ab initio Simulation Package (VASP) version 5.4.1 for DFT calculations, where it was vital to utilize parallel computing with more than hundreds of cores for the description of a nanoparticle whose diameter exceeds 2.5 nm. Three kinds of bimetallic structures, i.e., core-shell, random-alloy, and core-randomly-alloyed-shell structures, were considered in this study. The d-band centers, which are an index of the oxygen reduction reaction catalytic activity, were estimated from their density of states. We observed that the d-band center at the outermost layer of bimetallic core-shell nanoparticles quickly converged to that of pure monometallic's by increasing the number of shell atoms. We are currently constructing Behler-Parrinello neural-network potentials [1] for the bimetallic nanoparticles using the data obtained this year by Atomistic Machine-learning Package (AMP) of Prof. Andrew Peterson and his coworkers at Brown University[2]. We expect that the force fields will enable us to estimate of vibrational entropy contributions to the stability of those nanoparticles, and to model more realistic structures.

Furthermore, we worked on refining a proto-

col for finding a transition state (TS) structure on a metal surface. Though tremendous efforts have been devoted to develop the TS structure optimization techniques in first principle simulations, still there is considerable room for improvement; a robust and computationally efficient method for locating TS is highly desirable to investigate chemical reactions on the surface of a large nanoparticle. Here we focused on a three-step strategy which combines Nudged Elastic Band (NEB), and Climbing-Image-NEB (CI-NEB) and the dimer method, examining various initial vectors for the dimer method. The VTST tools of Henkelman's group were used with VASP for NEB, CI-NEB and the dimer method. The calculations were performed on the GPGPU nodes of the ISSP system B. We employed eight surface reactions on Pt(100) surface [3] as a benchmark set to see the effects of the initial modes. We found that our improved initial vector reduced the computational costs for the dimer method by 17% on average.

References

- [1] J. Behler and M. Parrinello: Phys. Rev. Lett. **98** (2007) 146401.
- [2] A. Khorshidi and P.A. Peterson: Comput. Phys. Commun. **207** (2016) 310.
- [3] A. Nikodem, A.V. Matveev, B.X. Zheng, and N. Rösch: J. Chem. Theory Comput. **9** (2012) 588.

First-Principles Study on New Group-IV Semiconductor Alloys

Yuki NAGAE and Masashi KUROSAWA

*Graduate School of Engineering, Nagoya University,
Furo-cho, Chikusa-ku, Nagoya 464-8603*

Group-IV semiconductor alloys have been one of the promising materials for optoelectronic applications of intra- and interchip optical wirings in silicon-based high-performance large-scale integrated circuits. Si-Sn binary alloy ($\text{Si}_{1-x}\text{Sn}_x$) is an interesting material since its energy bandgap (E_g) is theoretically expected to correspond to a wavelength (1550 nm; $E_g=0.8$ eV) that is preferable for optical communication applications [1]. However, the formation of high-Sn-content $\text{Si}_{1-x}\text{Sn}_x$ alloy is still a great challenge owing to the low thermal equilibrium solubility limit of Sn atoms in Si bulk ($\sim 0.1\%$) [2]. Recently, we have experimentally achieved the formation of polycrystalline $\text{Si}_{1-x}\text{Sn}_x$ (poly- $\text{Si}_{1-x}\text{Sn}_x$) and epitaxially grown $\text{Si}_{1-x}\text{Sn}_x$ (epi- $\text{Si}_{1-x}\text{Sn}_x$) layers on insulators with a Sn content as high as 40% [3, 4]. On the other hand, some theoretical calculations have been examined for predicting the energy band structure of $\text{Si}_{1-x}\text{Sn}_x$. These studies mainly investigated the threshold Sn content causing indirect-direct crossover, which is expected to be 31–55% [5–9]. To design the energy band alignment needed to realize multi-quantum-well (MQW) structures composed of $\text{Si}_{1-x}\text{Sn}_x$ layers with various Sn contents, the investigation of not only the E_g of $\text{Si}_{1-x}\text{Sn}_x$ alloy but also the valence and conduction band offsets is important to the

design of both electron and hole confinement structures for enhancing carrier recombination. Ranjan and Das [10] and Menéndez and Kouvetakis [11] used a regression model based on the elastic theory to predict the valence band offset (VBO) of strained $\text{Ge}_{1-x-y}\text{Si}_x\text{Sn}_y$ using the referenced deformation potential.

In this work, we performed density functional theory (DFT) calculation to predict the VBOs of $\text{Si}_{1-x}\text{Sn}_x$ with various Sn contents while considering the atomic displacement and configuration with Sn atomic incorporation into Si. We theoretically investigated the VBO of $\text{Si}_{1-x}\text{Sn}_x$ only by the first-principles calculation of the electronic properties of $\text{Si}_{1-x}\text{Sn}_x$. In order to examine the consistency of our theoretical prediction, we compare our theoretical data with some experimental data [3, 4] and conventional results of $\text{Si}_{1-x}\text{Sn}_x$.

We investigated the energy band offset of $\text{Si}_{1-x}\text{Sn}_x$ alloy and compared it with conventional theoretical estimation and experimental results. By estimating the CNL of each $\text{Si}_{1-x}\text{Sn}_x$ alloy, we could compare it with the VBO of $\text{Si}_{1-x}\text{Sn}_x$ alloys with different Sn contents (Fig. 1). As a result, we estimated the bowing tendency of the VBO of $\text{Si}_{1-x}\text{Sn}_x$ due to the effect of the variation in atomic configuration on the electronic state of $\text{Si}_{1-x}\text{Sn}_x$; we estimated a bowing parameter of

1.15±0.02 eV. The obtained Sn content dependence of VBO showed a similar tendency to the experimental results of $\text{Si}_{1-x}\text{Sn}_x$ with Sn content ranging between 0 and 40%, which cannot be ignored for designing band alignment. By estimating the energy band offset using calculations of $E-k$ dispersion and the VBO, we could estimate the dependences of the VBM and CBM in the entire Sn content range not only in the low-Sn-content region; we could also find the possibility of making type-I MQW with a suitable E_g for optoelectronic applications.

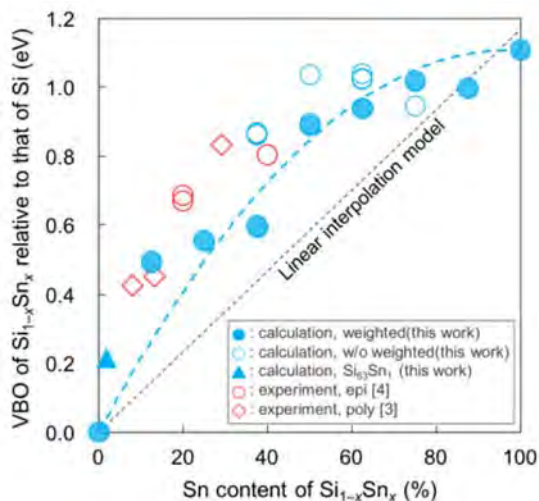


Fig.1: VBO of $\text{Si}_{1-x}\text{Sn}_x$ relative to the VBM of Si. The closed blue circles are calculation results weighted by the formation probability of each $\text{Si}_{1-x}\text{Sn}_x$. The open blue circles represent all atomic configurations of $\text{Si}_{1-x}\text{Sn}_x$ (not weighted). The red circles and diamonds correspond to experimental values of epi- $\text{Si}_{1-x}\text{Sn}_x$ [4] and poly- $\text{Si}_{1-x}\text{Sn}_x$ [3], respectively. The values estimated with the interpolation model by Sun [12] are indicated as reference. The closed blue triangle is for calculated $\text{Si}_{63}\text{Sn}_{37}$ as reference in this work. Copyright 2017 The Japan Society of Applied Physics [13].

References

- [1] P. Moontragoon, R. A. Soref, and Z. Ikonic, *J. Appl. Phys.* **112**, 073106 (2012).
- [2] T. B. Massalski, in *Binary Alloy Phase Diagrams*, ed. J. L. Murray, L. H. Bennet, and H. Baker (American Society for Metals, Metals Park, OH, 1986).
- [3] M. Kurosawa, M. Kato, T. Yamaha, N. Taoka, O. Nakatsuka, and S. Zaima, *Appl. Phys. Lett.* **106**, 171908 (2015).
- [4] M. Kato, M. Kurosawa, T. Yamaha, N. Taoka, O. Nakatsuka, and S. Zaima, presented at 9th Int. Conf. Silicon Epitaxy and Heterostructures (ICSI 9), 2015.
- [5] R. A. Soref and C. H. Perry, *J. Appl. Phys.* **69**, 539 (1991).
- [6] J. Tolle, A. V. G. Chizmeshya, Y. Y. Fang, J. Kouvetakis, V. R. D'Costa, C. W. Hu, J. Menéndez, and I. S. T. Tsong, *Appl. Phys. Lett.* **89**, 231924 (2006).
- [7] P. Moontragoon, Z. Ikonic, and P. Harrison, *Semicond. Sci. Technol.* **22**, 742 (2007).
- [8] N. Amrane and M. Benkraouda, *Am. J. Mater. Sci. Eng.* **1**, 12 (2013).
- [9] Y. Nagae, M. Kurosawa, S. Shibayama, M. Araidai, M. Sakashita, O. Nakatsuka, K. Shiraishi, and S. Zaima, *Jpn. J. Appl. Phys.* **55**, 08PE04 (2016).
- [10] R. Ranjan and M. K. Das, *Opt. Quantum Electron.* **48**, 201 (2016).
- [11] J. Menéndez and J. Kouvetakis, *Appl. Phys. Lett.* **85**, 7 (2004).
- [12] G. Sun, R. A. Soref, and H. H. Cheng, *J. Appl. Phys.* **108**, 033107 (2010).
- [13] Y. Nagae, M. Kurosawa, M. Araidai, O. Nakatsuka, K. Shiraishi, and S. Zaima, *Jpn. J. Appl. Phys.* **56**, 04CR10 (2017).

Study of Charge-trapping Site of High Performance Polymer Electret Material

Seonwoo KIM and Yuji SUZUKI

The University of Tokyo, 7-3-1 Hongo, Bunkyo-ku, Tokyo 113-8656

Electret is a dielectric with quasi-permanent charge, and it can generate electrostatic field without additional voltage supply. Electret energy harvester have electrodes covered with electret material. External vibration causes relative movement of electrodes, leads electrons to flow through load circuit connected to electrodes. Enhancing electret's performance and understanding alignment behavior of anisotropic dielectric fluid [1] are considered to be promising method to improve power output of electret energy harvester. In this report, the authors portrait on attempt to develop high-performance electret material with analytical approach.

Electret's performance can be evaluated by its characteristics such as charge density, long-term stability, and dielectric breakdown voltage. Even electrets materials satisfying these respects were reported within these years [2], theoretical model to estimate / evaluate performance of electret material is not yet developed. In this research, as a first step, electron trapping site of polymer electret has been studied.

Amorphous polymer CYTOP (Asahi Glass Co., Ltd) is studied with ab-initio computational software package NWChem [3]. Basis set of 6-

31G* was used to express effect of polarization of fluorine. B3LYP density functional is used to solve the Schrodinger equation. Figure 1. shows image of CYTOP monomer. As an early step, CTL-A and CTL-S is studied. Oligomer systems are made with 4 CYTOP monomers, combined with different end-group (COOH for CTL-A, CF₃ for CTL-S). After pre-process of molecular dynamic rough geometry optimization is made, the geometry of the system is precisely optimized with ab-initio method. After geometry optimization, the energy of systems is calculated before/after charge is trapped. The calculation is

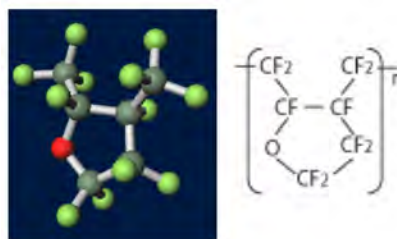


Fig. 1. CYTOP monomer

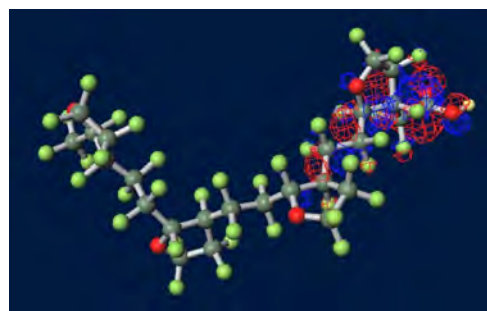


Fig. 2. Localization of trapped electron near carboxyl acid (CTL-A)

performed with SGI ICE XA ISSP system B F4cpu nodes. Every calculation was held with 4 nodes. In case of CTL-A, the calculation costs of geometry optimization are 02:46:16(Wall time), 66:18:13(CPU time). For energy calculation, 0:29:31(Wall time), 11:43:36(CPU time).

With calculated orbital energy, site of trapped charge is visualized. Fig. 2. shows the case of CTL-A. Charge concentration near carboxyl end is significant. In the case of CTL-S, the

localization tendency was not shown.

References

- [1] K. Kittipaisalsilpa et al.: 29th IEEE Int. Conf. Micro Electro Mechanical Systems (MEMS'16), Shanghai, pp. 37-40 (2016)
- [2] K. Kashiwagi et al.: J. Micromech. Microeng. **21** (2011) 125016.
- [3] M. Valiev et al.: Comput. Phys. Commun. **181** (2010) 147.

Magnetization Processes Based on Magnetic Dipole Moments

Shuji OBATA

*School of Science & Engineering, Tokyo Denki University
Ishizaka, Hatoyama, Hiki, Saitama 350-0394, Japan*

The electronic binding energies J_{ij} of 3d electrons in transition metals are induced from the tight binding interactions of the directed magnetic moments μ_i bonded in the Hund's rule. These 3d and 4s electrons construct eigenstates in external field environments. The magnetization processes are calculated by use of the Hamiltonian

$$\hat{H} = \sum_{i \leq j} J_{ij} \hat{\mu}_i \cdot \hat{\mu}_j + \sum_{i \leq j} W_{ij} + \sum_j \mu_j \cdot \mathbf{H} \quad (1)$$

including magnetic dipole moment interactions composed of classical-spin magnetic fields

$$W_{ij} = \frac{1}{4\pi\mu_0 d_{ij}^3} \{ (\mu_i \cdot \mu_j) - 3(\mu_i \cdot \mathbf{e}_{ij})(\mu_j \cdot \mathbf{e}_{ij}) \}. \quad (2)$$

The third term is magnetization energy in the external field \mathbf{H} . Distance vector is set as $\mathbf{d}_{ij} = \mathbf{e}_{ij} d_{ij}$ between the dipole moments at i and j . The static field energies J_{ij} do not affect to the hysteresis energy transitions for \mathbf{H} . Thus in this study, magnetization processes are simulated in a Fe₃O₄ doughnut film using the Hamiltonian

$$\hat{H} = \sum_{i \leq j} W_{ij} + \sum_j \mu_j \cdot \mathbf{H}. \quad (3)$$

This energy system produces the domain structures, the magnetization curves and the Barkhausen effects, which fairly coincide with the experimental data. The dipole moment freedom is tentatively selected to 26 directions to compose the energy minimum structures.^{[1][2]}

The Fe₃O₄ hysteresis curve is shown in Fig.1, where H_C coincides with experimental data. At the external field $\mu_0 H = -0.06$ T marked in Fig.1 as \circ , the domain structures by $\mu_i \cdot \mathbf{H}$ are drawn in Fig.2, where the total energy map by Eq.(3) is drawn in Fig.3 as -3.0×10^{-23} J: dark blue $\sim 3.0 \times 10^{-23}$ J: red. In these simulated results, diagonal zig-zag domain walls are not observed as in experimental data. This mismatch indicates the necessity of molecular spin states obtained using the interactions J_{ij} using Eq. (1).

In the ISSP system, the Fortran programs of the nano-Fe₃O₄ magnetizations are executed by about 500 line programming. The used times are about 18 hours using a large scale PC system for drawing the Fig.1~3. The programming for many PC cluster system are developing now.

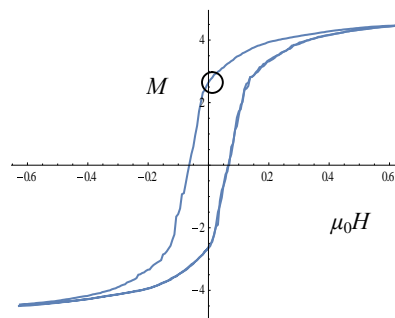


Fig.1. Fe₃O₄ hysteresis curve of a thin film ring : R=16,r=4, y=3 lattices.

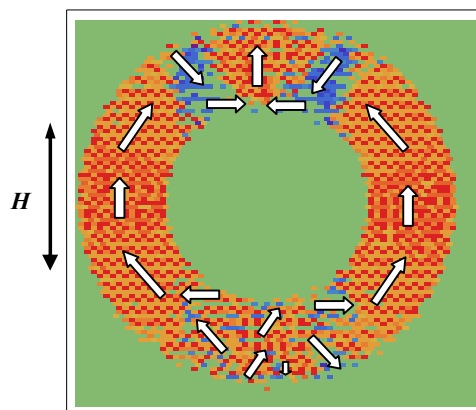


Fig.2. Fe₃O₄ spin direction structures in the ring system. Ordered areas are domains.

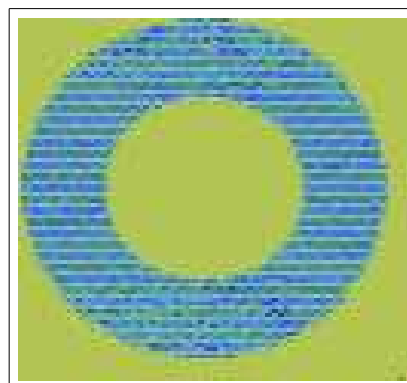


Fig.3. Fe₃O₄ energy map in the ring system. The variations are small.

- 1) S. Obata: Mater. Trans. **55** No 10 (2014) 1591-8.
- 2) S. Obata: IEEJ Trans. FM, **133** No 9 (2013) 489.

Molecular Dynamics Simulation of Organic Semiconductors

Kazume NISHIDATE and Masayuki HASEGAWA

Faculty of Engineering, Iwate University

Ueda 4-3-5, Morioka, Iwate 020-8551

We have investigated the energetics and work function (WF) of graphene (GR) with depositing pentacene ($C_{22}H_{14}$, PEN) and perfluorinated pentacene ($C_{22}F_{14}$, PFP) using the electronic structure calculations based on the density functional theory (DFT) with van der Waals (vdW) corrections[1]. Where the molecules are chemically adsorbed on the metals by exchanging electrons or forming hybridized orbitals, while they are physisorbed on GR through the vdW interactions in the flat laying configurations.

To study the WF of GR covered by the organic molecules, we put two PEN or PFP molecules on GR sheet to obtain plane averaged results for the local potential. The coverages are 0.75 ML (PEN) and 1.01 ML (PFP). Where the DFT-D2, DFT-D3, and the optB86b-vdW gave the same results for the adsorption configurations since the vdW corrections only affect the energetics but not the electric structure in direct way. A special attention was paid to the computational conditions to obtain converged results. We used the Γ -centered $4 \times 4 \times 1$ Monkhorst-Pack k-point mesh and very high cutoff energy of 1 keV. Present result for the WF for GR (4.23 eV) is compared to the experimental value (4.3 eV) and as well as to the theoretical value reported by other research group (4.26 eV) showing a good consistency. When the PEN molecules are adsorbed on GR, the vacuum level is shifted downward (-0.06 eV), whereas the vacuum level shift is upward (+0.10 eV) in the adsorption of the PFP molecules on GR. This tendency is different

from that of the PFP adsorbed on the Au(111), Cu(111), and Ag(111) surfaces where only the negative vacuum-level shifts have been predicted. It has been known that the electronic structure is only weakly perturbed by the benzene adsorption on GR. This is also the case in the adsorption of PEN and PFP molecules on GR. Energy diagrams obtained in the present study are shown in the Figure 1.

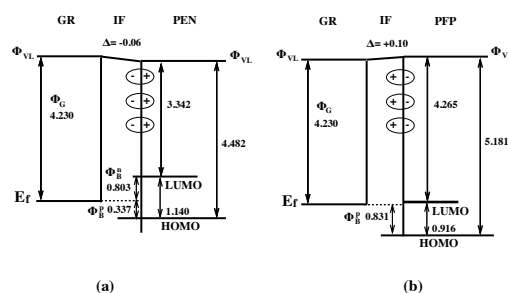


Figure 1: Energy diagrams for (a) PEN on GR and (b) PFP on GR. The vacuum levels Φ_{VL} are shifted by Δ through the dipole layers induced at the interface to the molecular surface. E_f is the Fermi level and Φ_G is the WF of the pristine graphene. Φ_B^p (Φ_B^n) is the hole (electron) injection barrier from GR to the molecules. All the energy values are in units of eV.

References

- [1] K. Nishidate, N. Yoshimoto, P. Chant-ngarm, H. Saito and M. Hasegawa: *Molecular Physics*, Vol. 114, 2993-2998, 2016.

First principles calculations of electronic structures, magnetism, and electric field effects in metal thin films and organometallic complexes

Kohji NAKAMURA

Department of Physics Engineering,

Mie University, Tsu, Mie 514-8507

Electric field effect to magnetism of metal thin films: Magnetocrystalline anisotropy (MCA) at Fe/MgO interfaces with insertions of 3d (Co, Ni), 4d (Ru, Rh, Pd), and 5d (Os, Ir, Pt) elements in an external electric field was investigated.[1] The MCA energy and the electric-field-induced MCA modification is found to dramatically depend on the inserted elements. Large MCA modification may be achieved by heavy-metal insertions, in which the strength of spin-orbit coupling of inserted elements and the position of the Fermi level relative to *d*-band level play key roles.

Search for the ground-state electronic configurations of organometallic molecules: The ground-state electronic configurations of the organometallic metallocenes, MCp₂, M = V, Cr, Mn, Fe, Co, and Ni, were investigated using constraint density functional theory combined with non-empirical U_{eff} approach in linear-response theory.[2] The relative stability of the various *d*-orbital electronic configurations is found to be sensitive to the U_{eff} values. Using the calculated non-empirical U_{eff} values, the

electronic configurations are in agreement with the experiments: $^4A_{2g}$, $^3E_{2g}$, $^6A_{1g}$, $^1A_{1g}$, $^2E_{1g}$, and $^3A_{2g}$ for the VCp₂, CrCp₂, MnCp₂, FeCp₂, CoCp₂, and NiCp₂, respectively

Electric-field-driven superconductivity at diamond (110): Hole states in an electric-field-driven superconductivity at diamond(110) were examined.[3] The surface-bound hole states, confined near the surface by an application of external electric field, is found to play a key role in superconductivity. Indeed, there is a critical electric field for observing the superconductivity, which attributes to the second surface-bound hole state. It further demonstrated that the transition temperature of superconductivity reaches to about 1K at electric field of 1.2V/Å, which corresponds to the surface carrier density of about $6 \times 10^{13} \text{cm}^{-2}$.

References

- [1] K. Nakamura et.al., J. Magn. Magn. Mater. **429** (2017) 214.
- [2] K. Nawa et.al., Phys. Rev. B **94** (2016) 0351361.
- [3] T. Hattori et.al., submitted.

Development and application of first-principles simulator for time-dependent electron-transport calculation

Yoshiyuki EGAMI

*Division of Applied Physics, Faculty of Engineering, Hokkaido University
Kita 13, Nishi 8, Kita-ku, Sapporo, Hokkaido 060-8628*

Nowadays, computational simulations with a high accuracy and efficiency have attracted much attention in both science and technology. For example, in the research and development of electronic devices, such numerical investigations play important roles to understand relationship between atomic and electronic structures of materials and electric, magnetic and optical characteristics of devices. A large number of notable studies using first-principles calculations have been performed so far to elucidate the relationship. However, most of the calculations are based on the density functional theory which describes the static characteristics of electrons in the steady state, and there remains to be discussed a time-dependent behavior of electrons.

In order to demonstrate the time-dependent transport properties of electrons through the nanoscale materials, we developed the impulse response (IR) method [1] based on the real-space finite-difference approach [2] within the framework of the time-dependent density functional theory. In this subject, for the IR method, we have worked on the improvement of the efficiency of parallel computing in the spatial dimensions since we cannot parallelize the calculations in the direction with respect to time due to the sequential evolution of scattering wave functions. This work has been performed with a few hundred cores on FUJITSU PREMEHPC FX10 in System C.

On the other hands, we have calculated the

electron transport properties of the molecular junction consisting of a transition metal complex molecule using the conventional time-independent electron transport simulator[3, 4] in order to compare the characteristics obtained by the IR method. As the results, in a $\text{Mn}(\text{dmit})_2$ molecular junction, spin-dependent properties are observed owing to the spin polarization derived from Mn atom, which are suitable as a spin filtering device. In particular, for a down-spin electron transport depending on the relative angle θ between two planar ligands, a non-monotonic behavior with θ in the conductance spectrum is found. It is confirmed that the d -orbitals of Mn atom plays a key part to exhibit such behavior. This work has been performed on System B.

References

- [1] Y. Egami and K. Hirose: JPS Conf. Proc. **1**, 016012 (2014).
- [2] K. Hirose *et al.*: *First-Principles Calculations in Real-Space Formalism*, (Imperial College Press, London, 2005).
- [3] Y. Egami, K. Hirose and T. Ono: Phys. Rev. E **82**, 56706 (2010)..
- [4] Y. Egami, S. Iwase, S. Tsukamoto, T. Ono and K. Hirose: Phys. Rev. E **92**, 033301 (2015).

Magic Angles in Energetics of Graphene Bilayer

Kazuyuki Uchida

Department of Physics,

Kyoto Sangyo University, Kyoto

Energetics for bilayer of graphene disks has been explored, to analyze the magic angles where the system has locally minimal energy. In this work, we have successfully clarified physical origin of the magic angles. This is the first time that magic angles are seriously discussed for interfaces where van-der Waals interactions are playing a dominant part.

We have calculated energy E for bilayers of graphene disks a function of the twist angle θ between the two layers. In Fig. 1, we show our model used in this work. The nearest-neighbor C-C bond length within a layer is fixed to be 1.42\AA . The bond angle among the three nearest neighbor C atoms within a layer is fixed to be 120° . The inter-layer distance is fixed to be 3.35\AA . We have used Lenard-Jones potential to describe van-der Waals interactions between the two layers.

We have found that the energy E oscillates as a function of the twist angle θ between the two layers, which is consistent with a previous report [1]. We have compared the atomic

structures of the systems which have the locally minimal energy and that of the system which have the locally maximal energy, finding that Moire patterns in the stacking structures of the two layers are closely related with the energy of the systems. Detail will be shown elsewhere [2].

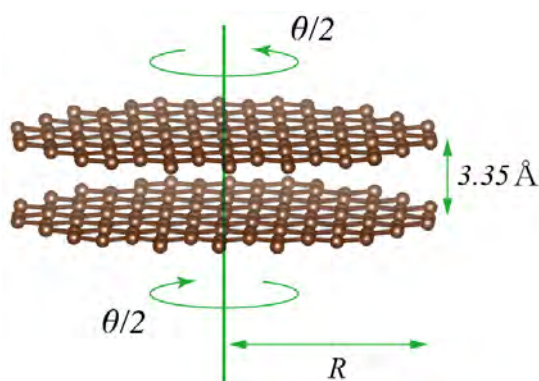


Fig. 1: Bilayer of graphene disks.

References

- [1] Bin Liu Min-Feng Yu, and Yonggang Huang, PRB **70**, 161402(R) (2004).
- [2] in preparation.

Atomic structures and electronic properties of atomic-layered materials

Yoshitaka FUJIMOTO

*Department of Physics, Tokyo Institute of Technology
Oh-okayama, Meguro, Tokyo 152-8551*

Graphene shows various unique electronic properties. In particular, graphene possesses very high carrier mobilities, and therefore is expected to be a potential device material for future nanoelectronics. Graphene is reported to be sensitive to adsorbates, and is also good candidates for promising sensor applications due to the high carrier mobility as well as the high sensitivity to adsorbates.

We here report polluting or toxic gas (NO and NO₂) adsorption effects on energetics and electronic properties of B-doped and N-doped graphene bilayers using first-principles electronic-structure calculations in the framework of the density-functional theory [1]. It is found that NO and NO₂ molecules are adsorbed with chemical bonds on the B-doped graphene bilayer. It is also found that the charge transfer takes place between the NO or the NO₂ molecule and the B-doped graphene layer.

We examine the stabilities of the NO and NO₂ molecules adsorbed on the B- and N-doped graphene bilayers. For the N-doped cases, NO and NO₂ molecules are not chemically but physically adsorbed with relatively small adsorption energies (E_a) as well as the long distances (d) between the molecule and the dopant atom ($d > 2.6 \text{ \AA}$). For the B-doped cases, the NO and NO₂ molecules can bind chemically with the large adsorption energies ($|E_a| > 1.1 \text{ eV}$) as well as the short distances ($d < \sim 2 \text{ \AA}$). Interestingly, the B atom protrudes from the planar graphene sheet when the NO₂ molecule binds with a chemical bond between the O atom in the NO₂ molecule and the B atom in the B-doped graphene bilayer, whereas it still resides in the planar sheet when

the NO molecule binds with a chemical bond between the N atom in the NO molecule and the B atom in the graphene layer.

We also examine the electronic properties of the NO and NO₂ molecules adsorbed on the B-doped graphene bilayer. The adsorption of the NO (NO₂) molecule clearly induces the charge transfers between the N (O) atom in the NO (NO₂) molecule and the B atom in the graphene due to the orbital hybridizations between the NO (NO₂) molecule and the B-doped graphene bilayer. Interestingly, by the NO molecule adsorption, electrons move from the NO molecule to the B-doped graphene with an amount of ~ 0.03 electrons, while for the adsorption of the NO₂ molecule, they move from the B-doped graphene to the NO₂ molecule with an amount of ~ 0.18 electrons. It can be seen that the charge transfer in the case of the adsorption of the NO₂ molecule is considerably larger than that in the case of the NO molecule. This is because the distance between the NO₂ molecule and the B-doped graphene is shorter compared with that between the NO molecule and the B-doped graphene.

We further examine work functions of the B-doped bilayer graphenes with adsorptions of the NO and the NO₂ molecules. Our calculated work function of the pristine AB-stacked bilayer graphene is 4.50 eV. When the B atom is doped into the graphene bilayer, the work function increases to $\sim 5 \text{ eV}$ since a B atom has one deficit electron compared with a C atom. When the NO₂ molecule is adsorbed, its work function further increases up to beyond 5 eV. On the other hand, when the NO molecule is adsorbed, the work function diminishes dramatically below that of the pristine bilayer

graphene. The variation of the work function induced by the adsorption of different types of adsorbates is mainly attributed to the charge transfer: In the case of the NO_2 molecule, the charge transfer takes place from the B-doped graphene layer into the NO_2 molecule, whereas it takes place from the NO molecule into the B-doped graphene layer.

In summary, we have examined adsorption effects of the polluting gas molecules on the energetics and the electronic properties of B-doped and N-doped graphene bilayers using first-principles density-functional calculations. The NO and NO_2 molecules can bind with chemical bonds on the B-doped graphene bilayer. By the adsorptions of the NO molecule and the NO_2 molecule, the charge transfers take place between the NO (NO_2) molecule and the B-doped graphene layer. The B-doped graphene bilayer is expected to be useful as sensors for the NO and the NO_2 molecules.

References

- [1] Y. Fujimoto and S. Saito, *Chem. Phys.* **478**, 55 (2016).

Study on electronic structures in perovskite-type lead-halide mixed crystals

Takayuki Makino

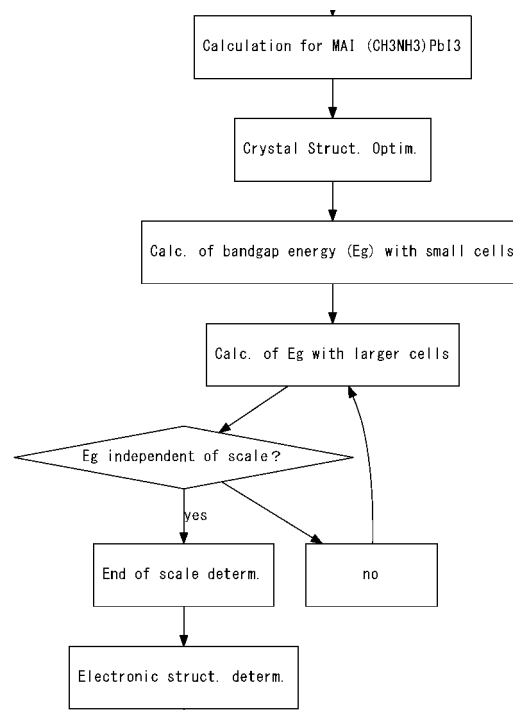
*Department of Electric and Electronics Engineering,
University of Fukui, Bunkyo Fukui, Fukui 910-8557*

Perovskite type halide compound is known to exhibit several interesting properties. They are, for example, strong excitonic effect and photovoltaic action. Deeper understandings for mixed crystal are important from both technological and basic viewpoints [1]. In this research, we intend to compare calculation and experimental data.

We have used the Quantum-ESPRESSO package to optimize the crystal structure and perform the band structure calculations. In this work, we use a set of the optimized norm-conserving Vanderbilt pseudopotentials generated by Schlipf and Gygi. We also confirmed the unit cell size necessary for the mixed crystal calculations. Flow chart is shown at the right hand side. We confirmed that evaluated bandgap energy is similar to that evaluated by Brivio *et al*[2].

We then moved into study of the electronic structure perovskite-lead chloride compound. As has been done for perovskite iodides, we optimized crystal structural parameters, followed by the calculation of electronic structures. The research plan of FY 2017 covers the mixed crystals between

iodide and chloride. We are calculating the electronic states, though the calculation is now at its beginning. Specifically, it aims to determine the dependence of Cl concentration and their positions.



References

- [1] J. H. Heo and S. H. Im: *Nanoscale* **8** 2554 (2016).
- [2] F. Brivio *et al.*, *APL Materials* **1**, 042111 (2013).

Theoretical analysis of H/D isotope effect in hydrogen-bonded organic conductor

Masanori TACHIKAWA

Quantum Chemistry Division,

Yokohama City University, Seto 22-2, Kanazawa-ku, Yokohama 236-0027, Japan

We have performed the computational analysis of H/D isotope effect on the novel hydrogen-bonded material, catechol-fused ethylenedithio-tetrathiafulvalene (H₂Cat-EDT-TTF) (H-TTF) [1]. H-TTF is a hydrogen-bonded π -electron system which was found to reveal $C2/c$ symmetry in 50-293 K, while its isotopologue, κ -D₃(Cat-EDT-TTF)₂ (D-TTF), showed the phase transition at 185 K from $C2/c$ to $P-1$. To elucidate the origin of such difference, we calculated the potential energy curves (PECs) for the hydrogen transfer along the H-bonds in these conductors. We found that both the π -stacking and the hydrogen nuclear quantum effect drastically affected the hydrogen transfer energy. With taking account of both effects, we obtained symmetric single-well effective PEC for H-TTF, which indicated that the hydrogen was always located at the center of the H-bond. By contrast, the effective PEC of D-TTF was low-barrier double-well, indicating that the position of the H-bonded deuterium would change according to the temperature. We concluded that the π -stacking and the nuclear quantum effect were the key factors for the

appearance of phase transition only in D-TTF [2].

We also theoretically investigated a significant contraction of the hydrogen-bonding O...O distance upon H/D substitution in recently developed purely organic crystals, κ -H₃(Cat-EDT-ST)₂ (H-ST) and its isotopologue κ -D₃(Cat-EDT-ST)₂ (D-ST). The optimized O...O distance in H-ST was found to be longer than that in D-ST due to the anharmonicity of the potential energy curve along the O-H bond direction, which was in reasonable agreement with the experimental trend [3].

References

- [1] T. Isono, H. Kamo, A. Ueda, K. Takahashi, A. Nakao, R. Kumai, H. Nakao, K. Kobayashi, Y. Murakami, H. Mori: *Nat. Commun.* **4** (2013) 1344.
- [2] K. Yamamoto, Y. Kanematsu, U. Nagashima, A. Ueda, H. Mori, and M. Tachikawa, *Phys. Chem. Chem. Phys.* (Communication), **18** (2016) 29673-29680.
- [3] K. Yamamoto, Y. Kanematsu, U. Nagashima, A. Ueda, H. Mori, and M. Tachikawa, *Chem. Phys. Lett.*, in press (2017).

Strain of β -FeSi₂(100) ultra-thin film

Ken HATTORI

*Graduate School of Materials Science, Nara Institute of Science and Technology
Takayama, Ikoma, Nara 630-0192*

Using scanning tunneling microscopy (STM) and low-energy electron diffraction (LEED), author's group has been studied the epitaxial growth of β -FeSi₂(100) nano-films on Si(001) prepared in ultra-high vacuum [1]. The β -FeSi₂[010] and [001] directions are Si<110> with lattice mismatches of +1.5% and +2.0%, respectively. The spot-intensity profiles in the LEED measurements have suggested the β -FeSi₂ surface structure; 1) the stacking of the surface top-layer of Si, 2nd-layer of Fe, 3rd-Fe, 4th-Si, 5th-Fe and repetition of Si/Fe/Fe/Si/Fe layers to bulk, and 2) in-plane relaxation of top-layer Si atoms from a rectangle configuration in the ideal to a square one in the real reconstruction.

The structure was also confirmed by the comparison with the STM simulation images calculated using Simulation Tool for Atom TEchnology (STATE)-Senri [2] in SCC-ISSP system; four Si atoms in the square configuration forms one atomic protrusion in the STM calculation. Recently the authors' group has confirmed such a slab structure using high-angle annular dark-field scanning transmission electron microscopy (HAADF-STEM) in atomic resolution. The HAADF-STEM showed β -FeSi₂(100) nano-films consists of units of the quintuple layers (QL) (Si/Fe/Fe/Si/Fe) with a bottom Si layer on a Si(001) substrate. Figure 1 shows a model for β -FeSi₂(100) with 3 QL on Si(001). The red and green balls are Fe and Si in *beta*-FeSi₂, respectively. The cyan, orange, pink and green balls are 1st-, 2nd-, 3rd- and 4th/5th-layer Si atoms, respectively, in Si, respectively.

Interestingly, the STM and HAADF-STEM displayed the bending of β -FeSi₂ over Si substrate steps; the bending strain was estimated to be \sim 3–4% in the ratio of the height dif-

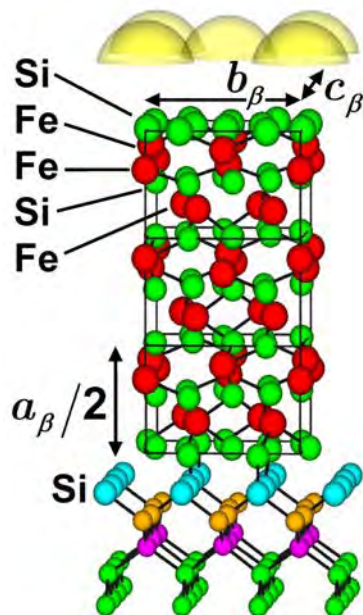


Figure 1: A model of β -FeSi₂(100) with three quintuple layers (QL) on Si(001). Red and green balls represent Fe and Si atoms, respectively, in β -FeSi₂. Cyan, orange, pink and green balls represent 1st, 2nd, 3rd and 4th/5th-layer Si atoms, respectively, in Si. a_β , b_β and c_β denote unit-lengths of β -FeSi₂[100], [010] and [001], respectively. Yellow hemispherical balls represent schematic atomic protrusions in the STM calculation.

ference (Δz) to length (L). On the other hand, the in-plane compression of β -FeSi₂ was smaller than the ideal values (1.5% and 2.0%) within the error. These experimental results suggest the relaxation of the in-plane compress strain by the bending formation.

In this project we calculated energy increases by the compression and bending of free-standing β -FeSi₂(100) using STATE-Senri.

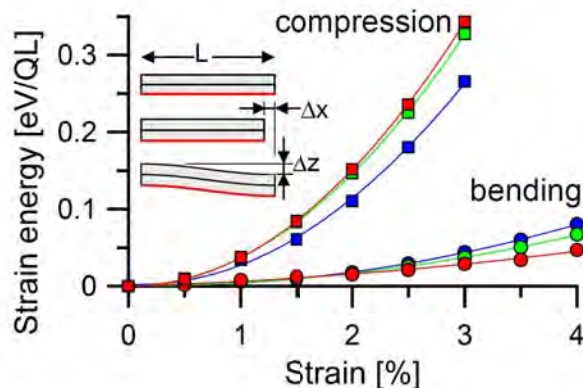


Figure 2: Calculated strain energies of β -FeSi₂(100). Blue, green and red squares (circles) represent energy increases divided by QL number for 1, 2 and 3 QL models, respectively, as a function of compression (bending) strain, $|\Delta x|/L$ ($\Delta z/L$).

The compression models were (100)1×1 units for 1 QL, 2 QL and 3 QL with the bottom Si layer consisting of 6, 11, and 16 layers having 32, 56, and 80 atoms, respectively. The atomic positions in the bottom layer were fixed to those with the same relative x and y components normalized by unit lengths in [010] and [001], respectively, to the stable bulk structure. The other positions were relaxed at the residual force of ≤ 0.05 eV/Å,

Troullier-Martins norm-conserving pseudo potentials were used for Si and Fe atoms. The wave functions and charge densities were expanded by a plane-wave set with cut-off energies of 25 and 225 Ry, correspondingly. $4 \times 4 \times 1$ k-points mesh was used for the k-space integration. The spin polarization was not taken into account in the calculations. The blue, green and red squares in Fig. 2 displays the energy increases divided by the number of QL for 1, 2 and 3 QL models, respectively, as a function of the compression ($|\Delta x|/L$) from the stable structures with L .

Similarly the energy increases by the bending strain were calculated as shown by blue, green and red circles in Fig. 2, for 1, 2 and 3 QL (100)1×1 units, respectively. Here, z components of the fixed bottom layer atoms were modulated by $(|\Delta z|/2) \cos(\pi x/L)$, thus, the actual calculations were done with 2×1

units under $2 \times 4 \times 1$ k-points mesh.

Figure 2 indicates that the energy increases in the compression at 1.5–2.0% are larger than those in the bending at 3–4%, which implies that the nano-film system is prefer to bend in order to release the large energy increase due to the compression strain, in principle. We should note here that the stable in-plane lattice constants depend on the film thickness. For the 3 QL model, the [010] and [001] lattice constants were 0.3% smaller than the bulk ones, but the above trend is not changed. Figure 2 also indicates no drastic difference in energy per QL for the 1-3 QL models.

The author thank Prof. Morikawa in Osaka University, Dr. Yanagisawa in Ryukyu University, and Dr. Hamada in NIMS for their great support in STATE-Senri calculations.

References

- [1] O. Romanyuk, K. Hattori, M. Someta, and H. Daimon: Phys. Rev. B **90** (2014) 155305.
- [2] Y. Morikawa: Phys. Rev. B **63** (2001) 033405, and references therein.

First-principles study on the defects in semiconductors

Jun YAMAUCHI

Faculty of Science and Technology, Keio University

3-14-1 Hiyoshi, Kohoku-ku, Yokohama-shi, Kanagawa 223-8522

As the size of devices on integrated circuits decreases, the behavior of dopant atoms make relatively larger effect on the device performance. Especially, it is very important to understand the unfavorable defects including the dopant atoms. The experimental observations on each defect is extremely difficult. One of the major difficulties for detecting dopant configurations is the very weak signals from the defects of very low concentration comparing to those from the matrix semiconductors. However, recently, as a solution for the above problem, it is suggested to use powerful synchrotron radiation facilities to measure the X-ray photoelectron spectroscopy (XPS) signals of defects. On the other hand, there have been few reliable first-principles core-level XPS calculations for impurity defects in semiconductors, because the local potential boundary condition of defect model systems has not yet been sufficiently evaluated. To obtain reliable shifts in the XPS binding energy, it is necessary to take a sufficiently large supercell for a defect.

To investigate the dependence of the substrate semiconductors on the XPS binding energies, we carried out a comprehensive study on the As 3d core-level XPS binding energies for As defects in crystalline Si using a first-principles calculation with careful evaluation of the local potential boundary condition for the model system. To represent a core hole in

the 3d orbitals, we adopted the arsenic pseudopotential including the 3d orbitals as valence ones, and the spherical hole approximation assuming that one core hole occupies degenerated core states equally. It is found that the effect of this approximation on the relative XPS binding energy is negligible. We adopted cubic supercell corresponding to 1000 Si atoms and also considered the charged state and spin effect. The code used in this study is xTAPP, which is a hybrid paralleled density functional theory calculation program with plane-wave basis[1].

It is found that, while the spin polarization does not make large effect on the formation and XPS binding energy of defects, the charge state change those energies up to several tenth of eV in some cases. Among the examined defect structures, vacancy related defects, where one vacancy is surrounded by substitutional arsenic atoms, well explain the experimentally observed XPS peak.

References

- [1] xTAPP (eXtended Tokyo Ab initio Program Package)
(<http://xtapp.cp.is.s.u-tokyo.ac.jp>)
- [2] J. Yamauchi, Y. Yoshimoto, and Y. Suwa: *J. Appl. Phys.* **119** (2016) 175704.

Effects of heavy elements in surface nanostructures

Yoshihiro GOHDA

*Department of Materials Science and Engineering, Tokyo Institute of Technology
J1-3, Nagatsuta-cho 4259, Midori-ku, Yokohama 226-8502, Japan*

Spin-orbit coupling of heavy elements, especially in nanostructures, has potentials of novel physical properties. For example, bilayer Bi(111) films have been predicted theoretically as two-dimensional topological insulators [1]. In recent experiments, atomically-flat Bi(110) ultrathin films have successfully grown on Si(111) $\sqrt{3} \times \sqrt{3}$ -B surfaces [2]. Since Si(111) $\sqrt{3} \times \sqrt{3}$ -B surfaces have no dangling bonds, properties of Bi ultrathin films are expected to be similar to those of freestanding one. Contrary to previous studies [3], where even-layer thickness films have stable black-phosphorous-like structures and odd-layer ones have less-stable bulk-like structures, the preference of even-layer thickness was not obtained [2]. Furthermore, it is difficult to distinguish black-phosphorous-like structures and bulk-like structures by scanning-tunneling-microscope images.

In the present study, the atomic structures and electronic properties of Bi(110) ultrathin films are studied by first-principles calculations using the OpenMX code [4], where pseudo-atomic orbitals and norm-conserving pseudopotentials are used. For even-layer thickness films, we obtained black-phosphorous-like structures, which is consistent with previous studies [3]. In contrast, for odd-layer thickness ones with 5 monolayers or more, the optimized structures have characteristics of both black-phosphorous-like and bulk-like structures. The atomic structure together with the electron-density rearrangement compared to the isolated atoms are shown for the 5-monolayer case in Fig. 1 (a). The outermost two monolayers form the black-phosphorous-like structure, whereas the inner one monolayer has essentially no chemical bonding with neighboring layers. The formation energy relative to the

bulk Bi as a function of the thickness of the films is shown in Fig. 1 (b). The formation energy decreases as the thickness increases. Furthermore, our result demonstrates that there is no clear preference for even or odd numbers of the layer-thickness, as far as the thickness is more than 5 monolayers. As the spin-orbit coupling of Nd dominates the magnetic anisotropy of Nd-Fe-B permanent magnets [5], the spin-orbit coupling of other heavy elements including Bi should be useful to control the anisotropy of magnetic materials, which must be an interesting target of further studies.

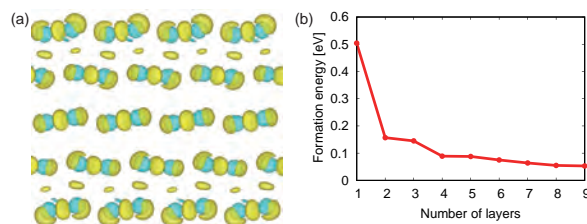


Figure 1: (a) The atomic structure together with the electron-density increase compared to the isolated atoms for the 5-monolayer case and (b) the formation energy per atom relative to the bulk Bi as a function of the thickness of the films.

- [1] S. Murakami, *Phys. Rev. Lett.* **97**, 236805 (2006); M. Wada, S. Murakami, F. Freimuth, and G. Bihlmayer, *Phys. Rev. B* **83**, 121310(R) (2011).
- [2] I. Kokubo, Y. Yoshiike, K. Nakatsuji, and H. Hirayama, *Phys. Rev. B* **91**, 075429 (2015).
- [3] T. Nagao, J. T. Sadowski, M. Saito, S. Yaginuma, Y. Fujikawa, T. Kogure, T. Ohno, Y. Hasegawa, S. Hasegawa, and T. Sakurai, *Phys. Rev. Lett.* **93**, 105501 (2004).
- [4] T. Ozaki, *Phys. Rev. B* **67**, 155108 (2003).
- [5] Y. Tatetsu, S. Tsuneyuki, and Y. Gohda, *Phys. Rev. Appl.* **6**, 064029 (2016).

Geometric and electronic structures at edge of 2-dimensional honeycomb sheets

Noriaki TAKAGI¹, Ryuichi ARAFUNE², Naoya KAWAKAMI¹, and Emi MINAMITANI³

¹*Department of Advanced Materials Science, University of Tokyo
Kashiwa-no-ha, Kashiwa, Chiba 277-8561,*

²*International Center for Materials Nanoarchitectonics, National Institute for Materials,
Science, 1-1 Namiki, Ibaraki 304-0044,*

³*Department of Materials Engineering, The University of Tokyo, 7-3-1 Hongo,
Bunkyo-ku, Tokyo 113-8656, Japan..*

The discovery graphene has fueled the competition to explore exotic new honeycomb materials and to uncover their hidden properties. One-atom layer honeycomb sheets consisting of heavy elements such as Bi, Si, Ge and Sn atoms have gathered lots of attention. These materials are promising candidates of two-dimensional (2D) topological insulator because the large spin-orbit interactions open the energy gaps, leading to the topological edges states [1, 2].

Recently, we have investigated the geometric and electronic structures of Bi thin films grown on Si(111) and Au(111) substrates mainly by using scanning tunneling microscopy (STM). We found that the Bi thin films on Si(111) have two types of step edges; One shows a regular step edge and the other exhibits a reconstruction. Interestingly, the latter reconstructed edge hosts a localized 1D electronic state [3]. In addition, we found the superstructure formed by the Bi

adsorption on Au(111). We carried out density functional theory (DFT) calculations (1) to construct the structural model of the reconstructed edge in Bi films on Si(111) and elucidate the origin of the 1D state and (2) to construct the structure model of the superstructure for Bi on Au(111).

The DFT calculations were carried out by the plane-wave-based Vienna Ab initio Simulation Package (VASP) [4, 5] with the projected augmented wave method [6]. While we did not find reasonable structural model for the reconstructed Bi edge yet, we found a good model for the superstructure of Bi on Au(111).

Reference

- [1] S. Murakami: Phys. Rev. Lett. **97**, 236805 (2006).
- [2] M. Ezawa, Phys. Rev. Lett. **109**, 055502 (2012).
- [3] N. Kawakami, C.-L. Lin, M. Kawai, R. Arafune and N. Takagi, Appl. Phys.

Lett. **107**, 031602 (2015).

[4] G. Kresse and J. Furthmüller: Phys. Rev. B **56**, 11169 (1996).

[5] G. Kresse and J. Furthmüller: Comput. Mater. Sci. **6**, 15 (1996).

[6] P. E. Blöchl: Phys. Rev. B **24**, 17953 (1994) 17953.

Adsorbed states of magnetic molecules at solid surfaces

Noriaki TAKAGI¹ and Emi MINAMITANI²

¹*Department of Advanced Materials Science, University of Tokyo*

Kashiwa-no-ha, Kashiwa, Chiba 277-8561

²*Department of Materials Engineering, The University of Tokyo, 7-3-1 Hongo,*

Bunkyo-ku, Tokyo 113-8656, Japan.

Adsorption of metal phthalocyanines (MPcs) on solid surfaces has gathered considerable attention because these molecules exhibit unique properties [1-3]. MnPc, FePc and CoPc are typical members of MPc family and the adsorption of these molecules on solid surfaces has been intensively studied. Recently, we have investigated the magnetism of FePc on noble metal surfaces, especially the relation between the spin state and the molecule-surface (Mol-S) interaction, by using scanning tunneling microscopy (STM) and spectroscopy (STS) and photoelectron spectroscopies. We have elucidated that the S=1 spin state of the bulk FePc is converted when the molecule directly contacts Cu(110) [4]. In contrast, the S=1 state is preserved by inserting atom-thick oxide layer between the molecule and the Cu substrate [4]. On Au(111), two unpaired spins of S=1 FePc exhibit Kondo effect because of the exchange coupling with the substrate electrons [5,6]. These examples indicate the spin state is sensitive to the molecule-surface interactions.

To understand systematically the relation of the spin state and the Mol-S

interaction, we investigated the spin state of FePc on Ag(111) by using soft X-ray photoelectron spectroscopy (SXPS) together with the density-functional theory (DFT) calculations. The evolution of SXPS spectra as a function of the amount of adsorbed FePc molecules shows that the S=1 spin state is converted to S=0 for the monolayer regime, and that S=1 preserves in the second layer on the monolayer. We performed the DFT calculations by using the plane-wave-based Vienna Ab initio Simulation Package (VASP) [7,8] with the projected augmented wave method [9]. The DFT calculations have found that the adsorption of FePc on Ag(111) changes the S=1 spin state of bulk FePc to S=0, consistent with the SXPS results. The present results show that there is a boundary between Ag and Au in the 11th group of periodic table concerning the conversion of S=1 to S=0 upon the adsorption.

Reference

[1] R. Bonnett: *Chem. Soc. Rev.* **24**, 19 (1995).

[2] C. C. Lanznoff and A. B. P. Lever: *Phthalocyanines, Properties and*

Applications (Wiley, New York, 1996).

[3] K. Kadish, and R. Guillard: *Applications of Phthalocyanines, The Porphyrin Handbook* (Academic Press, San Diego, 2003).

[4] N. Tsukahara *et al.*: Phys. Rev. Lett. **102**, 167203 (2009).

[5] N. Tsukahara *et al.*: Phys. Rev. Lett. **106**, 187401 (2011).

[6] E. Minamitani *et al.*: Phys. Rev. Lett. **109**, 086602 (2012).

[7] G. Kresse and J. Furthmüller: Phys. Rev. B **56**, 11169 (1996).

[8] G. Kresse and J. Furthmüller: Comput. Mater. Sci. **6**, 15 (1996) 15.

[9] P. E. Blöchl: Phys. Rev. B **24**, 17953 (1994).

Study on an automatic derivation technique of first-principles effective model based on the many body electron theory

Hirofumi SAKAKIBARA

*Department of Applied Physics and Mathematics,
Tottori University, Koyama-cho, Tottori, Tottori 680-8552*

The derivation of effective model is one of the central issues in the condensed matter physics. Especially in the low-temperature physics, the effective model is can be constructed by truncating the space which constructs the energy eigenvalues around the Fermi level. However, the states spanning such space are affected by electron process in higher energy scales. Therefore, we have to obtain the whole electron band structure before the truncation of the effective model.

By recent development of the implementation technique of the first-principles calculation and the computational resources, we can obtain the electron band structure for each material by several ours of calculation. Furthermore, the recent studies on the Hubbard-type model have shown that the critical temperature of high- T_c cuprates can be estimate as the realistic

values and the systematics with the curvature of the Fermi surface is reproduced [1,2]. Therefore, if we can systematically construct the effective model from the first-principles calculations, we have possibilities to salvage the new superconducting materials from the material database in principle.

To this end, we have firstly improved the derivation system of effective model. We have suggested the modified random phase approximation (named mRPA) method to overcome some difficulties recognized in the constrained RPA.

For the benchmark of mRPA, we have estimated the Hubbard interaction U in the HgBa₂CuO₄, which is the typical single-band high- T_c superconductor. As a result, the U in mRPA is larger than the value in cRPA ($U_{\text{cRPA}}=2.0\text{eV}$, $U_{\text{mRPA}}=3.9\text{eV}$). The reasons are follows: On one hand, in cRPA, the

screening effect by long-ranged Coulomb interaction is completely discarded [3]. On the other hand, even mRPA can treat the range truncation of the interaction exactly in principle, our recent test in the mRPA does not take any off-site interaction. In the future study including the off-site interaction in mRPA, the value of U may be modified to become close to the appropriate value of the single-band (extended) Hubbard model, which

has been studied to reproduce the low-energy process in the cuprates superconductors.

References

- [1] H. Sakakibara et al: Phys. Rev. Lett. **105** (2010) 057003.
- [2] H. Sakakibara et al: Phys. Rev. B **89** (2014) 224505.
- [3] H. Sakakibara et al: J. Phys. Soc. Jpn. **86** (2017) 044714.

Ab initio calculations of impurity states in the silicon cluster superlattice

Nozomi ORITA, Yasushi IWATA

*National Institute of Advanced Industrial Science and Technology
Tsukuba Central 2, Tsukuba, Ibaraki 305-8568*

Recently, Iwata *et al.* found out the crystallographic coalescence of silicon (Si) clusters into a bcc superlattice structure with a lattice constant of 2.134 nm by direct deposition of a Si cluster beam on a graphene substrate[1]. In the past year, we obtained a good model structure for the bcc Si cluster superlattice by *ab initio* calculations using OpenMX [2]. That structure is composed of Si_{211} clusters and the lattice constant is 2.167 nm, which is in good agreement with the experimental value, 2.134nm[3, 4]. The obtained structure and the band structure of the bcc Si_{211} cluster superlattices are shown in Fig. 1.

This year, we have investigated the effect of impurities for the bcc Si_{211} cluster superlattice. The Si_{211} cluster has 18 symmetrically equivalent atomic sites. An atom for each equivalent site was substituted by a boron (B) or a phosphorus (P) atom and the stable structure and the electronic state were calculated. The obtained band structures of the $\text{Si}_{210}\text{B}_1$ and $\text{Si}_{210}\text{P}_1$ cluster superlattices in which the each central Si atom of the Si_{211} cluster was substituted by the impurity are shown in Fig. 2. The impurity states are hidden in the surface states in the vicinity of the Fermi level and those band structures are almost same as that of the Si_{211} cluster superlattice. We obtained similar band structures for impurities at the other 17 equivalent sites.

We also calculated surface-oxidized $\text{Si}_{210}\text{B}_1$ and $\text{Si}_{210}\text{P}_1$ cluster superlattices. In those calculations, the twelve oxygen atoms terminate

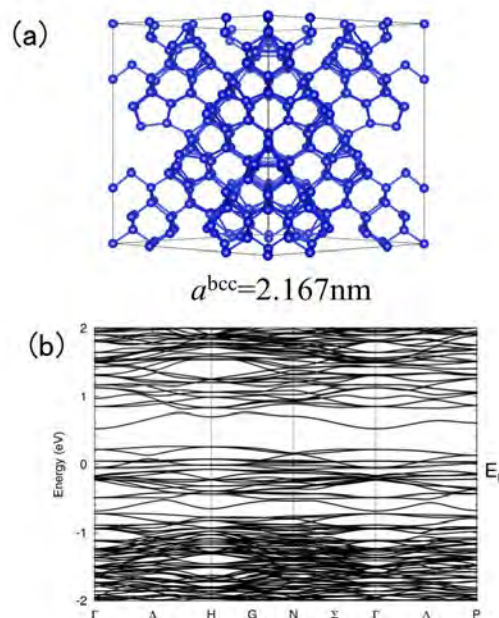


Figure 1: Crystal structure (a) and band structure (b) of the bcc Si_{211} cluster superlattices. E_F denotes the Fermi level

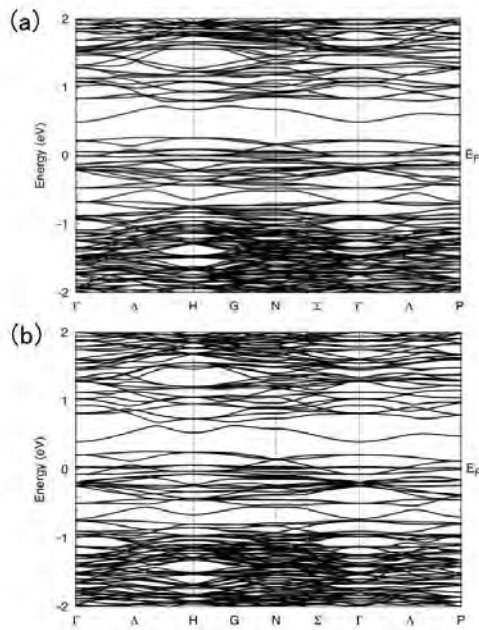


Figure 2: Band structures of the $\text{Si}_{210}\text{B}_1$ (a) and the $\text{Si}_{210}\text{P}_1$ (b) cluster superlattices. The impurity is located at the center of the cluster. E_F denotes the Fermi level

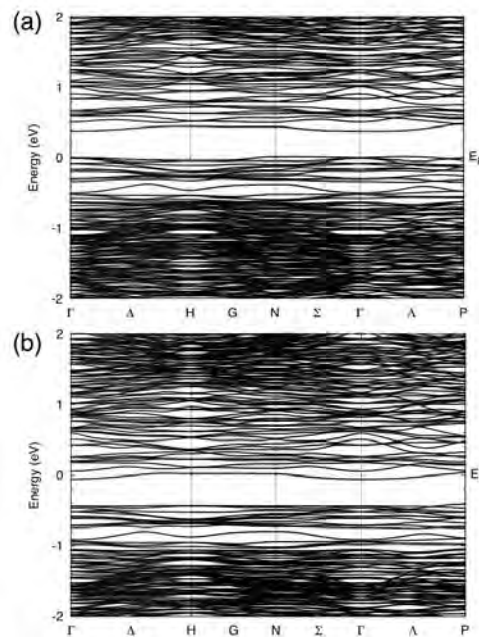


Figure 3: Band structures of the surface-oxidized $\text{Si}_{210}\text{B}_1$ (a) and $\text{Si}_{210}\text{P}_1$ (b) cluster superlattices. The B or P is located at the center of the cluster. E_F denotes the Fermi level

dangling bonds on the surface. The obtained band structures for a B and a P atom at the center of the clusters are shown in Fig. 3. In those cases, the B-doped and the P-doped surface-oxidized Si cluster superlattices indicate a p-type and an n-type conductivity, respectively. However, in some cases, depending on the position of the impurity, the B-doped and the P-doped surface-oxidized Si cluster superlattices became an n-type and a p-type semiconductor, respectively.

References

- [1] Y. Iwata, K. Tomita, T. Uchida, and H. Matsuhata, *Cryst. Growth Des.* **15** (2015) 2119.
- [2] T. Ozaki *et al.*, <http://www.openmx-square.org/>
- [3] Y. Iwata, N. Orita, T. Uchida, and H. Matsuhata, *Proc. Advanced Materials World Congress 2015*, Chapter 10, p. 5.
- [4] Y. Iwata, N. Orita, T. Uchida, H. Amekura, J. Hasegawa, K. Horioka, and H. Matsuhata, *EMN Meeting on Quantum Matter 2016*.

Study of interaction between radiation damage and interstitial atom

Kazuhito Ohsawa

Institute for Applied Mechanics,

Kyushu University, Kasuga-koen, Kasuga, Fukuoka 816-8580

Metal properties usually deteriorate by the presence of hydrogen (H). In particular, the degradation of Fe, W, and their alloys by H is paid attention in the field of irradiation damage, which is related to the safety of fusion and fission reactors. Stable configurations of H atoms trapped in a mono-vacancy have been reported in some previous works. So, we investigated stable configurations of di-vacancy in BCC transition metals and H trapped in the di-vacancy. Formation energies of di-vacancy and vacancy hydrogen complex (VHC) are estimated by first-principle calculations based on density functional theory.

It is possible to be two types of di-vacancies in BCC lattice, as shown in Fig. 1. In Fe lattice, $\langle 100 \rangle$ di-vacancy is more stable than $\langle 111 \rangle$ di-vacancy. While, $\langle 111 \rangle$ di-vacancy is more stable in Cr, Mo, W lattice.

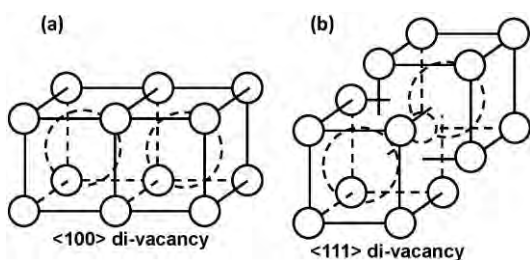


Fig. 1: Two types of di-vacancies in BCC lattice.

The binding energies of di-vacancy and VHC are calculated, as shown in Fig. 2. The di-vacancy formation $V + V \rightarrow V_2$ is usually exothermic reaction. But di-vacancy in W is unstable. Binding energies of VHC are also calculated in the case of $VH_6 + VH_6 \rightarrow V_2H_{12}$. The presence of H usually enhances di-vacancy formation except for Cr. In particular, W and its alloys will be installed in fusion reactors which are exposed to intense H plasma. The abnormal properties of vacancy type lattice defects in W materials will be an important subject in the field of plasma facing material.

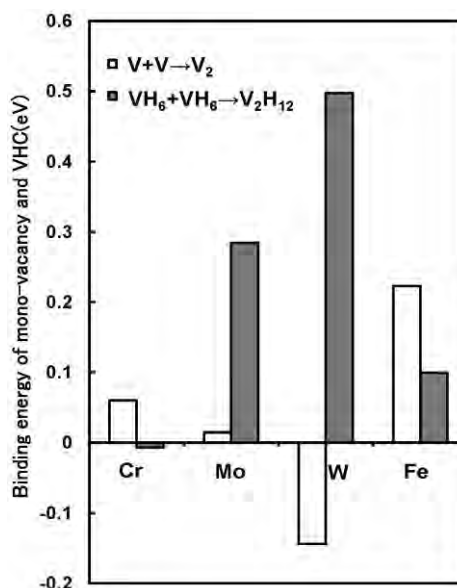


Fig. 2: Binding energy of V and VH_6 .

Study on structure, formation, and physical properties of multiatomic vacancies and clusters of 2D semiconductors

Hiroyuki KAGESHIMA

*Interdisciplinary Graduate School of Science and Engineering, Shimane University
Nishi-Kawatsucho, Matsue, Shimane 690-8504*

Our project has been focused on the physical and structural properties of defects, surfaces and interfaces of two dimensional (2D) semiconductors such as graphene, h-BN, and transition metal dichalcogenide (TMD). MoS₂ is one of the 2D semiconductors consisting of two elements as h-BN is. In addition, the projected atomic structure of MoS₂ is honeycomb as that of h-BN is. Therefore, it is expected that physical properties of MoS₂ is similar to those of h-BN. We study properties of MoS₂ vacancies based on the first-principles method and compare them with those of h-BN vacancies [1, 2]. The calculations were performed based on the first-principles calculation with the GGA density functional, plane wave bases, and pseudopotentials. Program package PHASE [3] was employed.

The results show that vacancies for both h-BN and MoS₂ are more stable when they are more negatively charged (Fig. 1). Almost all of the calculated vacancies prefer the negative charge states to the neutral and positive charge states. In addition, they show that the vacancy atomic structures change with the charge states. We successfully explain both of these properties based on gap state properties. The highest occupied states for the neutral states are located close to the valence band maximum in band gap, and many vacancy states appear in the band gap as unoccupied states.

Our results also show that the anion vacan-

cies are much easily formed for MoS₂. The formation energy of V_S is only 0.64 eV in the Mo-rich condition at conduction band minimum. The reason comes from the rather strong ionic nature of chemical bonds of MoS₂. On the other hand, the rather strong covalent nature of chemical bonds of h-BN enlarges the formation energy of anion vacancies.

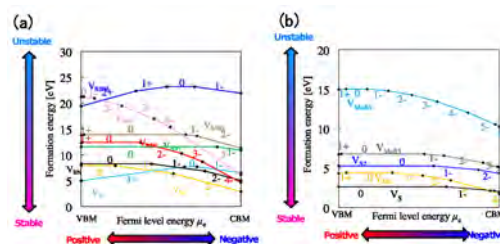


Figure 1: Charge state dependent formation energies of vacancies (a) of h-BN in the N-rich condition and (b) of MoS₂ in the S-rich condition. The numbers along lines show the charge states.

References

- [1] S. Urasaki, and H. Kageshima, Jpn. J. Appl. Phys. **56**, 025201 (2017).
- [2] S. Urasaki and H. Kageshima, 2016 International Conference on Solid State Devices and Materials, Tsukuba, Japan, PS-13-02.
- [3] <https://azuma.nims.go.jp/cms1>

First-Principles study on the electric-double layer capacitance of MXene compound Ti_2CT_x

Yasunobu ANDO

CD-FMat,

AIST, Tsukuba Central 2, 1-1-1 Umezono, Tsukuba, Ibaraki, 305-8568

MXenes are a new, large family of layered materials synthesized from MAX phases by simple chemical treatments. Due to their enormous variations, MXenes have attracted great attention as promising candidates as anode materials for next-generation secondary batteries. However, specific capacitance of MXene supercapacitors is lower than that of active-carbon ones. Theoretical investigation of the electric-double layer (EDL) at electrode interfaces is necessary to improve their capacitance.

Ab initio molecular dynamics (AIMD) simulation based on the density functional theory (DFT) is performed to estimate the EDL capacitance from a potential profile $V(z)$ and a charge distribution $q(z)$ induced by the ions at water- Ti_2CT_2 (T=O, F) interfaces. Potential profiles $V(z)$ of both Ti_2CO_2 and

Ti_2CF_2 decrease about 1.0 eV steeply in a region of only 3 Å from a Ti layer, which is the same profile at the platinum interfaces. On the other hand, induced charge distribution $q(z)$ depends on the species of surface termination. Induced electrons are introduced at Ti layers in the case of O surface termination. However, Ti_2CF_2 is not capable to store electrons at Ti layers because it is mono-valence anions. It indicates that effective surface-position of MXenes depends on the surface terminations. Our results are revealed that small induced charge leads the low EDL capacitance at MXene interfaces. This is because interface polarization due to strong interaction between water and Ti_2CT_x induces net charge. The surface net charge hinders the introduction of ion-induced charges.

Electronic structure of light rare earth permanent magnets

Akai Group^{a,b}^a*Institute for Solid State Physics, University of Tokyo
Kashiwa-no-ha, Kashiwa, Chiba 277-8581*^b*Elements Strategy Initiative Center for Magnetic Materials,
National Institute for Materials Science,
Sengen, Tsukuba, Ibaraki 305-0047*

Introduction There has been a surge in the interest on high-temperature magnetic anisotropy of $4f$ - $3d$ intermetallics as motivated by practical applications of them as permanent magnets. Permanent magnets need strong magnetization and accordingly strong coercivity: magnetic anisotropy is considered to be the intrinsic origin of the coercivity. Magnetization mostly comes from $3d$ -electrons in Fe or Co and leading-order magnetic anisotropy is contributed from $4f$ -electrons in rare earth elements, while sub-leading $3d$ -electron magnetic anisotropy can also be of relevance at high temperatures. We are developing *ab initio* understanding of magnetic anisotropy toward a quantitative understanding and control of magnetic properties of several representative compounds in permanent magnets. Here $4f$ -electrons pose also a methodological challenge in *ab initio* calculations.

Target materials and methods In today's champion magnet, Nd-Fe-B alloy, the main phase is made of $\text{Nd}_2\text{Fe}_{14}\text{B}$ [1] which has 68 atoms, 4 formula units, in the complicated unit cell. Utilizing OpenMX and AkaiKKR [2], we have gone through the electronic states of $\text{R}_2\text{Fe}_{14}\text{B}$ permanent magnet compounds and RCO_5 compounds (R=rare earth) with the latter being a reference material to have our own theoretical insights in a relatively easy way. Thus complicated nature in the Nd-Fe-B champion magnets is being resolved one by one. Relativistic calculations to calculate magnetic anisotropy for $\text{R}_2\text{Fe}_{14}\text{B}$ can be computationally expensive but manageable

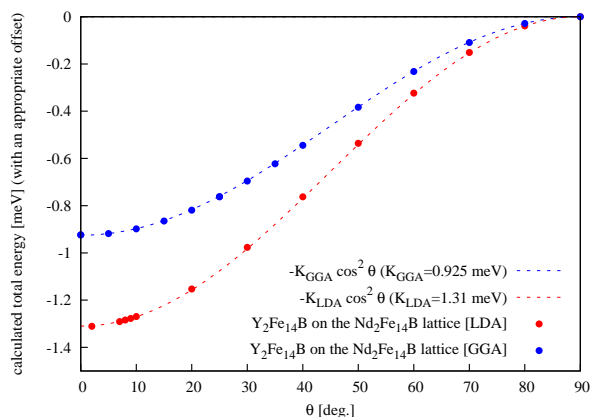


Figure 1: Calculated total energy for $\text{Y}_2\text{Fe}_{14}\text{B}$ artificially constructed on the experimental lattice of $\text{Nd}_2\text{Fe}_{14}\text{B}$ [1] as a function of the angle, θ , between the total magnetization and the c -axis. This is obtained with OpenMX fully relativistic runs with constrained non-collinear spin orientation. The energy gain in $\theta = 0$ reflects $3d$ -electron magnetic anisotropy in $\text{R}_2\text{Fe}_{14}\text{B}$ (R=rare earth). The data was obtained on system B in March 2017 at the cost of $O(10^2)$ points overall.

with OpenMX, which implements $O(N)$ methods. Great variety of magnetic properties in $\text{R}_2\text{Fe}_{14}\text{B}$ depending on the species of R has been known [3] to which KKR-CPA as implemented in AkaiKKR is suitable for systematically tracking the trends among rare earth with $(\text{R}_{1-x}\text{R}'_x)_2\text{Fe}_{14}\text{B}$ where $0 \leq x \leq 1$ can be continuously swept. Significant part of our computational projects was launched in the latter half of the fiscal year 2016 and here we report

our progress up to the anisotropy of d -electrons (as shown in Figs. 1 and 2) and magnetization (as shown in Fig. 3). Results concerning the magnetic anisotropy from $4f$ -electrons are now being elaborated to be out in a separate few publications in the near future.

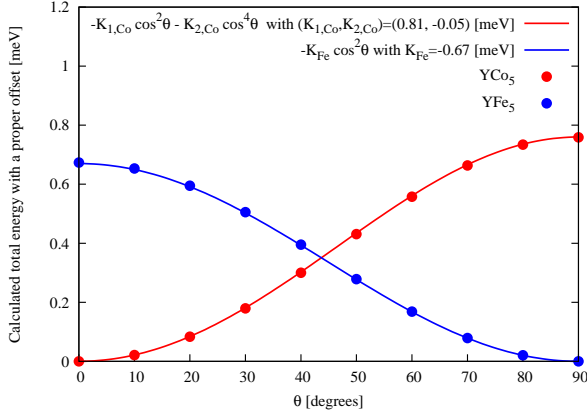


Figure 2: Calculated total energy for $Y\text{T}_5$ ($\text{T}=\text{Co},\text{Fe}$) on a computationally optimized lattice with OpenMX as a function of the angle, θ , between the total magnetization and the c -axis. The data collection procedure is the same as is applied for the data shown in Fig. 1.

Results [1/2]: magnetic anisotropy The leading-order uni-axial magnetic anisotropy can be described by the following term [4]:

$$\mathcal{H}_{\text{aniso}} = -K_1 \cos^2 \theta, \quad (1)$$

where θ is the angle between the bulk magnetization in the ferromagnetic order and an easy-axis, which is c -axis for the present cases of $\text{R}_2\text{Fe}_{14}\text{B}$ ($\text{R}=\text{Nd}, \text{Pr}, \text{and Y}$) and $\text{R}'\text{Co}_5$ ($\text{R}'=\text{Y}$). Calculated results for $3d$ -electron contribution in $\text{R}_2\text{Fe}_{14}\text{B}$ as shown in Fig. 1 indicates $K \simeq 1$ [meV/formula unit] which amounts to 0.7 [MJ/m^3]¹. The result is in good agreement with the experimental number for $\text{Y}_2\text{Fe}_{14}\text{B}$ near the ground state, $K \simeq 0.8$ [MJ/m^3] [3].

Trends in $3d$ -electron magnetic anisotropy have been inspected with the case of RCo_5 as shown in Fig 2. We make the following observations.

¹Experimental lattice constants for $\text{Nd}_2\text{Fe}_{14}\text{B}$ ($a=8.8$ [\AA] and $c=12.20$ [\AA]) [3] are tentatively taken here.

1. a higher-order term, $(-K_2 \cos^4 \theta)$, contributes to the Co-anisotropy on top of the leading-order one written as Eq. (1). The quantitative relation between them, $K_2/K_1 \simeq -0.06$, seems to be in a reasonable agreement with the experimental result $K_2/K_1 \simeq -0.02$ as had been found in a past work [5].

2. Co and Fe contributes the opposite sign of anisotropy.

Implication of the second observation is serious for permanent magnet applications: a possible optimization of magnetization could be reached via the celebrated Slater-Pauling curve which points to a material-design principle that an appropriate mixture of Fe and Co would give us the best magnetization. We see that uni-axial magnetic anisotropy could be sacrificed during such course of magnetization optimization. Thus a non-trivial generalization of the Slater-Pauling curve is to be sought after where the overall performance in both of magnetization and anisotropy would be optimized.

Results [2/2]: magnetization Practical application of $\text{Nd}_2\text{Fe}_{14}\text{B}$ often involves alloys such as $(\text{Nd}_{1-x}\text{Dy}_x)_2\text{Fe}_{14}\text{B}$ in elevating the high-temperature coercivity to an industrially acceptable level or $(\text{Nd}_{1-x}\text{Pr}_x)_2\text{Fe}_{14}\text{B}$ when a light-rare-earth alloy is taken as the raw ingredients to fabricate a low-cost magnet. Thus it is important to address the intrinsic magnetism of such alloys, being at least of technological relevance. Also the known variation of magnetic properties with respect to the species of rare earth in $\text{R}_2\text{Fe}_{14}\text{B}$ [3] is to be put under a good theoretical control to come up with another material design principle to make the best use of rare-earth mixtures. Along these lines of motivations we have looked at the magnetization of $(\text{Nd}_{1-x}\text{Pr}_x)_2\text{Fe}_{14}\text{B}$ as shown in Fig. 3 to computationally interpolate the stoichiometric limits utilizing AkaiKKR. Mass generation of the data to explore the overall magnetic trends in $(\text{R},\text{R}')_2\text{Fe}_{14}\text{B}$ is now under progress to be combined with machine-learning approach and reference experimental data: the idea is to distill potentially useful composition candidates which could have been overlooked

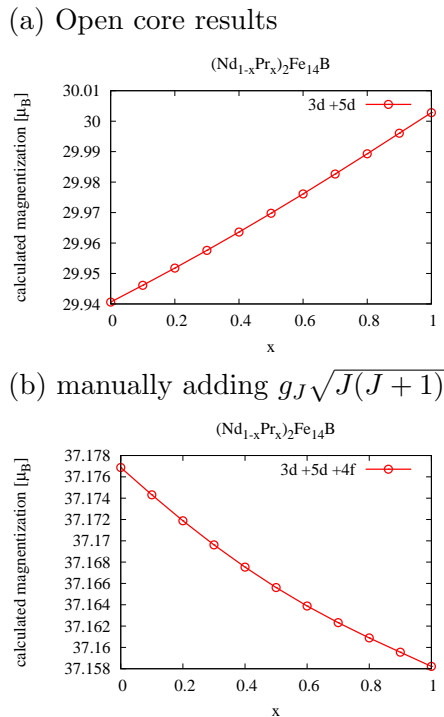


Figure 3: Calculated magnetization per formula unit of $(R_{1-x}R'_x)_2\text{Fe}_{14}\text{B}$ ($R=\text{Nd}, R'=\text{Pr}$) as a function of the composition parameter. Alloying of Nd and Pr has been described within Coherent Potential Approximation (CPA) and the data are collected utilizing AkaiKKR. (a) Open core results to show the d -electron contribution and (b) 4f-electron contribution has been included by manually adding $g_J\sqrt{J(J+1)}$ [$(g_J, J) = (8/11, 9/2)$ for Nd and $(4/5, 4)$ for Pr] as appropriately weighted with x .

on all-manual work done by strictly-limited human power.

Discussions We have successfully captured the qualitative trends in magnetization and magnetic anisotropy among $\text{Y}(\text{Co}, \text{Fe})_5$ and $\text{R}_2\text{Fe}_{14}\text{B}$ ($R=\text{Nd}, \text{Pr}, \text{Y}$), while absolutely correct description on a quantitative level is yet to be achieved by a more comprehensive incorporation of realistic energy scales. Possible improvements might come in the following two-fold way:

1. Electronic correlation in $3d$ -bands, however small in an intermetallic compound, is not quite negligible. In order to describe such many-body physics, DFT+U

or self-interaction correction can be done and are partly in progress in bringing the calculated results closer to experimentally known data.

2. The true macroscopic properties of permanent magnets involves extrinsic effects coming from classical dipolar magnetic fields. In principle they can also be incorporated in *ab initio* simulations while description of microstructure and various defects on the mesoscopic scale involves non-trivial physics on other level.

Conclusions and outlook Trends in magnetism among rare-earth permanent magnet compounds has been successfully addressed *ab initio* and the combined calculation framework (AkaiKKR+OpenMX) has been put onto our mass data production line with stoichiometric data points addressed with OpenMX and compositional interpolation taken care of with AkaiKKR. Together with a few schemes of implementation of *ab initio* description of $4f$ -electron anisotropy by fully relativistic calculations, we expect that the mass data generation would take another few $O(10^4)$ points on system B in the upcoming fiscal year.

References

- [1] J. F. Herbst: Rev. Mod. Phys. **63** (1991) 819.
- [2] both available via MateriApps <http://ma.cms-initiative.jp/ja/listapps> and runs out of the box on System B.
- [3] S. Hirosawa, Y. Matsuura, H. Yamamoto, S. Fujimura, M. Sagawa, and H. Yamauchi: J. Appl. Phys. **59** (1986) 873.
- [4] M. Matsumoto, H. Akai, Y. Harashima, S. Doi, and T. Miyake, J. Appl. Phys. **119** (2016) 213901.
- [5] J. M. Alameda, D. Givord, R. Lemaire, and Q. Lu: J. Appl. Phys. **52** (1981) 2079.

First-principles molecular spin dynamics theory of the complex magnetic structures in Mn-Pt alloys

Takashi UCHIDA

Hokkaido University of Science

4-1, 7-15, Maeda, Teine-ku, Sapporo 006-8585

Mn-Pt alloys show four different types of antiferromagnetic (AF) structures below their Néel temperatures depending on the composition and temperature. Mn_3Pt with Cu_3Au structure shows D-phase (triangular structure) and F-phase (collinear AF). MnPt with CuAu-I structure shows II-phase (collinear AF) and III-phase (collinear AF). We have recently applied the first-principles molecular spin dynamics (MSD) method to Mn_3Pt and explained the magnetic phase transitions from the D-phase to a high-temperature ordered phase in terms of the temperature dependence of the electronic structure [1]. As a preparation for the systematic study on the disordered alloys $\text{Mn}_{3-x}\text{Pt}_{1+x}$ ($x = 0 \sim 1$), in the present research, we have investigated the electronic and magnetic structures of ordered MnPt alloy.

The MSD theory is formulated by incorporating the first-principles TB-LMTO Hamiltonian into the MSD approach for itinerant magnets on the basis of the functional integral method and the isothermal MSD technique [1, 2]. The MSD approach allows us to determine automatically the magnetic structure of a large system with several hundred atoms in a unit cell at finite temperatures. In the present MSD analysis, we solved the isothermal MSD equations of motion by using site-dependent effective medium. We used the recursion method to calculate the local electronic structure in determining the effective medium and in calculating magnetic forces at each time step of

the MSD equations of motion. We utilized the MPI parallel calculation scheme in the recursion calculation. The site-dependent effective medium is determined by the local coherent potential approximation (CPA) equation. In the present case with tetragonal lattice, we have included the orbital dependence of the effective medium and the charge potential which is determined by the charge neutrality condition at each site. The magnetic structure is calculated on the supercell with $4 \times 4 \times 4$ CuAu-I unit lattice, which is embedded in a large cluster consisting of $5 \times 5 \times 5$ supercells, each of which are connected by the periodic boundary condition. The lattice parameter was fixed to the room temperature value [3].

The calculated magnetic structure of MnPt at 25 K was shown to be a collinear AF structure (II-phase) in agreement with experiment [3]. The calculated d -electron density of states (DOS) reveals a dip at the Fermi energy, being consistent with the previous LMTO calculation [4] with assuming the magnetic structure of II-phase.

References

- [1] T. Uchida, N. Kimura, and Y. Kakehashi: J. Korean Phys. Soc. **62** (2013) 1748; Y. Kakehashi, S. Akbar, and N. Kimura, Phys. Rev. **B57** (1998) 8354.
- [2] T. Uchida, Y. Kakehashi, and N. Kimura: J. Magn. Magn. Mater. **400** (2016) 103.
- [3] E. Krén *et al.*: Phys. Rev. **171** (1968) 574.
- [4] A. Sakuma: J. Phys. Soc. Jpn. **69** (2000) 3072.

Calculation of polarons, vibration modes, and positron trapping from first principles

Hannes Raebiger

*Department of Physics, Yokohama National University
Graduate School of Engineering
Tokiwadai, Hodogaya-ku, Yokohama 240-8501*

We employ first principles calculations to study not only electronic behavior, but also vibration modes in solids, and positron trapping in molecules. Solids are mainly studied by density-functional theories, whereas molecular systems are studied by Hartree-Fock theory. We push the limits of electronic structure theory, also by including positronic densities via multi-component theory [1], as well as by explicit calculation of nuclear wavefunction in order to investigate non-adiabatic phenomena at phase transitions [2].

Positron trapping in molecules

Positrons are a versatile probe to probe various properties of diverse materials. Positrons are used not only to probe defects in bulk materials [3] and recently also for medical purposes, including positron emission tomography [4]. The latter involves positron trapping to organic molecules, which is a poorly studied field. Moreover, for clinical applications, this positron trapping cannot be modeled by study of isolated molecules in vacuum, so we focus on the effect of an aqueous environment to the positron trapping properties of organic molecules. It is well known that in addition to negative ions, also strongly polar molecules may bind positrons [5]. We investigate positron binding to glycine (Gly) and its zwitterion (GlyZI) form, and their aqueous complexes $\text{Gly} \cdot n \text{H}_2\text{O}$ and $\text{GlyZI} \cdot n \text{H}_2\text{O}$, and show that also these systems do exhibit a crit-

ical dipole moment μ_{cr} , such that molecules with dipole moment $\mu > \mu_{\text{cr}}$ bind positrons. However, we demonstrate that μ is not a sufficient quantity to describe binding properties to such complex systems, and that positron binding to molecular systems also strongly depends on the intramolecular bonding [6].

Localization of vibration modes around defects in 2D materials

2D and quasi-1D bulk materials have unique phonon properties, which allow, e.g., to determine sample thickness based on shifts in typical vibration modes [7]. In collaboration with experiment, we show that defects in MoS_2 give rise to new Raman active vibration modes, which are unique to different types of defects [8]. We discover new vibration modes, which are both localized near defect sites, as well as scattered, such as to exhibit large vibration amplitudes far away from the defects. Thus, we have shown that Raman spectroscopy combined with first principles calculation offer a non-invasive probe to observe both defect species, as well as to evaluate defect concentrations etc.

Non-adiabatic metal-insulator transition in magnetic semiconductors

Mn-doped GaAs is an important and widely studied material for magnetic semiconductors. In addition to its exotic magnetic properties,

it exhibits a critical metal-insulator transition (MIT) as Mn concentration x is increased up to, and beyond $\sim 1\%$. We study this material by self-interaction corrected density-functional calculations [9], and for the first time, reproduce a critical MIT in a first principles calculation [2]. We find both delocalized, metallic states Φ_M , as well as localized, insulator states Φ_I , whose relative stability depends on x : Φ_M is stable for $x > 1\%$, and Φ_I is stable for $x < 1\%$. Moreover, around the critical concentration $\sim 1\%$, both states coexist. We calculate the adiabatic potential energy surface that joins these states, which exhibits an anharmonic double-well structure. We then numerically evaluate nuclear wavefunctions for nuclear motion Q along this adiabatic potential, showing that the system must be described by an anharmonic superposition state $c_I(Q)\Phi_I + c_M(Q)\Phi_M$ [2]. Thus, the MIT criticality in this system arises due to excitonic phases [?]; this implies that for critical x , Mn-doped GaAs is an excitonic insulator, and in this sense, our work proves the realization of an excitonic insulator material.

References

- [1] M. Tachikawa: Chem Phys. Lett. **350** (2001) 269.
- [2] S. Bae and H. Raebiger: Phys. Rev. B (Rapid Communications) **94** (2016), 241115(R).
- [3] F. Tuomisto and I. Makkonen: Rev. Mod. Phys. **85** (2013) 1583.
- [4] M. Reivich et al.: Circ. Res. **44** (1979) 127.
- [5] O. Crawford, Proc. Phys. Soc. (London) **91** (1967) 279.
- [6] M. Nummela, H. Raebiger, D. Yoshida, and M. Tachikawa: J. Phys. Chem. A **120** (2016) 4037.

- [7] K. Osada S. Bae M. Tanaka H. Raebiger K. Shudo T. Suzuki: J. Phys. Chem. C **120** (2016) 4653.
- [8] S. Bae, N. Sugiyama, T. Matsuo, H. Raebiger, K. Shudo, K. Ohno: Phys. Rev. Applied **7** (2017) 024001.
- [9] S. Lany and A. Zunger: Phys. Rev. B **80** (2009) 085202.
- [10] W. Kohn: Phys. Rev. Lett. **19** (1949) 416.

Search for new electronic properties of new nanoscale interfaces

Katsuyoshi KOBAYASHI

*Department of Physics, Ochanomizu University
2-1-1 Otsuka, Bunkyo-ku, Tokyo 112-8610*

We started a theoretical study on the electronic states of IV-VI monolayers on alkaline-earth chalcogenide surfaces in 2015. We performed more detailed study on the same system in 2016.

It was theoretically proposed by several groups that IV-VI monolayers are two-dimensional (2D) topological crystalline insulators (TCIs). However, it was also pointed out that the planar structure of free standing IV-VI monolayers is not stable, and the TCI states are broken by structural deformation [1]. In order to maintain the planar structure of IV-VI monolayers we consider the system of IV-VI monolayers supported by substrates. First we consider alkali halide surfaces for supports. However, it was found that the interaction between IV-VI monolayers and alkali halides is weaker than that between IV-VI monolayers. This means that single IV-VI layers are not stable on alkali halide surfaces. Therefore we consider alkaline-earth chalcogenide surfaces as a candidate for supports having strong interaction with IV-VI monolayers. In 2015 we performed energetic calculations using 1×1 unit cell. In 2016 we extend the calculations up to 2×2 unit cell. For the total-energy calculations we used the VASP code.

The IV-VI monolayers investigated are GeS, GeSe, GeTe, SnS, SnSe, SnTe, PbS, PbSe, and PbTe. The alkaline-earth chalcogenides are MgO, MgS, MgSe, CaO, CaS, CaSe, CaTe, SrO, SrS, SrSe, BaO, and BaS. Various combinations of these monolayers and supports are investigated. We found that the combinations favorable for stable IV-VI monolayers on surfaces are SnTe-SrS, SnTe-SrSe, SnTe-CaTe, SnTe-BaS, SnSe-CaS, SnSe-CaSe, SnS-MgSe,

and GeSe-MgSe. In the structural optimization we found a structure of IV-VI monolayers shown in Fig. 1. This structure consists of tetragons and octagons of IV-VI networks. It is essentially the same structure as those found theoretically for Bi monolayers [2, 3, 4].

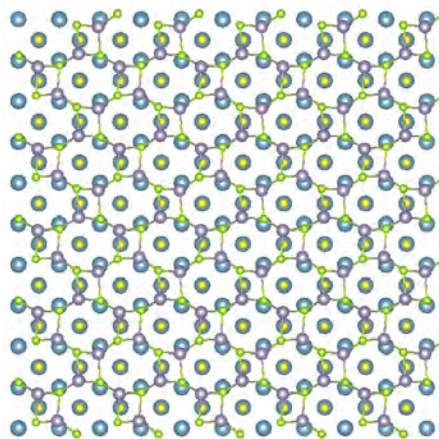


Figure 1: Top view of a tetragonal-octagonal structure of IV-VI monolayer on an alkaline-earth chalcogenide surface. The tetragonal-octagonal structure is shown by the network.

References

- [1] K. Kobayashi: Surf. Sci. **639** (2015) 54.
- [2] L. Kou *et al.*: 2D Materials **2** (2015) 045010.
- [3] P. Li and W. Luo: Sci. Rep. **6** (2016) 25423.
- [4] F. Ersan *et al.*: Phys. Rev. B **94** (2016) 245417.

Thermo-Chemical Wear Mechanism of Diamond Cutting Tools

Yutaka Uda, Shoichi Shimada

Osaka Electro-Communication University, Hatsu-cho, Neyagawa, Osaka 572-8530

Sakuro Honda

Technology Research Institute of Osaka Prefecture, Ayumino, Izumi, Osaka 594-1157

Diamond is the only ideal cutting tool material for high efficient ultraprecision cutting of accurate three-dimensional metal works such as molds for precise optical components with high aspect ratio. However, it is well known that diamond cutting tools show severe wear in cutting of heat-resistant materials such as ferrous metals and nickel. On the other hand, in cutting of electroless nickel deposits, in which 10-14% phosphorus (P) is solid-soluted, remarkably less tool wear is observed than in case of pure nickel [1,2]. However, the essential mechanisms of tool wear and its suppression by P addition have not yet been understood well. To understand these mechanisms, first principles analyses were carried out using double-grid method for real-space electronic-structure calculations package RSPACE [3].

The $C_{10}H_{14}$ cluster was used as the model of diamond (100) surface. The dangling bonds

other than that of the radical carbon atom at the bottom layer of diamond were terminated by hydrogen atoms. The atomic and back bond populations of the radical carbon were 4.11 and 0.894, respectively. The thin Ni (100) surface model was composed of 24 Ni atoms. The dimension of the model $x \times y \times z$ was $2a \times 2a \times a$, where a is lattice constant of Ni. The atomic populations of all Ni atoms were 10.0. The model has periodic boundaries in x and y directions and aperiodic boundary in z direction. The Ni-P surface model was prepared by randomly distributing of 6 P atoms at the octahedral holes of the Ni model. The atomic populations of Ni atoms decreased from 9.29 to 9.72 and those of P atoms increased from 6.28 to 6.39. The result suggests that strong ionic bonding occur between Ni and P atoms.

The atomic and bond populations in combined structures of diamond with Ni after optimization are shown in

Fig.1. White and yellow figures express atomic and bond populations, respectively. By the interaction with Ni, the atomic population of radical carbon increases to 4.91 and those of Ni atoms interacting with radical carbon decreases

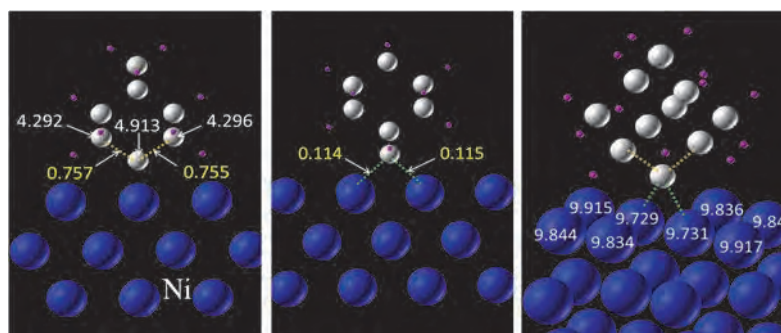


Fig. 1 Atomic and bond populations in combined structure of diamond with Ni surface after optimization.

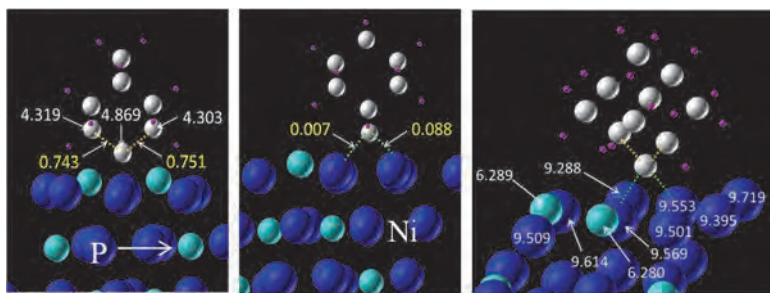


Fig.2 Atomic and bond populations in combined structure of diamond with Ni surface after optimization.

to 9.73. The result suggests that the strength of ionic bond between carbon and Ni increases. As the population of back bonds of radical carbon decrease to 0.76 from the original value of 0.89, the strength of covalent bond of back bonds decreases and the radical carbon has a chance to dissociate from the diamond surface when it has a large kinetic energy due to cutting temperature. On the other hand, in case of interacting with Ni-P, both of decrease of back bond population and increase of atomic population of radical carbon are remarkably suppressed as shown in Fig.2.

The dissociation energy of the radical carbon was estimated as shown in Figure 3. Diamond model is lifted up from optimum stable structure leaving the radical carbon on work surface. By optimization after lifting of a certain distance, the radical carbon moves

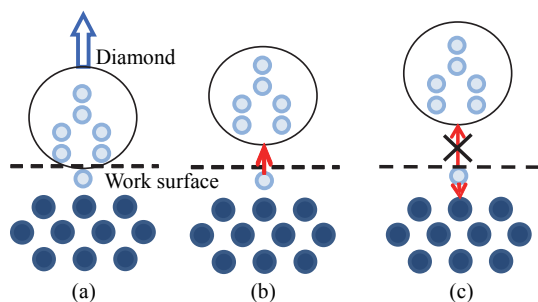


Fig.3 Estimation of dissociation energy of radical carbon atom interacted with work surface.

toward the main body of diamond. However, at a lift up distance larger than the critical value, the radical carbon stays on the work surface. The dissociation energy of the radical carbon can be estimated from the difference between the

total energy of the combined structure at the critical lift up distance and that of optimum stable structure. Although the atomic structure was not optimized in pulling up process, the dissociation energies of radical carbon by different work materials can be relatively compared. The dissociation energies estimated are 5.01eV and 5.70eV when the diamond is contacting with Ni and Ni-P, respectively. The results suggest that the essential wear mechanism is the dissociation of carbon atoms on diamond surface due to the interaction with nickel atoms on work surface. P atoms addition reduces the dissociation because the interaction is suppressed.

References

- [1] C.K. Syn, J.S. Taylor, R.R. Donaldson: Proc. SPIE, **676** (1986) 128.
- [2] J.M. Oomen, L. Eisses: Precision Engineering, **14**, (1992) 206.
- [3] K. Hirose, T. Ono: First-Principles Calculations in Real-Space Formalism – Electronic Configurations and Transport Properties of Nanostructures -, Imperial College Press, London, (2005).

Electron-Phonon Interactions in Isotopic Diamond Superlattice

Yuki Bando, Masayuki Toyoda, and Susumu Saito
Department of Physics, Tokyo Institute of Technology
 2-12-1 Ookayama, Meguro-ku, Tokyo 152-8550 Japan

The isotopic diamond superlattices that are periodic arrays of layers of carbon isotopes, such as ^{12}C and ^{13}C , with diamond structure, have been known to confine carriers to the layers of the lighter isotope (^{12}C) due to the isotope effect on the electron-phonon interaction [1]. This phenomena has a great potential to realize the band-gap engineering in diamonds and to utilize diamonds as electronic devices. In this study, the electron-phonon interactions have been quantitatively investigated for the isotope diamond superlattices using the adiabatic Allen-Heine-Cardona calculations based on the density functional perturbation theory [2]. The calculations were performed by using ABINIT code [3] on the cpu nodes of system B. The visualized images of the crystal structures were created by using XCrySDen [4].

Figure 1(a) shows the crystal structures of the superlattices. The stacking direction is along [001] and each structure is labeled as $\{m,n\}$ that means it consists of periodic arrays of m atomic layers of ^{12}C and n atomic layers of ^{13}C . The tetragonal unit cells of the superlattices have a lower symmetry than the original $Fd\bar{3}m$ symmetry and thus the electron-phonon interaction would modify the electronic structure in such a way that it breaks the original symmetry. One of such examples is schematically shown in Fig. 1(b), where the six identical electron pockets in diamonds are separated into two groups in superlattices: two pockets along Γ - Z line and four along Γ - M line.

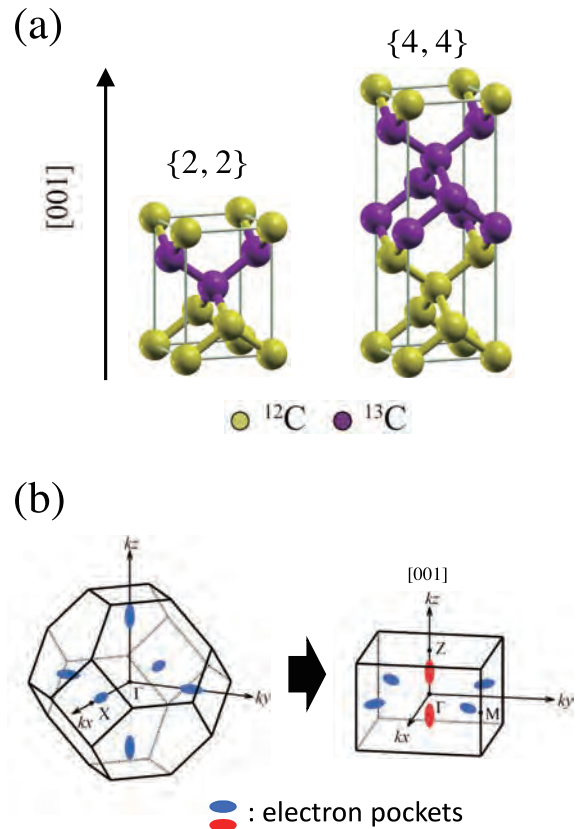


Figure 1: (a) Tetragonal unit cells of $\{2,2\}$ and $\{4,4\}$ isotope diamond superlattices (see text for the definition of the labels). (b) Schematic image of the electron-pockets in the fcc (simple diamond) and tetragonal (superlattices) Brillouin zones.

The zero point renormalization (ZPR) of the Kohn-Sham band gap has been calculated for the isotope superlattices. Figure 2 shows the calculated Kohn-Sham eigenvalues around the valence band (VB) top and conduction band

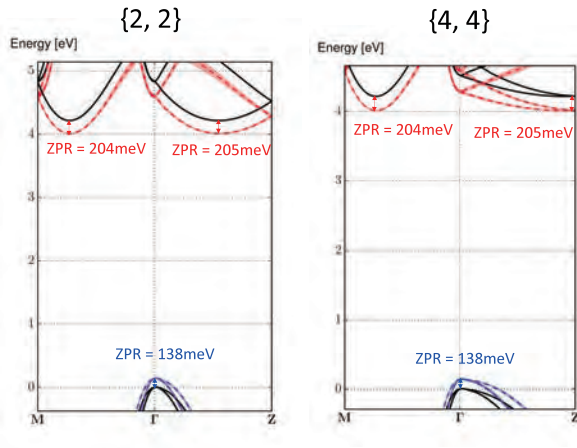


Figure 2: Calculated zero-point renormalized Kohn-Sham eigenvalues of the valence bands (blue) and conduction bands (red). The Kohn-Sham eigenvalues without renormalization are also plotted by the black line for comparison.

(CB) bottoms, as well as the renormalized eigenvalues. The Kohn-Sham band structure is shown by the black solid lines and the renormalized band structure is by the colored (red for CB and blue for VB) dashed lines. For both of the $\{2,2\}$ and $\{4,4\}$ systems, the renormalization of the indirect band-gap is 342 meV. This value is in exact agreement with the renormalization of the band gap calculated for a simple diamond lattice of a carbon isotope with a virtual mass number $^{12.5}\text{C}$. This result shows that the isotope effect is mass-averaged, being consistent with our previous study of the phonon modes of the this layer isotope superlattices.

Interestingly, we found that there is a slight difference in the ZPR of the CB bottoms between those along Γ -M and Γ -Z lines. The difference is as small as 1 meV, but it might possibly be due to the symmetry breaking as discussed above. In order to confirm this symmetry breaking ZPR effect, further study is necessary.

References

- [1] H. Watanabe, C.E. Nebel, and S. Shikata, *Science* **324** (2009) 1425.
- [2] S. Ponce, et al, *Phys. Rev. B* **90** (2014) 214304
- [3] X. Gonze, et.al, *Computer Physics Communications* **180** (2009) 2582-2615
- [4] A. Kokalj, *Comp. Mater. Sci.*, **28** (2003) 155.

Theoretical research on dissociation of N_2 for designing new ammonia catalysis supporting Ru

Yoichi KAMIHARA

*Department of Applied Physics and Physico-Informatics, Keio University
3-14-1 Hiyoshi, Yokohama, Kanagawa 223-8522*

In the Haber-Bosch process NH_3 is synthesized from gaseous N_2 and H_2 with an Fe-based catalyst for over 100 years[1]. In 21st century, it has been reported that Ru-loaded $[Ca_{24}Al_{28}O_{64}]^{4+}(e^-)_4$ (Ru/C12A7: e^-) works as an efficient catalyst for NH_3 synthesis[2]. C12A7: e^- , the first room temperature stable electride, which has a low work function (2.4 eV) comparable to that of potassium metal, with chemically and thermally stability. C12A7: e^- contains 12Ca-Al-O cage structures in a unit cell. In this report, three virtual Ru/C12A7: e^- lattices are modeled by layered slab models. These N_2 adsorption energies are quantified for these models.

A first reaction step in the synthesis of ammonia is



where (*) stands for an empty site on the surface. The adsorption energies (E_{ad}) of nitrogen were calculated using

$$E_{ad} = 2E_{N-Ru/C12A7} - 2E_{Ru/C12A7} - E_{N_2} \quad (2)$$

where $E_{Ru/C12A7slab}$ and $E_{N-Ru/C12A7}$ stand the total energies of the Ru/C12A7 clean surface and Ru/C12A7 surface with an adsorbed nitrogen atom respectively. E_{N_2} is the total energy of a nitrogen molecule.

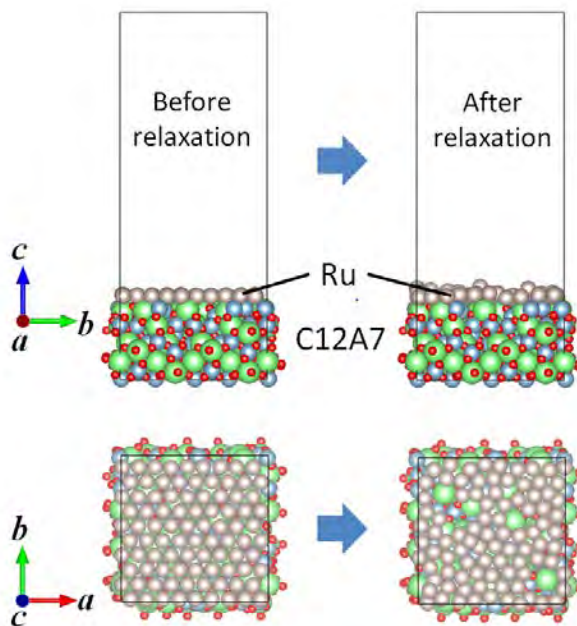


Figure 1: Structure of slab model of 1 Ru layer on C12A7 before and after optimization of internal structure. Green, blue and red symbols represent Ca, Al and O ions, respectively.

Each calculation has been carried out based on density functional theory (DFT) using Projector Augmented Wave (PAW) method[3] implemented in the Vienna *ab-initio* Simulation Package (VASP)[4]. Generalized gradient approximation (GGA) of Perdew-Burke-Ernzerhof (PBE) functional[5] was adopted for exchange-correlation energy.

The Ru supported by C12A7 surface were

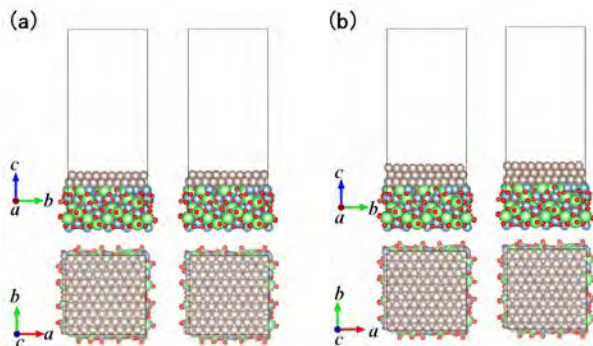


Figure 2: Structure of slab model of 2 and 3 Ru layers on C12A7 before (left) and after (right) optimization of internal structure. Green, blue and red symbols represent Ca, Al and O ions, respectively.

modeled as periodically repeating C12A7, Ru (0001) and vacuum for simplify the system. Supercell was made by $(2 \times 2 \times 1)$ of C12A7 unitcell, N layer(s) ($N = 1, 2, 3$) of Ru (0001) surface (90 atoms per layer) and vacuum region of 4.2 nm. The energy cut off for plane waves was 500 eV. The Brillouin zone was sampled at the Γ point only. Fractional occupancies of the bands were obtained allowed using a Gaussian smearing method with width $\sigma = -0.05$ [6].

Fig. 1, Fig. 2(a) and Fig. 2(b) show the schematic image of slab structures of 1, 2 and 3 layer(s) of Ru on C12A7 before and after optimization of internal structures for the lattices respectively. For 1 Ru layer model, Ru atoms move along the C12A7 surface. Therefore C12A7 surface is partially exposed to vacuum. As for 2 and 3 Ru layers model, such an atomic coordination's movement are smaller than that of 1 Ru layer model.

After ionic optimization, a nitrogen atom laid on a hollow site of the obtained surface model of N layer(s) ($N = 1, 2, 3$) of Ru (0001) on C12A7(Fig. 3). Adsorption energies E_{ad} of 1 Ru layer model, 2 Ru layers model and 3 Ru layers model are calculated as -1.74 eV,

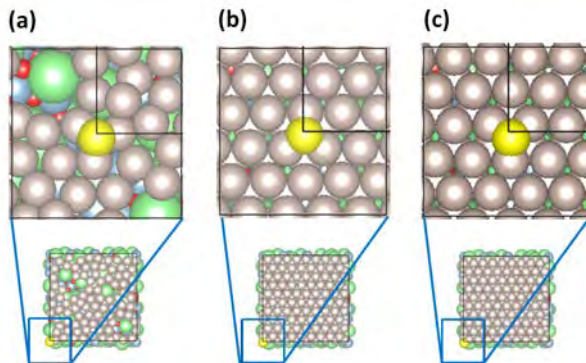


Figure 3: The configurations of the surfaces adsorbed nitrogen atoms on (a)1 Ru layer model (b)2 Ru layers model (c)3 Ru layers model. Green, blue, red and yellow symbols represent Ca, Al, O and N ions, respectively.

-0.21 eV and -0.48 eV respectively. A nitrogen atom is more stable when it adsorbed on the surface of 1 Ru layer model, than that of 2 or 3 Ru layers model.

In our calculation, the supporting C12A7 makes matrix structures composed of several Ru atoms and the Ca-Al-O cages. The matrix surface structures would works to enhance the catalytic activity in the process of dissociative adsorption for 1 Ru layer model. As for 2 and 3 layers model, further calculation is required.

References

- [1] F. Haber: Z. Elektrochem. Angew. P. **16** (1910) 244.
- [2] M. Kitano, *et al.*: Nature Chemistry **4** (2012) 934.
- [3] P. E. Blöchl: Phys. Rev. B **50** (1994) 17953.
- [4] G. Kresse and J. Hafner: Phys. Rev. B **47** (1993) 558.
- [5] J. P. Perdew, K. Burke and M. Ernzerhof: Phys. Rev. Lett. **77** (1996) 3865.
- [6] https://cms.mpi.univie.ac.at/vasp/vasp/Finite_temperature_approaches_smearing_methods.html

Ab-initio Analysis on Structures of Amorphous Iron Oxide for Secondary Battery

Kenji TSURUTA, Keiichi MITANI, Satoshi OHMURA^a, and Atsushi ISHIKAWA

Graduate School of Natural Science and Technology, Okayama University, Okayama 700-8530

^a *Department of Civil Engineering and Urban Design, Hiroshima Institute of Technology, Hiroshima 731-5193*

Corundum-structure hematite α - Fe_2O_3 is one of the most common mineral on the earth, and plays important roles in various industrial sectors such as steel, medical and electronics. Especially, hematite nanoparticles have recently attracted much attention for lithium-ion batteries, sensors, biomedical, and photoelectro-chemical (PEC) applications. In addition, the iron-oxide nanoparticles are found in nature as biogenous secondary materials [1]. It has been identified that the biogenous iron-oxide has an amorphous structure containing several impurities such as Si and P. They have exhibited to possess high capacity in using anode material of Li-ion secondary battery.

In the present study, we investigate structural properties of a Si/P co-doped hematite using the density-functional theory. The generalized gradient approximation (GGA) + U functional, the Perdew-Burke-Ernzerhof functional for the local spin density approximation of exchange-correlation, and the projector-augmented wave based pseudo-potential for the core electrons have been employed for the electronic-structure calculations. The *ab-initio* molecular dynamics simulations with the *NPT* ensemble have been performed to obtain thermal equilibrium states of the Si/P co-doped systems of an anti-ferromagnetic (AFM) state at the room temperature, as well as a non-doped amorphous structure modeled by rapid quenching from high-temperature (3000K) melt. We have adopted the Vienna *Ab initio* Simulation Package (VASP) for these *ab-initio* simulations.

The pair distribution functions $g_{\alpha\beta}$ for the co-doped and the non-doped amorphous Fe_2O_3 models are shown in Fig. 1. In $g_{\text{O}\text{O}}(r)$ of the amorphous Fe_2O_3 , the peak in the vicinity of $r = 1.5\text{\AA}$ indicates that oxygen dimers are formed in a disordered structure of the iron oxide at the AFM state. This feature is consistent with previous theoretical calculations for Fe_2O_3 [2]. We find that all the $g_{\alpha\beta}(r)$ agree very well with each other; overlaps between both distributions for Fe-Fe, O-O and Fe-O are 97.5%, 95.8% and 98.7% respectively. Thus the Si/P co-doping has been shown to be an efficient route for amorphization of iron oxides.

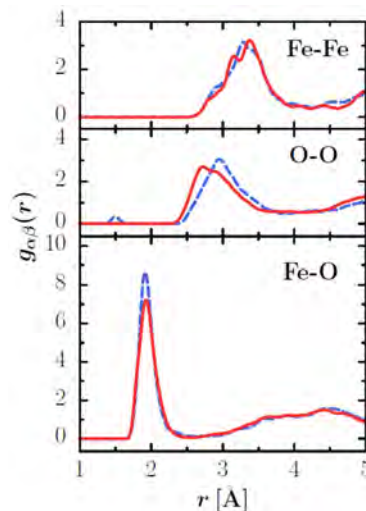


Fig. 1: Partial pair distribution functions $g_{\alpha\beta}(r)$ for non-doped amorphous (dashed lines) and Si/P co-doped Fe_2O_3 (solid lines).

References

- [1] H. Hashimoto *et al.*, ACS Appl. Mater. Interface **6**, 5374-5378 (2014).
- [2] M. Misawa *et al.*, J. Phys. Soc. Jpn. **83**, 105002 (2014).

First-Principles Momentum Dependent Local Ansatz and Application to Momentum Distribution Function and Quasiparticle Bands in Fe Compounds

Yoshiro KAKEHASHI

*Department of Physics and Earth Sciences, Faculty of Science, University of the Ryukyus,
1 Senbaru, Nishihara, Okinawa, 903-0213, Japan*

Quantitative aspects of the density functional theory (DFT) are well-known to become unstable with increasing Coulomb interaction strength as found in ϵ -Fe, Fe-pnictides, and cuprates. In order to describe correlated electrons quantitatively and to remove the difficulties in the DFT, we have recently proposed the first-principles momentum dependent local ansatz (MLA) wavefunction theory on the basis of the tight-binding LDA+U Hamiltonian [1].

In the first-principles MLA, we introduce the three kinds of momentum dependent correlators (*i.e.*, intra-orbital correlator, inter-orbital charge-charge correlator, and inter-orbital spin-spin correlator), and takes into account all the two-particle excited states with the momentum-dependent amplitudes, so that it describes exactly the weak interaction limit, and describes well correlated electrons from the weak to strong Coulomb interaction regime.

In this project, we have performed the numerical calculations of the ground-state properties of iron-group transition metals from Sc to Cu using the first-principles MLA.

We found large Hund's rule correlation energy in Mn and Fe (3000 K), which are missing in the magnetic energy calculations in the LDA+DFT. The Hund rule correlations also enhance the amplitudes of local moments. We found that calculated amplitudes of local moments quantitatively explain the experimental values estimated from the inner core photoelectron spectroscopy and susceptibility [2].

We also found large deviation of the momentum distribution function from the Fermi-

Dirac function in the late transition metals. Figure 1 shows a systematic change of the mass enhancement factors m^*/m calculated from the jump of the momentum distribution function. We found significant enhancement of m^*/m in the late transition metals. The result explains a systematic change of the experimental data obtained from the low-temperature specific heats [2].

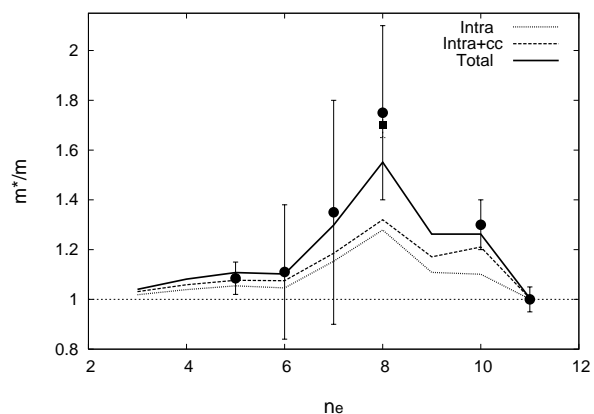


Figure 1: Calculated mass enhancement factor (m^*/m , solid curve) as a function of conduction electron number n_e . Experimental results: closed circles, closed squares.

References

- [1] Y. Kakehashi and S. Chandra, J. Phys. Soc. Jpn. **85**, 043707 (2016); **85**, 064714 (2016).
- [2] Y. Kakehashi and S. Chandra, J. Phys. Soc. Jpn. **85**, 084708 (2016); **86**, 034711 (2017).

Electronic State and Proximity Effects around Interface in Layered Superlattices

Kunitomo HIRAI

*Department of Physics, Nara Medical University
Kashihara, Nara 634-8521*

The purpose of the present research is to elucidate characteristics of electronic state in superlattices with layered structures, in particular, to illustrate proximity effects of each layer on adjacent layers in the superlattices. This research of a first-principles electronic structure calculation is performed by means of the Korringa-Kohn-Rostoker (KKR) Green function method within the framework of the local spin density (LSD) functional formalism.

The calculation by means of the KKR method was so far carried out for superlattices of ferromagnetic layers with nonmagnetic spacer layers such as Fe/Cr, Fe/V, Fe/Cu, . . . ones, with magnetizations of two successive Fe layers being aligned parallel or antiparallel. Oscillatory interlayer exchange coupling between ferromagnetic layers with respect to spacer thickness was investigated, and relation between bulk effects inherent in the spacer layer and the proximity effects due to the ferromagnetic layers was analyzed. In the calculation, every atom in a monolayer stacked in the superlattices is assumed to be equivalent, and there is one site in each monolayer. This assumption can be justified for the superlattices with ideal interfaces without structure, but not for those with realistic interfaces with structures like steps, islands, or such, and hence there are two or more sites in each monolayer for the superlattices with realistic interfaces.

A need of the calculation for superlattices with more sites in each monolayer arises also for layered superlattices of ordered alloys or

compounds, which now attract broad interests particularly in viewpoint of spintronics. We then start preparation of the calculation for superlattices with more sites in each monolayer, which results in increase of the number of atoms in a unit cell and involves vast increase of computation times. In the preparation of the calculation, installation of parallelization with use of the OpenMP into program codes of the KKR methods is intended, together with parallelization with use of the MPI which was already achieved, that is, installation of hybrid parallelization is intended.

The installation of the OpenMP has not been achieved within the present term, which was the last one, and it is really unfortunate that the proximity effects in the superlattices with realistic interfaces are not amply investigated. In the last place, I thank the Supercomputer Center, Institute for Solid State Physics, the University of Tokyo for the longtime use of its facilities.